Neuroscience

Driver lines for studying associative learning in Drosophila

Yichun Shuai, Megan Sammons, Gabriella Sterne, Karen Hibbard, He Yang, Ching-Po Yang, Claire Managan, Igor Siwanowicz, Tzumin Lee, Gerald M. Rubin, Glenn Turner, Yoshinori Aso

Janelia Research Campus, Howard Hughes Medical Institute, 19700 Helix Drive, Ashburn, VA 20147, USA • Technion-Israel Institute of Technology, 1 Efron St., Haifa 32000, Israel • Department of Biomedical Genetics, University of Rochester Medical Center, Rochester, NY, USA • Life Sciences Institute, University of Michigan, Ann Arbor, USA

Reviewed Preprint

Published from the original preprint after peer review and assessment by eLife.

About eLife's process

Reviewed preprint version 1
February 8, 2024 (this version)

Sent for peer review
November 23, 2023

Posted to preprint server
November 2, 2023

Abstract

The mushroom body (MB) is the center for associative learning in insects. In Drosophila, intersectional split-GAL4 drivers and electron microscopy (EM) connectomes have laid the foundation for precise interrogation of the MB neural circuits. However, investigation of many cell types upstream and downstream of the MB has been hindered due to lack of specific driver lines. Here we describe a new collection of over 800 split-GAL4 and split-LexA drivers that cover approximately 300 cell types, including sugar sensory neurons, putative nociceptive ascending neurons, olfactory and thermo-/hygro-sensory projection neurons, interneurons connected with the MB-extrinsic neurons, and various other cell types. We characterized activation phenotypes for a subset of these lines and identified the sugar sensory neuron line most suitable for reward substitution. Leveraging the thousands of confocal microscopy images associated with the collection, we analyzed neuronal morphological stereotypy and discovered that one set of mushroom body output neurons, MBON08/MBON09, exhibits striking individuality and asymmetry across animals. In conjunction with the EM connectome maps, the driver lines reported here offer a powerful resource for functional dissection of neural circuits for associative learning in adult Drosophila.

eLife assessment

This **important** collection of over 800 new cell type-specific driver lines will be an invaluable resource for researchers studying associative learning in Drosophila. Thoroughly characterized and well documented, this collection will permit researchers to selectively target neurons that deliver information to, or receive it from, the memory center of the fly brain called the Mushroom Body. Given the wealth of new drivers and the genetic access they provide to over 300 cell types, this **compelling** work will be of interest not only to researchers studying the mechanisms of associative learning but more generally to those dissecting sensorimotor circuits in the fly nervous system.

Introduction

In the insect brain, the mushroom body (MB) serves as the center for associative learning (**Figure 1A-C**; reviewed in Modi et al., 2020; Davis, 2023). Information regarding conditioned stimulus (CS), such as odors and colors, is conveyed by projection neurons (PNs) to the calyx, the input region of the MB. In Drosophila, approximately 2,000 Kenyon cells (KCs), the MB's primary intrinsic neurons, represent the identity of sensory stimuli by their sparse activity patterns (Perez-Orive et al., 2002; Turner et al., 2008). Dopaminergic neurons (DANs) mediate signals of the unconditioned stimulus (US), such as sugar reward or electric shock punishment, to the MB (Burke et al., 2012; Kirkhart and Scott, 2015; Liu et al., 2012; Mao and Davis, 2009; Schwaerzel et al., 2003). DANs and MB output neurons (MBONs) collectively form 15 compartmental zones that tile down the length of the KC axons in the MB lobes (Aso et al., 2014a; Tanaka et al., 2008). Memories are stored as altered weights of synaptic connections between KCs and MB output neurons (MBONs) in each compartment (Hige et al., 2015a; Owald et al., 2015). Relative activity levels of MBONs across compartments represent the valence of the learned CS and drive memory-based behaviors (Aso et al., 2014b; Owald et al., 2015).

The recently completed electron microscopy (EM) connectomes of the Drosophila brain in larvae and adults revealed thousands of interneurons upstream of DANs, which convey reinforcement signals to the MB, and downstream of MBONs, which link the MB to premotor pathways and other higher-order brain centers (Dorkenwald et al., 2023; Eichler et al., 2017; Eschbach et al., 2020; Li et al., 2020; Scheffer et al., 2020; Winding et al., 2023; Zheng et al., 2018). Functional investigation of these interneuron cell types has been limited by the lack of cell-type-specific driver lines.

Using the intersectional split-GAL4 method (Luan et al., 2020, 2006), we previously generated 93 split-GAL4 driver lines that allowed for precise genetic access to 60 MB cell types, including most of the KCs, DANs, MBONs and other modulatory neurons in the MB lobe regions (Aso et al., 2014a). These lines have been instrumental in revealing the neural circuit logic by which the MB forms associative memories (Aso et al., 2019, 2014b; Awata et al., 2019; Berry et al., 2018; Dolan et al., 2018; Felsenberg et al., 2017; Handler et al., 2019; Hattori et al., 2017; Hige et al., 2015a, 2015b; Ichinose et al., 2015; König et al., 2019; Martinez-Cervantes et al., 2022; Masek et al., 2015; McCurdy et al., 2021; Pavlowsky et al., 2018; Plaçais et al., 2017; Sayin et al., 2019; Shyu et al., 2017; Tsao et al., 2018; Vogt et al., 2016; Wu et al., 2017; Yamada et al., 2023; Zhang et al., 2019).

Since the MB split-GAL4 lines were generated, new genetic and computational tools have expanded the cell types that can be targeted and facilitated the split-GAL4 design. Critically, a new collection of ZpGAL4DBD and p65ADZp hemidrivers became available (Dionne et al., 2018; Tirian and Dickson, 2017) and the expression patterns of the original GAL4 driver lines were imaged with higher-resolution confocal microscopy and Multi-Color-Flip-Out (MCFO) stochastic labeling method to reveal the morphology of individual neurons (Meissner et al., 2023; Nern et al., 2015). Additionally, advanced tools for computational neuroanatomy were developed to aid the design of split-GAL4 driver lines (Bogovic et al., 2020; Costa et al., 2016; Masse et al., 2012; Meissner et al., 2023; Otsuna et al., 2018). Leveraging these tools and resources, we have generated a collection of new split-GAL4 lines labeling MBONs, including the majority of atypical MBONs that have dendritic input both within the MB lobes and in adjacent brain regions (Rubin and Aso, 2023). In this report, we introduce a novel collection of approximately 800 split-GAL4 lines, covering sensory neurons for sugar, wind and nociception, projection neurons for olfactory, thermo/hygro-sensory and gustatory signals, ascending neurons from ventral nerve cord (VNC), cell types within the MB, and interneurons that connect with DANs and/or MBONs. While our primary objective was to generate driver lines for studying associative learning, the collection

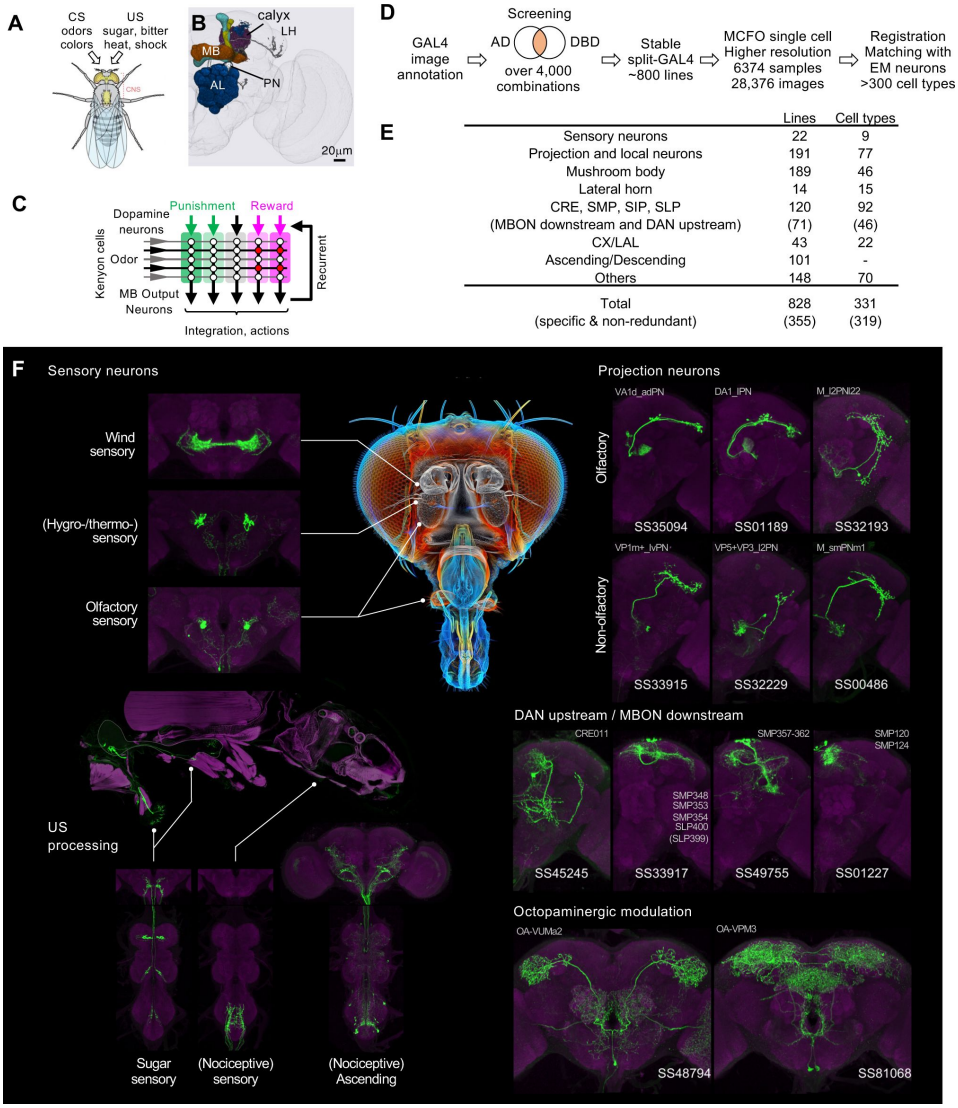

Figure 1

Generation and annotation of split-GAL4 lines

(A) In associative learning, flies adjust their behavioral responses to conditioned stimuli (CS), such as odors and colors, based on the contingency with innately rewarding or punishing unconditioned stimuli (US), such as sugar, bitter, shock and heat. A schematic of *Drosophila* melanogaster is from (Namiki et al., 2018).
(B) An image of the right half of an adult fly brain showing the mushroom bodies (MB). Projections neurons (PN) convey information from the antennal lobes (AL) to the calyx of the MB and the lateral horn (LH).
(C) A simplified diagram of the mushroom body circuit. The identity of sensory stimuli is represented by sparse activity patterns of Kenyon cells (KCs). A subset of dopaminergic neurons (DANs) respond to punishment/reward. Dopamine modulates weights of synapses between KCs and MB output neurons (MBONs) depending on the activity status of KCs. The skewed activity patterns of MBONs across compartments in response to the learned stimulus drive memory-based actions and feedback pathways to DANs.
(D) A summary of the workflow to generate split-GAL4 lines.
(E) Coverage of the collection. The crepine (CRE), the superior medial protocerebrum (SMP), the superior intermediate protocerebrum (SIP) and the superior lateral protocerebrum (SLP) are MB adjacent brain areas where MBONs and DANs most often have arborizations. CX, central complex. LAL, lateral accessory lobes.
(F) Examples of cell types covered by the collection. Expression patterns of CsChrimson-mVenus (green) are shown with neuropil counterstaining of Bruchpilot (Brp) with nc82 antibody (magenta). The whole body image came from Gr64f-Gal4 with muscle counterstaining (magenta). Putative cell types are bracketed.

also includes cell types tailored for various other functions. We provide a lookup table that maps the corresponding EM neurons in the hemibrain connectome for these drivers to facilitate connectome-guided investigation of neural circuits. This expanded collection of driver lines will be instrumental for many future studies of Drosophila associative learning and beyond.

Results and Discussions

Split-GAL4 design and anatomical screening

To gain genetic access to the cell types that convey CS and US information to the MB and those mediating memory-based actions, we designed screening to examine the expression patterns of over 4,000 intersections of split-GAL4 hemidrivers (**Figure 1D**). We selected 1,183 split-GAL4 lines representing various cell types in the central brain and the VNC for further characterization. For these lines, we employed higher resolution confocal microscopy and visualized the individual neurons that compose each split-GAL4 pattern with the MCFO method. We eventually identified 828 useful lines based on their specificity, intensity and non-redundancy. These fly lines are now publicly available through the webpage of the Janelia Flylight team project (*http://www.janelia.org/split-gal4*), where we have deposited a total of 28,376 confocal images from 6,374 tissue samples to document their expression patterns. We included lines with off-targeted expression, as they can be valuable for anatomical, developmental or functional imaging experiments, even if not suitable for behavioral experiments. Additionally, we retained drivers that intersected unintended cell types from the screening. Examples of confocal microscopy images are shown in **Figure 1F** and **Figure 1-figure supplement 1**.

We have annotated our split-GAL4 lines by matching the labeled neurons to their counterparts in the hemibrain connectome volume (Scheffer et al., 2020). We utilized confocal images registered to a standard brain, and matched neuronal cell types in each split-GAL4 line with those present in other lines and with the EM-reconstructed neurons (**Figure 2A-D**, see Materials and Methods). This light microscopy (LM) to EM matching process allows us to locate the cell type of each driver line in the connectome map, enabling users to select driver lines for further functional investigations based on their upstream and downstream synaptic partners (**Figure 2E**; **Figure 2-figure supplement 1**-**20**).

Among the 828 lines, 355 lines exhibit relatively high specificity to a non-redundant set of at least 319 cell types. **Figure 1E** provides an overview of the categories of covered cell types. Detailed information, including genotype, expression specificity, matched EM cell type(s), and recommended driver for each cell type, can be found in Supplementary File 1. A small subset of these lines have been previously used in studies (Aso et al., 2023; Dolan et al., 2019; Gao et al., 2019; Scaplen et al., 2021; Schretter et al., 2020; Takagi et al., 2017; Xie et al., 2021; Yamada et al., 2023). All transgenic lines newly generated in this study are listed in Supplementary File 2.

Drivers for the MB cell types, MBON-downstream and DAN-upstream

Prior to the completion of the EM connectome map, we conducted parallel efforts to identify cell types downstream of MBONs or upstream of DANs using confocal images of GAL4 drivers registered to a standard brain (Bogovic et al., 2020). We searched for GAL4 drivers containing cell types with potential connections to MBONs or DANs by quantifying the number of voxels overlapping with MBON axons or DAN dendrites (Otsuna et al., 2018). We then built split-GAL4 intersections from selected pairs of drivers from the established hemidriver library (Dionne et al., 2018; Tirian and Dickson, 2017).

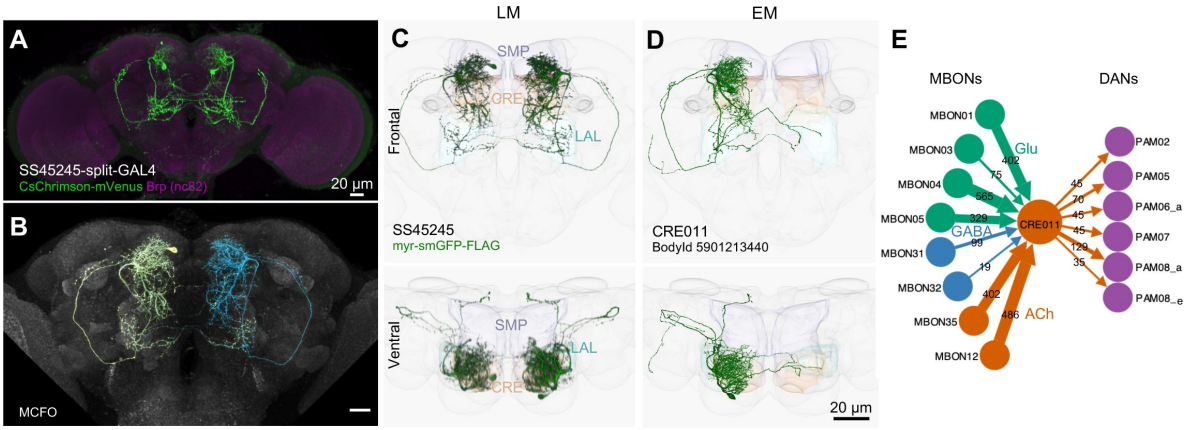

Figure 2

LM-EM match of CRE011 driver

(A) Expression pattern of SS45245-split-GAL4 in a brain.
(B) MCFO image of SS45245 showing individual labeled neurons.
(C) Frontal and ventral views of segmented light microscopy (LM) images of an exemplary split-Gal4 line (SS45245) visualized with a membrane reporter (myr-smGFP-FLAG) that was aligned to the JRC2018 standard brain. Frontal (top) and dorsal (bottom) projections are shown with outline of relevant neuropils.
(D) The skeleton reconstructed from electron microscopy (EM) data of the matched cell type CRE011 in the hemibrain connectome. The CRE011 cell on the right hemisphere is shown.
(E) Synaptic connectivity of CRE011 with MBONs and DANs in the MB derived from the hemibrain connectome.

After matching with EM-reconstructed neurons, these efforts resulted in split-GAL4 drivers encompassing 111 cell types that connect with the DANs and MBONs (**Figure 3**). Several of the cell types originally selected by LM were found to be not directly connected with MBONs or DANs. Nevertheless, these lines can be valuable for investigating other behaviors. For example, one such line, SS32237, was found to exhibit robust female-female aggression when activated (Schretter et al., 2020).

In the hemibrain EM connectome, there are about 400 interneuron cell types that have over 100 summed synaptic inputs from MBONs and/or synaptic outputs to DANs. Our newly developed collection of split-GAL4 drivers covers 30 of these major interneuron cell types (**Figure 3C**). While this constitutes a small fraction, it includes cell types with remarkable connectivity patterns. For instance, CRE011, presented as a single neuron per hemisphere, integrates over 2,000 inputs from 9 types of MBONs. This is the highest number of synaptic inputs from MBONs among all interneurons (**Figure 3C**). CRE011 provides cholinergic input to reward DANs (**Figure 2E**) and neurons in the lateral accessory lobe, a premotor center housing dendrites of multiple descending neurons (Kanzaki et al., 1994; Namiki et al., 2018). Another notable example is SMP108, which receives inputs from multiple glutamatergic MBONs and makes the highest number of cholinergic connections to DANs involved in appetitive memory (**Figure 3C**). We recently reported on SMP108's role in second-order conditioning (Yamada et al., 2023) and its upstream neurons labeled in SS33917 in transforming appetitive memory into wind-directed locomotion (Aso et al., 2023). Supplementary File 3 contains connectivity information of the MB major interneurons, along with the predicted neurotransmitters (Eckstein et al., 2023) and the available driver lines.

The current collection also contains 189 lines for cell types that have innervations within the MB (**Figure 3-figure supplement 1**). These lines offer valuable tools to study cell types that may have been overlooked previously. Notably, the SS48794 driver labels OA-VUMa2 octopaminergic neurons, which are the Drosophila counterparts to the honeybee OA-VUMmx1 neurons, the first neurons identified as mediating US signals in an insect brain (Hammer, 1993). Moreover, several drivers in this collection provide improved specificity. When combined with previous collections (Aso et al., 2014a; Rubin and Aso, 2023), we now have coverage for 7 types of Kenyon cells and 58 out of 68 cell types within the MB (excluding PNs) using split-GAL4 drivers. Overall, this amounts to about 87% coverage for non-PN cell types within the MB and about 10% coverage for MBON-downstream and DAN-upstream cell types (Supplementary File 3 and 4, **Figure 3B-C**).

Drivers for the antennal lobe projection neurons

In Drosophila, the primary CS pathway to the MB involves the antennal lobe PNs that convey olfactory signals. We have developed a set of driver lines for PNs and other cell types in the antennal lobe (Supplementary File 1). This set includes 191 lines, covering more than 48 of the approximately 190 PN types identified through EM connectome and LM studies (Bates et al., 2020; Li et al., 2020; Lin et al., 2007; Tanaka et al., 2004; Zheng et al., 2022), encompassing both uni- and multi-glomerular PNs (**Figure 4** and **5**; Supplementary File 5).

The antennal lobe, in addition to the 51 olfactory glomeruli, contains 7 glomeruli involved in processing thermo- and hygro-sensory information (Enjin et al., 2016; Frank et al., 2015; Gallio et al., 2011; Jenett et al., 2012; Liu et al., 2015; Marin et al., 2020; Stocker et al., 1990; Tanaka et al., 2012). We provide 8 lines that cover sensory neurons projecting into these non-olfactory glomeruli and 18 lines covering the projection neurons emanating from them (**Figure 6**; Supplementary File 1 and 5).

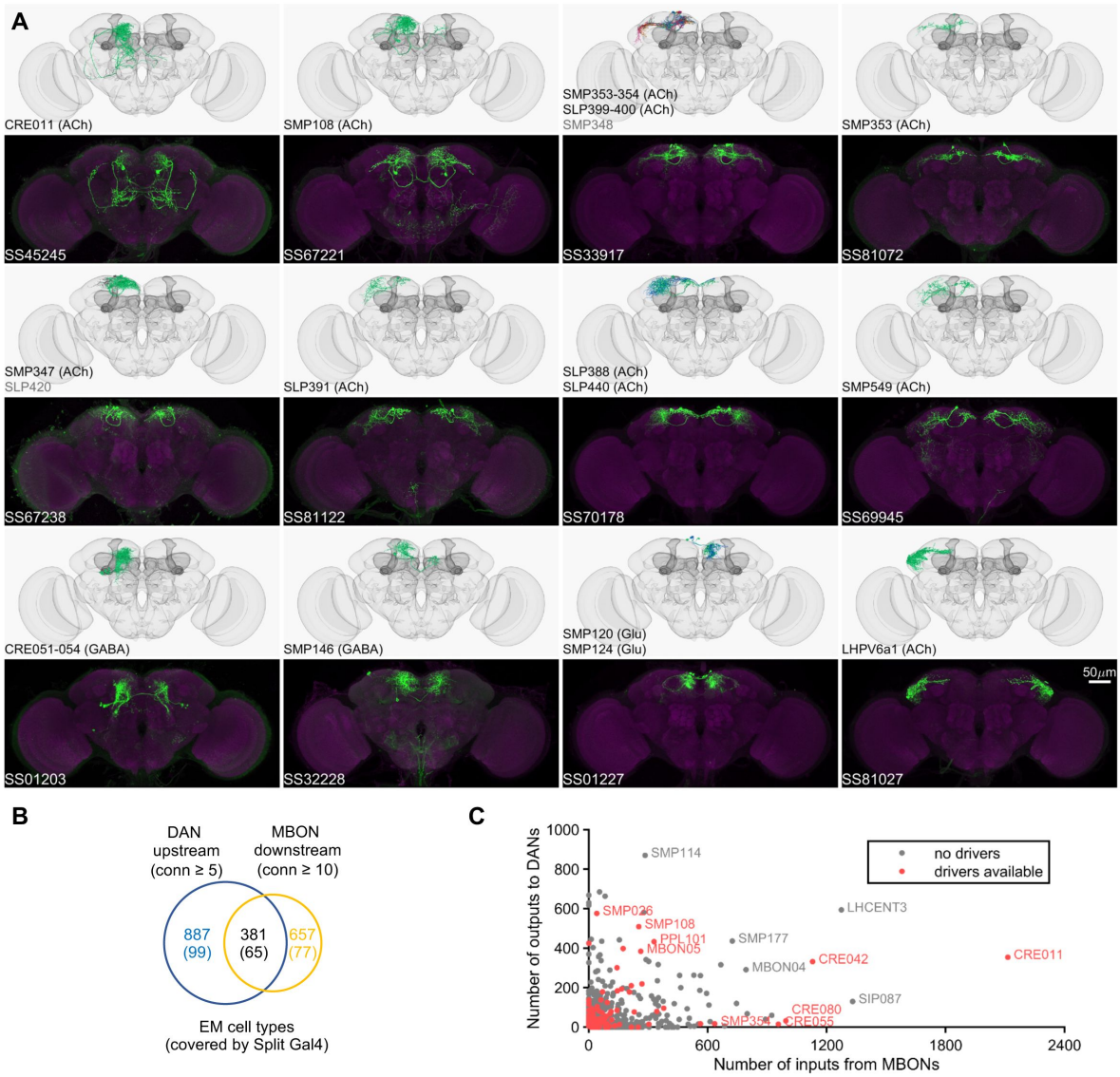

Figure 3

Drivers for MBON downstream and DAN upstream neurons.

(A) Examples of confocal microscopy images of split-GAL4 lines (bottom) and their matching cell types in the hemibrain connectome (top). CsChrimson-mVenus (green); Brp (magenta).
(B) The number of cell types that receive synaptic output from MBONs and supply synaptic input to DANs. Only cell types with connection (conn) over the indicated thresholds (i.e., more than 4 synapses for DAN upstream and more than 9 synapses for MBON downstream) were considered. The number of covered cell types are indicated in the brackets.
(C) A scatter plot of MB interneuron cell types connected with DANs and MBONs. Cell types covered by Split-GAL4 lines are highlighted in red.

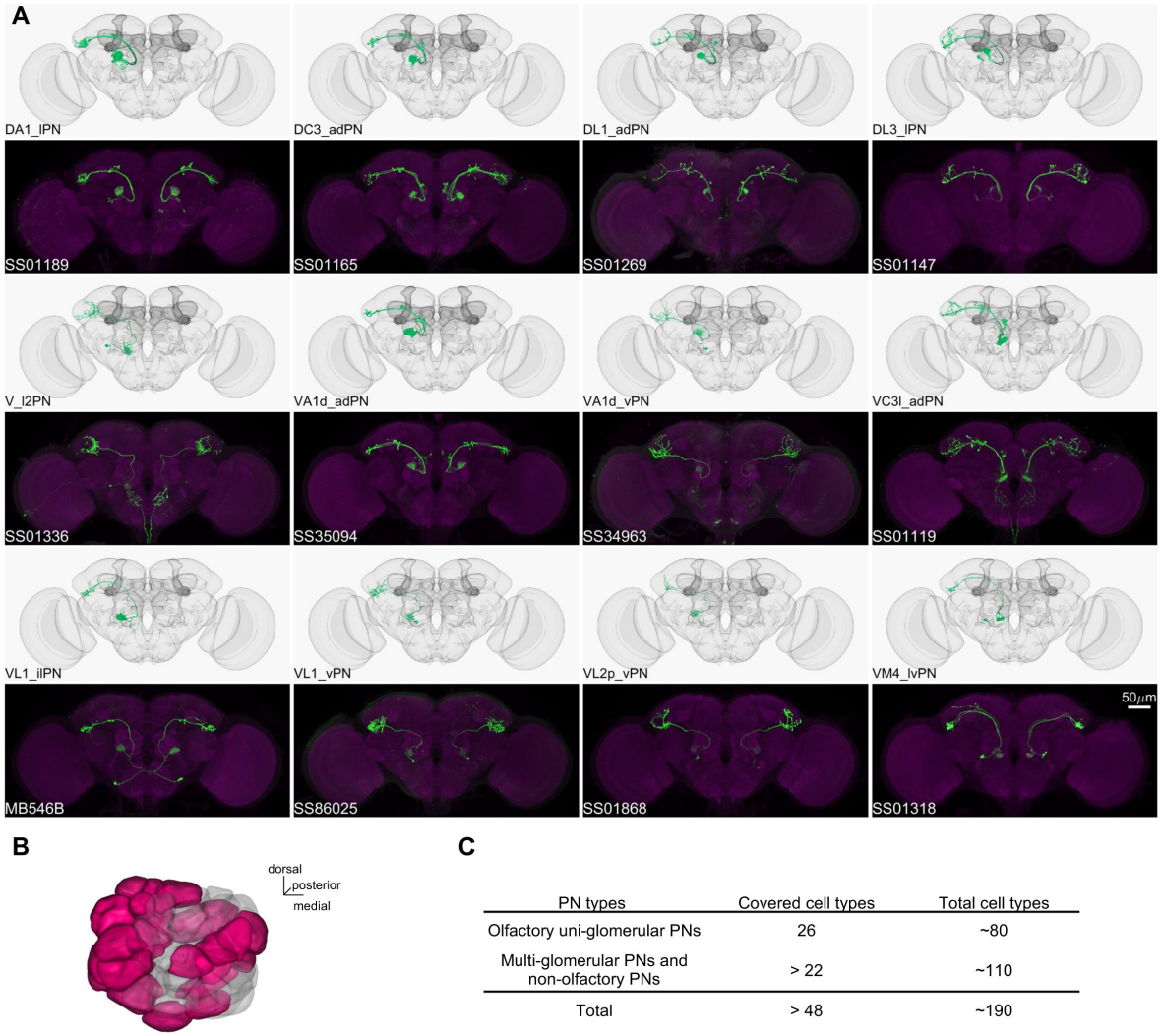

PN types	Covered cell types	Total cell types
Olfactory uni-glomerular PNs	26	~80
Multi-glomerular PNs and non-olfactory PNs	> 22	~110
Total	> 48	~190

Figure 4

Driver lines for uni-glomerular projection neurons

(A) Examples of covered uni-glomerular PN (uPN) cell types.
(B) Coverage of the 51 antennal lobe glomeruli. The new collection of split-GAL4 covers uPN in the colored glomeruli.
(C) Split-GAL4 coverage summary.

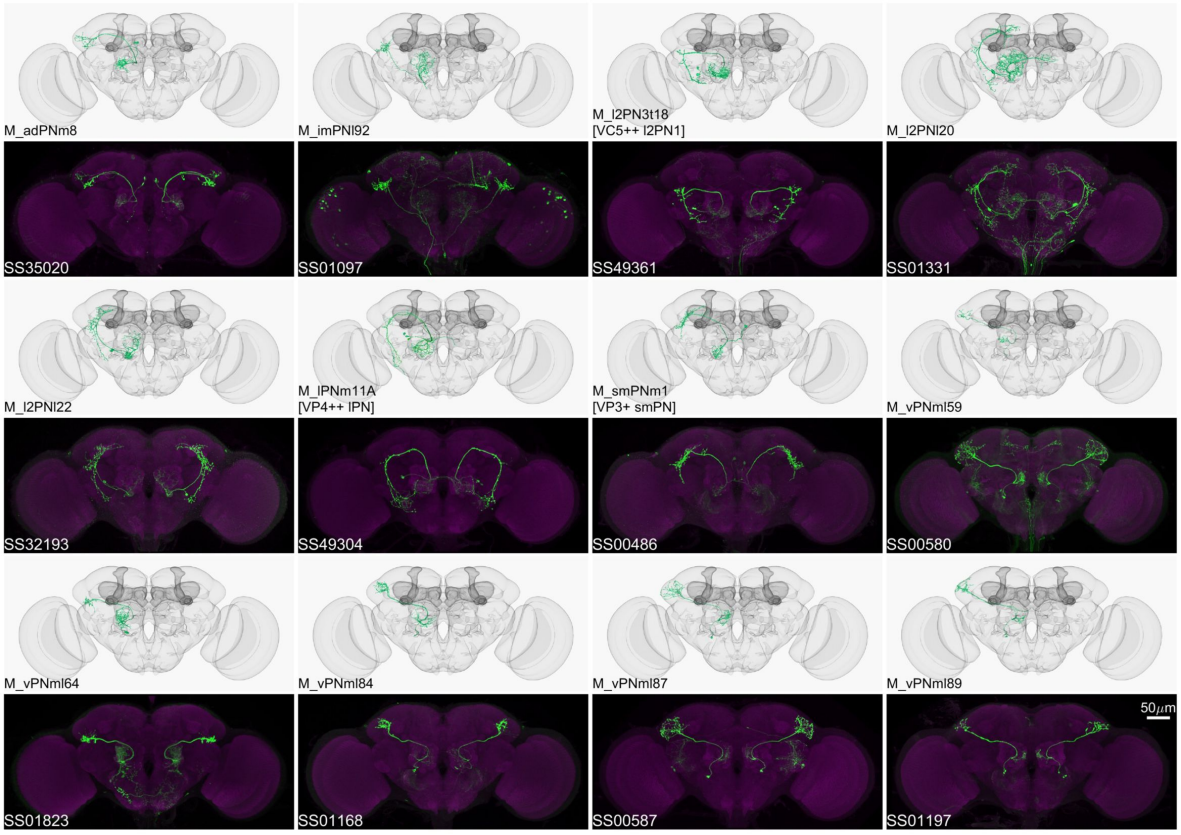

Figure 5

Driver lines for multi-glomerular projection neurons

Examples of multi-glomerular projection neurons (mPN) types. M_l2PN3t18 [VC5++ l2PN1], M_lPNm11A [VP4++ lPN], and M_smPNm1 [VP3+ smPN] are predicted to receive majority non-olfactory input (Marin et al., 2020).

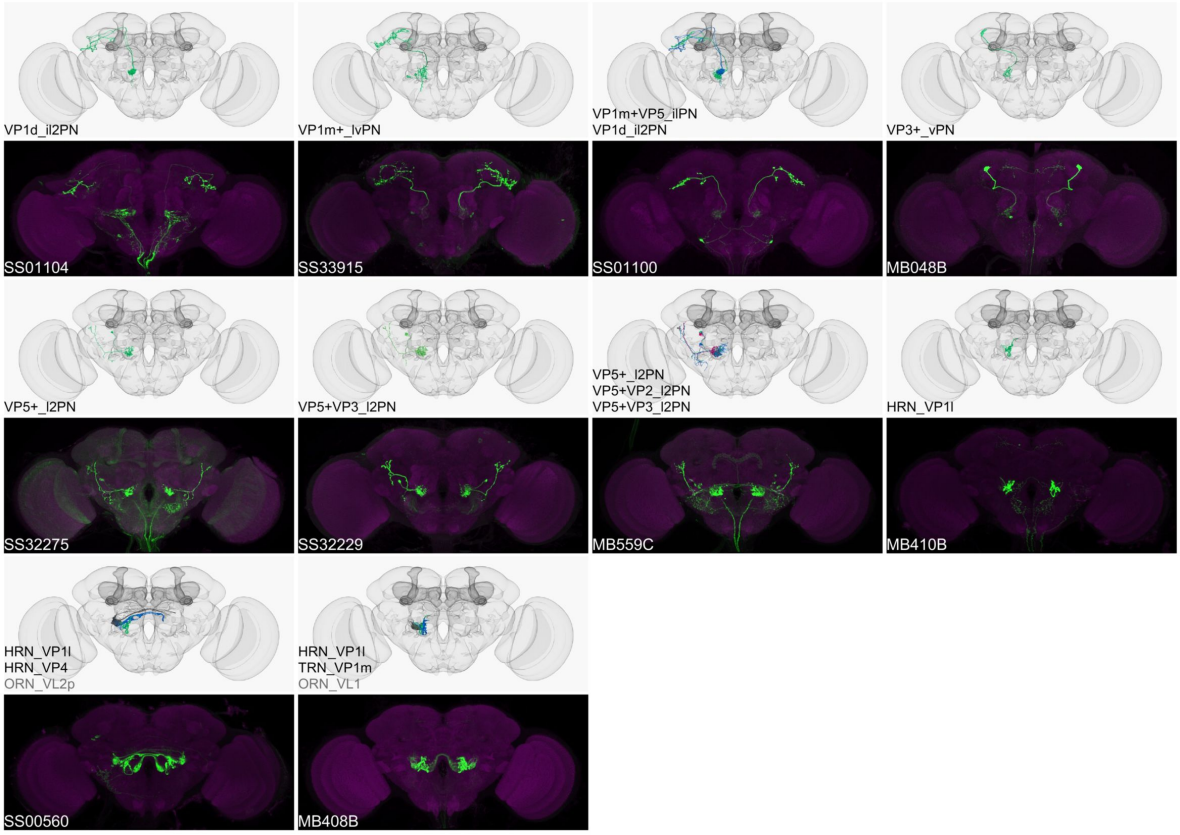

Figure 6

Driver lines for non-olfactory projection neurons and sensory neurons

Examples of thermo-/hygro-sensory PN types and sensory neurons covered by this collection

Drivers for reinforcement pathways

Our understanding of the neural pathways that encode the US has been greatly advanced by experiments that have tested the sufficiency of various neuronal cell types to substitute for the US (Aso et al., 2010; Aso and Rubin, 2016; Chiang et al., 2011; Claridge-Chang et al., 2009; Hige et al., 2015a; Huetteroth et al., 2015; Liu et al., 2012; Saumweber et al., 2018; Schroll et al., 2006; Yamagata et al., 2015). These experiments leveraged thermogenic or optogenetic tools expressed in specific neuronal cell types, especially DANs, to assess their functions in associative learning. The approach to directly stimulate DANs, although valuable, bypasses the earlier US processing pathways and potential feedback in the circuit. Because of this experimental caveat, it is preferable to activate neurons at the sensory level of reward or punishment pathways to faithfully replicate the natural activity of these DANs. In that way, DANs can be regulated by both US sensory pathways and feedback pathways from MBONs. That is likely to be essential for the successful execution of more continual learning tasks in which flies update memories based on the current and past experiences (Felsenberg et al., 2017; Jiang and Litwin-Kumar, 2021; McCurdy et al., 2021; Rajagopalan et al., 2022).

Our collection provides the starting point for generating the genetic tools needed for this approach. For example, we have generated drivers for the cell types in the thermo-sensory pathways, as well as PNs for odors with innate preference, such as CO2 and cVA (Datta et al., 2008; Lin et al., 2013; Suh et al., 2004). These cell types are candidates to convey the reinforcement signals to the MB and other brain regions for associative learning.

On the other hand, gustatory sensory neurons constitute the first layer of neurons that detect food-related sensory signals (taste), which are conveyed to the MB through largely uncharacterized pathways (Bohra et al., 2018; Burke et al., 2012; Deere et al., 2023; Kim et al., 2017; Miyazaki et al., 2015; Sterne et al., 2021). GAL4 driver lines that recapitulate expression patterns of gustatory receptors (GRs) have been generated and utilized for functional studies (Dahanukar et al., 2007; Harris et al., 2015; Miyamoto et al., 2012; Wang et al., 2004; Yavuz et al., 2014). However, these driver lines tend to contain a morphologically and functionally heterogeneous set of sensory neurons (see for examples: Chen et al., 2022; Thoma et al., 2016) and may contain off-targeted expressions. To address these limitations, we have developed split-GAL4 drivers specific to different subsets of gustatory sensory neurons by generating hemidrivers for GR-gene promoters and screening intersections with existing hemidrivers (**Figure 7A**).

We used this strategy to generate Gr64f-split-GAL4 lines and create clean drivers for reward sensory neurons. In fruit flies, sugar is detected by sensory neurons located on different taste organs of the body and also inside the brain (Fujii et al., 2015; Hiroi et al., 2002; Miyamoto et al., 2012; Rodrigues and Siddiqi, 1978). Gr64f-Gal4, in which Gal4 is expressed under the control of the promoter of the sugar receptor gene *Gr64f*, broadly labels sugar sensory neurons (Dahanukar et al., 2007 and **Figure 7 – figure supplement 1**). Gr64f-Gal4 expression can be found in heterogeneous sets of sensory neurons in the labellum, the tarsi and the labral sense organ (LSO) located along the pharynx. In addition, Gr64f-Gal4 also labels subsets of olfactory receptor neurons and neurons innervating the abdominal ganglion (Park and Kwon, 2011) (**Figure 7-figure supplement 1**), despite that whether these cells endogenously express Gr64f is yet to be confirmed. Such heterogeneity in Gr64f-Gal4 expression could limit its usage to substitute reward in complex associative learning.

To refine Gr64f-Gal4 expression, we intersected Gr64f-GAL4DBD with various AD lines selected based on the projection patterns of Gr64f-Gal4, and obtained 16 stable split-GAL4 lines that have expression in distinct subsets of Gr64f neurons (**Figure 7**). We examined the ability of these lines to serve as US in olfactory learning (Aso and Rubin, 2016) and their potency to drive local search behaviors (Corfas et al., 2019)(**Figure 8** and **Figure 8-figure supplement 1**). Additionally, we measured the walking speed of flies, as flies decrease walking while feeding (Thoma et al., 2016).

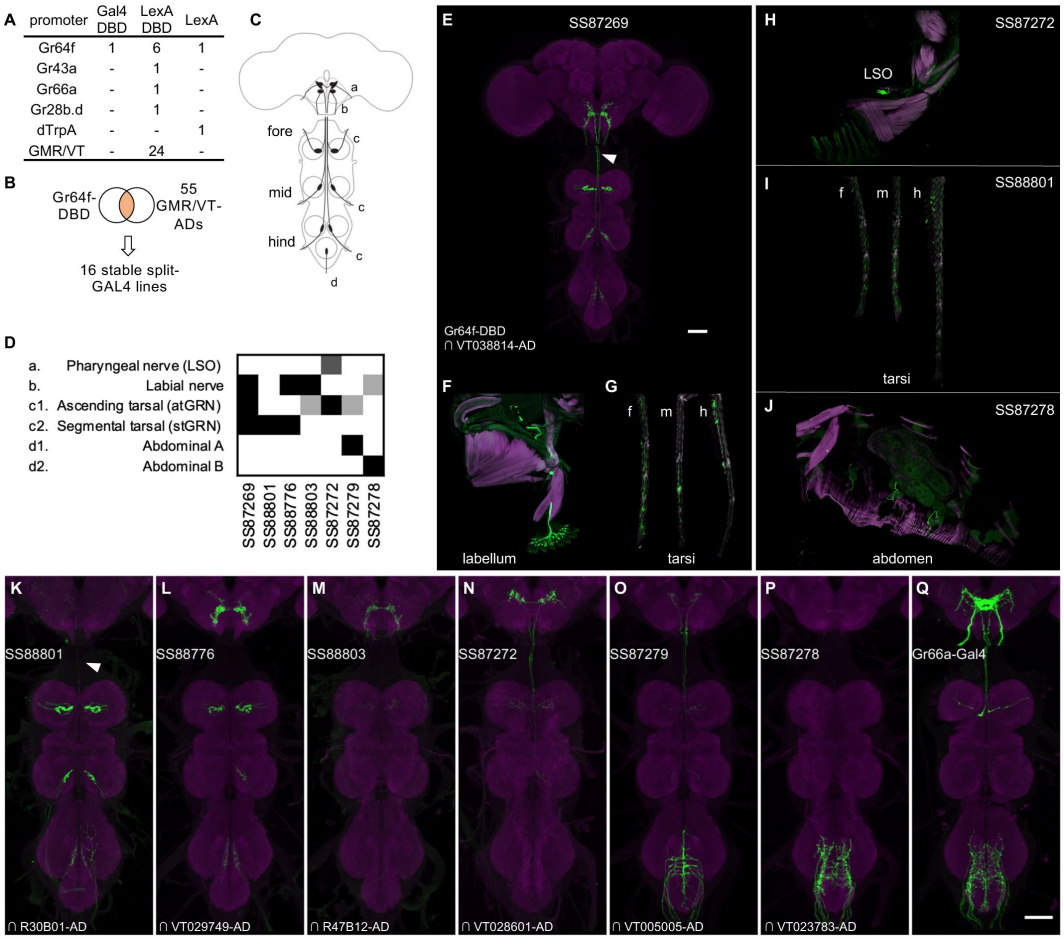

Figure 7

Driver lines for gustatory sensory neurons

(A) A summary of new transgenic lines generated by this study. In addition to Gr64f promoters, LexADBD lines were generated with Gr64f, Gr43a, Gr66a, Gr28b promoters and other GMR or VT promoters.
(B) Schematic of the screening strategy used here to subdivide the Gr64f-DBD pattern by intersecting it with GMR and VT AD lines.
(C) A schematic of the sensory neuron projection types that compose the Gr64f-DBD pattern.
(D) A summary of expression patterns of 6 of the Gr64f split-GAL4 lines derived from the screening strategy in (B), using the anatomical notation described in (C).
(E) Expression pattern of SS87269 in the brain and VNC. The arrow indicates an ascending projection of atGRN.
(F) Expression of SS87269 in the labellum.
(G) Expression of SS87269 in tarsi of fore (f), middle (m) and hind (h) legs.
(H) Expression of SS87272 in the labral sense organ (LSO).
(I) Expression of SS88801 in tarsi.
(J) Expression of SS87278 in the abdominal body wall.
(K-Q) Expression patterns of designated driver lines in the Gnathal Ganglia (GNG) and VNC. The arrow in K indicates the absence of ascending projections from stGRN.
Magenta in F-J indicates muscle counterstaining with phalloidin (actin filaments); magenta in other panels indicates neuropil counterstaining of Brp.

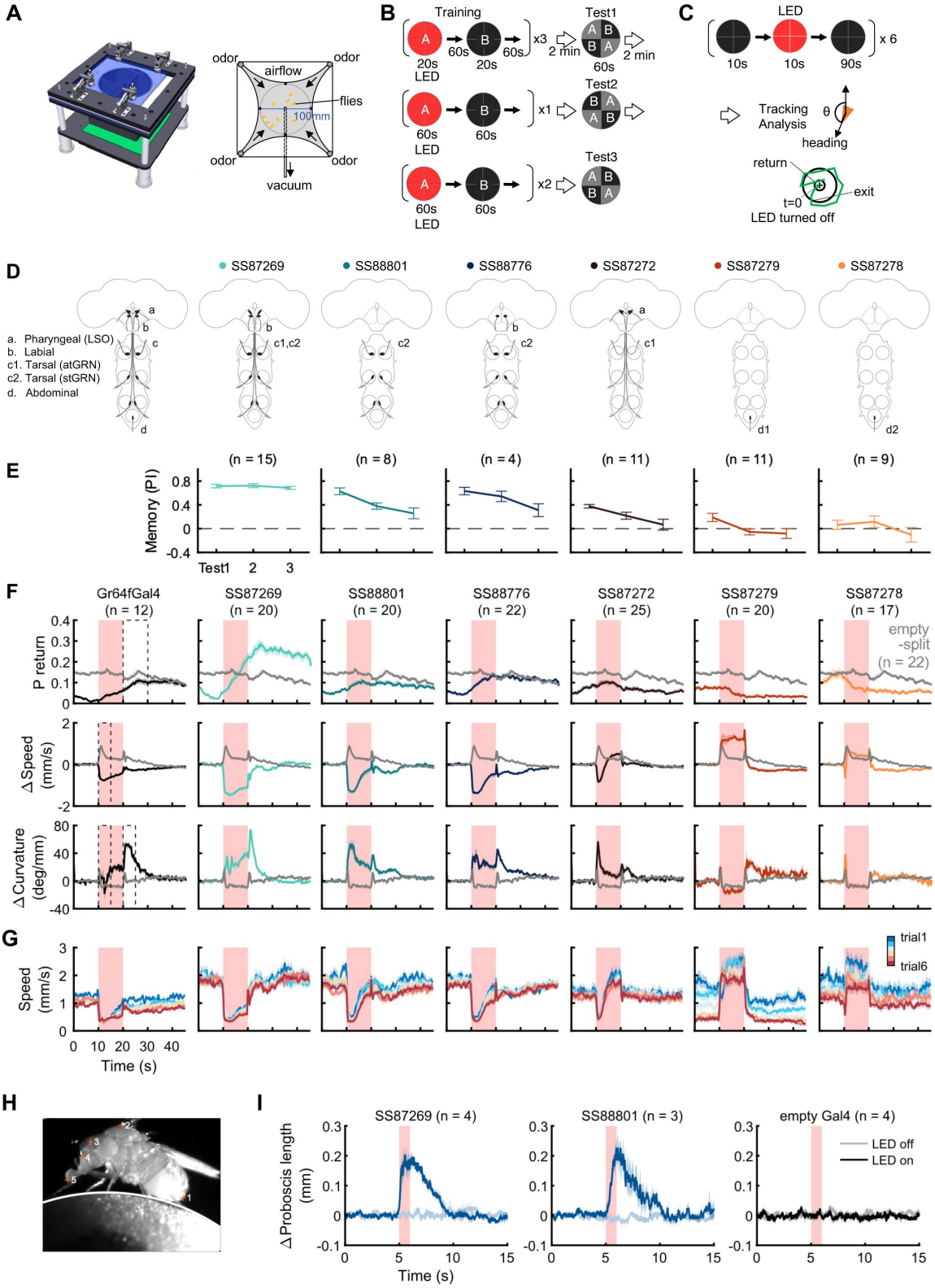
A
odor
airflow
odor
flies
100mm
odor
odor
vacuum
B
Training
A
20s
LED
60s
B
20s
60s
x3
2 min
Test1
A B
B A
2 min
60s
Test2
x1
Test3
x2
C
LED
10s
10s
90s
x 6
Tracking
Analysis
θ
heading
return
exit
t=0
LED turned off
D
SS87269
SS88801
SS88776
SS87272
SS87279
SS87278
a. Pharyngeal (LSO)
b. Labial
c1. Tarsal (atGRN)
c2. Tarsal (stGRN)
d. Abdominal
E
(n = 15)
(n = 8)
(n = 4)
(n = 11)
(n = 11)
(n = 9)
Memory (PI)
Test1 2 3
F
Gr64fGal4
(n = 12)
SS87269
(n = 20)
SS88801
(n = 20)
SS88776
(n = 22)
SS87272
(n = 25)
SS87279
(n = 20)
SS87278
(n = 17)
empty
-split
(n = 22)
P return
ΔSpeed (mm/s)
ΔCurvature (deg/mm)
G
trial1
trial6
Speed (mm/s)
Time (s)
H
I
SS87269 (n = 4)
SS88801 (n = 3)
empty Gal4 (n = 4)
LED off
LED on
ΔProboscis length (mm)
Time (s)

Figure 8

Behaviors with Gr64f-split-GAL4 lines

(A) In the optogenetic olfactory arena, odors are delivered from the periphery and sucked out from the central vacuum port to deliver odors only to defined quadrants. Red LEDs (627nm peak) enable programmed optogenetic activation of neurons expressing CsChrimson.

(B) Training and testing protocol for experiments shown in (E). The training protocol consisted of 3 x 20s optogenetic activation training followed by the first preference test, 1x 1 min training followed by the 2nd test, and additional 2x 1 min training followed by the last test. Odors delivered to the two zones and odor durations in each period are indicated. LED intensities were 4.3 μW/mm2 in early 20s training and 34.9 μW/mm2 in later training. Activation LED was applied with 1s ON and 1s OFF during pairing with odor A. Odors were trained reciprocally. Pentyl acetate and Ethyl lactate were used as odor A and B, respectively, in half of the experiments. The two odors were swapped in the other half of experiments.

(C) Protocol to characterize Gr64f split-GAL4 activation phenotypes in the absence of an odor. During each trial, flies were illuminated with a red LED light continuously for 10 seconds.

(D) Summary diagram of the expression patterns of the original Gr64f-GAL4 (far left) and 6 Gr64f-split-GAL4s. The expression of the original Gr64f-GAL4 in olfactory sensory neurons is not depicted here.

(E) Associative memory scores after the training protocol in (B). Mean, standard error of the mean (SEM), and the number of groups are shown.

(F) The kinematic parameters of trajectories measured with Caltech FlyTracker during split-GAL4 activation in the absence of odor as shown in (C). Each group of flies received 6 activation trials. Summarization was based on the trial average of each group. The number of groups is indicated. The thick lines and shadows are mean and SEM. Gray lines are Empty-split-GAL4 control. Dashed lines are time bins for data summary in **Figure 8-figure supplement 1**.

(G) Average walking speed in each of 6 trials.

(H) An image of a tethered fly on a floating ball. Flies were tracked for proboscis extension (PE) activity with the Animal Part Tracker (Kabra et al., 2022). The annotated points, in the order of numbers, consisted of the tip of the abdomen (1), the highest point on the thorax (2), the midpoint between the root of the antennae (3), the base of the proboscis (4) and the tip of the proboscis (5). PE activity was quantified as the change of proboscis length, i.e., the distance from the tip to the base of the proboscis, or the distance between points 4 and 5.

(I) SS87269 and SS88801 activation and proboscis extension. Each fly was recorded over 6 activation trials in which the 624 nm LED was turned on for 1 second. LED intensity for SS87269 and SS88801, 11 μW/mm2; for empty Gal4 (pBDPGal4), 50 μW/mm2. Less saturated traces indicate behavior during LED off trials, while more saturated traces indicate behavior during LED on trials.

Among the Gr64f-split-GAL4 lines, SS87269 emerged as the best driver for substituting sugar reward in olfactory learning given its specificity and the utility in long training protocols (**Figure 8E**). SS87269 expresses in the labellum and at least two types of tarsal sensory neurons, namely the ascending (atGRN) and the non-ascending segment-specific (stGRN) types (**Figure 7E-F**). The driver does not label pharyngeal sensory neurons, and importantly, it lacks expression in abdominal ganglion and olfactory sensory neurons that could be off-targeted neurons found in the original Gr64f-GAL4. When odor presentation was paired with the activation of SS87269 neurons, flies formed robust appetitive memories even after extended training with high LED intensity (**Figure 8E**, **Figure 8-figure supplement 1** and Video 1). Furthermore, and consistent with the

idea that this subset of sensory neurons encodes appetitive food-related taste information, flies with SS87269 activation showed proboscis extension and reduced locomotion (**Figure 8F-I**; **Figure 8-figure supplement 2**, Video 2 and 4). These flies also showed robust local search behavior during the post-activation period, i.e., an increased probability of revisiting the area where they experienced the activation (Video 3). Notably, the revisiting phenotype of SS87269 was stronger than the original Gr64f-GAL4 and any other Gr64f-split-GAL4 drivers (**Figure 8F** and **Figure 8-figure supplement 2A**).

Two other lines SS88801 and SS88776, which label stGRNs or stGRNs along with labial sensory neurons, respectively (**Figure 7K-L,I**), showed appetitive learning and reduced locomotion during activation (**Figure 8E-F**). Interestingly, however, the activation of stGRNs with SS88801 did not induce significant local search behaviors (**Figure 8F** and **Figure 8-figure supplement 2A**). This finding could be valuable for understanding circuits underlying local search behavior and invites further investigation to compare pathways from labial and tarsal sensory neurons to the MB and the central complex.

In contrast to SS87269, two other resulting lines, SS87278 and SS87279, express in cells that appear to convey aversive signals. Activation of these lines induced an increase in walking speed during activation and reduced the probability of return at the offset of LED activation (**Figure 8F** and **Figure 8-figure supplement 2**). Also, flies became progressively less mobile during the inter-trial interval period (**Figure 8G**). The reduced locomotion in the interval period was also observed with the original Gr64f-GAL4 (**Figure 8G**) and a bitter-taste driver, Gr66a-GAL4 (data not shown). With extended training using SS87278 and SS87279, the preference to the paired odor eventually became negative (**Figure 8E**). These drivers label distinct subsets of sensory neurons projecting to the abdominal ganglion (**Figure 7O,P**). The innervation of SS87278 inside the abdominal ganglion is similar to that of Gr66a-GAL4 (**Figure 7P**) (Dunipace et al., 2001), which is known to label multidendritic sensory neurons in the adult Drosophila abdomen (Shimono et al., 2009). Examining projection patterns in fly bodies with whole-animal agar sections, we found that sensory neurons in SS87278 also project to the abdominal body surface (**Figure 7J**), likely representing the class IV multidendritic neurons that detect multimodal nociceptive stimuli (Hwang et al., 2007; Ohyama et al., 2015). GAL4 expression in these aversive sensory neurons may thereby explain the compromised learning performance with the original Gr64f-GAL4.

Overall, the refinement of Gr64f-Gal4 expression with SS87269 now allows for specific manipulation of the rewarding subset of gustatory sensory neurons and thereby permits training with an extended number of trials. While we have not yet conducted anatomical screening, LexADBD lines generated with Gr64f, Gr43a, Gr66a, Gr28b.d promoters (**Figure 7A**) should enable similar refinement of these sensory neuron lines. We also made a small number of lines for cell types in the subesophageal zone (SEZ) area (**Figure 8-figure supplement 3**), which complement previous collections of drivers for gustatory interneurons (Otto et al., 2020; Sterne et al., 2021).

Lastly, we generated driver lines for putative ascending nociceptive pathways. We determined the activation preference for 581 combinations of ZpGAL4DBD and p65ADZp hemidrivers in the circular arena (**Figure 9A**, Supplementary File 1). We found one driver, SS01159, which showed the most robust avoidance of LED quadrants and demonstrated behavioral components that are characteristic to nociception, including backward walking, turning, increased speed, and jumping upon activation (**Figure 9B-D**, and Video 5). This driver labels a group of ascending neurons (**Figure 9E**), which likely carry nociceptive signals from the body and legs to the brain. We then generated drivers for subsets of these ascending neurons guided by single neuron morphologies of cells in SS01159 determined by MCFO stochastic labeling (Nern et al., 2015). Other than SS01159, the collection in total contains approximately 100 split-GAL4 lines covering ascending neurons.

While not completely matched to EM cell types due to only a portion of their morphologies being available in the hemibrain volume, these lines serve as a valuable resource for querying the reinforcement pathways.

Morphological individuality and asymmetry

Despite the recent progress in the EM connectome field, EM-based methods remain prohibitively expensive and morphological variability of neurons has been compared only across two individuals and three hemispheres (Schlegel et al., 2023). As a part of Janelia Flylight team project to generate cell-type-specific driver lines, we have imaged over 6,000 fly brains for the present study. While annotating those confocal images of split-GAL4 lines, we occasionally encountered samples with atypical morphologies (**Figure 10**). For example, one V_l2PN neuron, which typically projects to the lateral horn of the ipsilateral hemisphere, exhibited a peculiar morphology in one brain sample, where its axon crossed the midline and projected to the contralateral hemisphere, yet it still reached the correct target area within the lateral horn of the opposite side (**Figure 10A**). Another instance involved a DPM neuron, the sole serotonergic neuron of the MB lobes. While typical brain samples contain only one DPM neuron per hemisphere, we found a brain with two DPM neurons in one hemisphere (**Figure 10B**). In this case, the DPM projections exhibited an atypical innervation of the calyx of the mushroom body. We also found examples involving MBONs. The dendrites of MBON- α1 are typically confined inside the α lobe of the MB, but we discovered a case of MBON-α1 in addition projecting to the ellipsoid body (**Figure 10C**). MBON-α3 displayed striking variability in soma positions, but only subtle variability in axonal projections (**Figure 10D**). The table in **Figure 10E** summarizes additional examples of the atypical morphologies of MBONs. Overall in 1241 brain hemispheres examined, we found mislocalization of dendrites and axons in 3.14% and 0.97% of MB cell types, respectively. If this rate of mislocalization is generalizable to other brain regions, a fly brain of ~130,000 neurons (Dorkenwald et al., 2023) would have a few thousands of neurons with mislocalized dendrites or axons. These examples of atypical morphology were observed only once in dozens of samples, and thus can be considered as erroneous projections either resulting from stochastic developmental processes, or possibly caused by ectopic expression of reporter proteins on the plasma membrane at a high level.

In contrast to these rare, and seemingly erroneous, morphological variations, we observed much more frequent and reproducible variations in the composition as well as morphologies in the two MBONs labeled by MB083C, which may amount to “individuality”. This split-GAL4 driver line invariably labels two cells in each hemisphere in 169 brain samples examined with four different reporters and in both sexes (57 males and 112 females; **Figure 11-figure supplement 1**). In all samples, these MBONs arborized dendrites in the γ3 and β′1 compartments. An obvious mistargeting of the axon was observed in only one sample, suggesting highly consistent development of these MBONs (**Figure 11A-B**). However, MCFO method visualized two distinct morphologies of these MBONs: MBON08 arborizes dendrites in the γ3 compartment of both hemispheres, whereas MBON09 arborize dendrites in ipsilateral γ3 and contralateral β′1 (**Figure 11C-H**)(Aso et al., 2014a). β′1 compartment was always labeled in both hemispheres for all 169 samples, suggesting that MBON09 represents at least one of the two cells in each hemisphere. The second cell can be either MBON08 or MBON09. In MCFO experiments, we observed 21 instances of MBON08 (8 in the left and 13 in the right hemisphere) and 188 instances of MBON09 (**Figure 11I**). Based on the likelihood, we expect 65% of flies contain four MBON09, while the remaining 35% of flies likely have at least one MBON08. In 71 hemispheres, two cells were visualized in different colors of MCFO: 52 contained two MBON09 and 19 contained one MBON08 and MBON09. We never observed a brain with MBON08 on both hemispheres or two MBON08 in one hemisphere (**Figure 11J**). When MBON08 and MBON09 coexist, MBON09 arborized in the lateral part of the ipsilateral γ3 and MBON08 arborize in the medial part of the contralateral γ3 (**Figure 11E-H**). This seemingly extended γ3 compartment innervated by MBON08 is not part of γ4, because it did not overlap with DANs in the γ4 (**Figure 11-figure supplement 2A-B**).

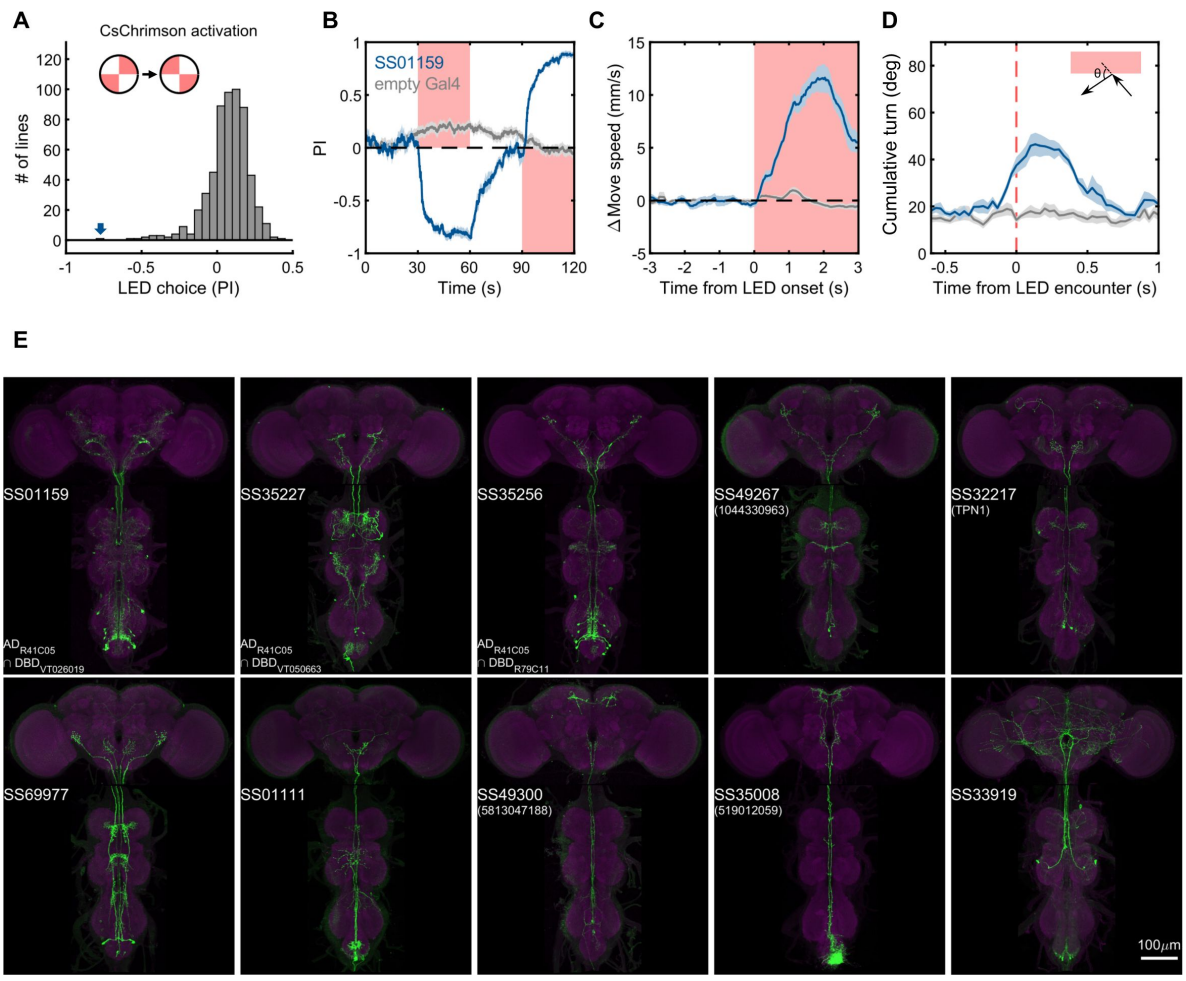

Figure 9

Examples of covered ascending neurons

(A) Activation preference screen of 581 split-GAL4 lines (342 lines from this study). SS01159 (blue arrow) is one of the lines that flies showed strong avoidance at optogenetic activation.
(B) Time course of flies' preference to quadrants with red LED light by SS01159>CsChrimson (blue) or empty-GAL4>CsChrimson (gray). A preference score to red LED quadrants was quantified from the distribution during the last 5s of two 30s activation periods. n = 8 groups for SS01159, n = 15 for empty Gal4. Mean (thick lines) and SEM (shadow) are plotted.
(C) The mean normalized movement speed at the LED onset for flies in the LED quadrants. The 3-s period before LED onset was used as the baseline for normalization.
(D) The mean cumulative turning angles in 5 movie frames (total elapsed time of 167 ms) when flies encountered the LED boundary. The boundary was defined as a 4-mm zone in between the LED and dark quadrants. Trajectories too close to the center (< 0.2*radius) or the wall (> 0.6*radius) of the arena were not analyzed.
(E) Examples of split-GAL4 lines for ascending neurons. SS35227 and SS35256 shared a split half (R41C05-AD) with SS01159. SS32217 matched with TPN1 (Kim et al., 2017). No cell types were assigned to the other lines shown due to missing information in the hemibrain volume.

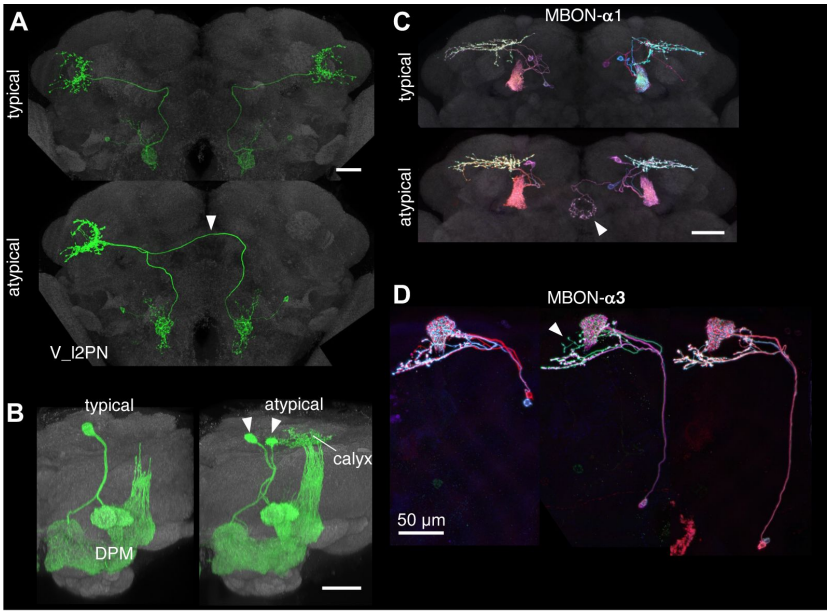

E

Cell Type	MB compartments	N hemisphere examined	Typical number of cells	Different number of cells (%)	Mislocalization (%) Dendrite	Mislocalization (%) Axon	mode of errors
MBON01	Y5, β'2a	16	1	0.0	0.0	12.5	mislocalization of axons
MBON02	β2, β'2a	96	1	1.0	1.0	1.0	mislocalization of axons
MBON03	β'2mp	56	1	0.0	0.0	0.0	
MBON05	Y4	50	1	0.0	0.0	0.0	
MBON06	β1	38	1	0.0	0.0	0.0	
MBON07	α1	105	2	0.0	22.9	1.9	dendrites outside the MB axon in the ellipsoid body third soma without neurites
MBON08/09	Y3, β'1	338	2	0*	*	0.6	see Figure 11
MBON11	Y1, pedc	136	1	0.7	0.7	1.5	dendrites in Y2 axon in the calyx lack of axon in α3
MBON12	Y2, α'1	106	2	0.0	0.0	0.0	
MBON13	α'2	82	1	0.0	1.2	0.0	dendrites outside the MB
MBON14	α3	44	1	0.0	0.0	2.3	additional axon branch
MBON18	α2sc	36	1	0.0	0.0	0.0	
MBON19	α2p3p	34	2	0.0	0.0	0.0	
MBON22	calyx	56	1	1.8	17.9	0.0	dendriets outside the calyx
MB-DPM	all	48	1	8.3	4.2	4.2	Second DPM axons/dendrites in the calyx

Figure 10

Stereotypy and erroneous projections

(A) V_l2PN from both hemispheres send axonal projections to the right hemisphere in an atypical case (arrowhead).
(B) In this atypical case, there are two MB-DPM neurons in one hemisphere (arrowhead) and the arborizations extend beyond the pedunculus into the calyx.
(C) MBON-α1 occasionally has additional arborizations in the ellipsoid body (arrowhead)
(D) The localization of MBON-α3 soma widely varied along the dorso-ventral axis. It occasionally had an additional axonal branch (arrowhead).
(E) A table to summarize normal and erroneous projections of MBONs and MB-DPM. In all the cases except for the DPM, “different number of cells” was likely due to stochastic expression of the drivers (i.e., lack of labeling) rather than biological difference. We defined “mislocalization” when axons or dendrites projected to outside of the normally targeted brain regions. For instance, dendrites of typical MBON07 are usually confined inside the α1, but were extended to outside the MB lobes in 22.9% of samples. Variable branching patterns inside the normally targeted brain regions were not counted as mislocalization here. In some MB310C-split-GAL4 samples, we observed a third soma attached to MBON-α1 but they lacked any neurites. We did not observe obvious mislocalization of dendrites or axons for MBON03, 5, 6, 12, 18 and 19. See **Figure 11** for variability of MBON08/09 in MB083C.

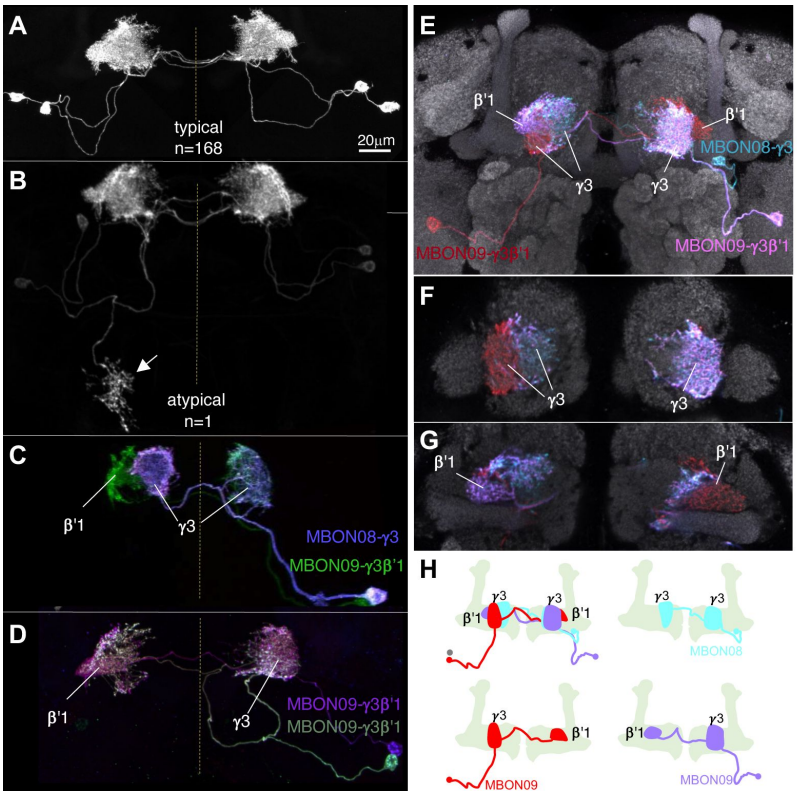

I

	Female	Male	Total
MBON08	7	14	21
MBON09	102	86	188
% MBON08	6.4	14.0	10.0
P only MBON09	0.77	0.55	0.65
P at least One MBON08	0.23	0.45	0.35

J

Left 2 cells	Right 2 cells	Left γ3	Left β'1	Right γ3	Right β'1	
08/08	08/08	+		+		
08/08	08/09	+	+	+		P=2% (No occurrence in 169 flies)
08/08	09/09	+	+	+		
08/09	08/08	+		+	+	
09/09	08/08	+		+	+	
08/09	08/09	+	+	+	+	P=3% (No occurrence in MCFO)
08/09	09/09	+	+	+	+	P=29%
09/09	08/09	+	+	+	+	
09/09	09/09	+	+	+	+	P=~65% of flies
MBON type		MB compartments				

Figure 11

Individuality and asymmetry of MBON08 and MBON09

(A) A typical image of two MBONs in MB083C-split-GAL4 driver.
(B) Abnormal axonal projection of MBON08/09 observed in one of 169 samples.
(C-D) MCFO images of MB083C driver from different flies show that the two cells can either be both MBON09-γ3β′1 (C) or one MBON09-γ3β′1 and one MBON08-γ3 (D).
(E-G) An example of MCFO image of MB083C, which visualized one MBON08 and two MBON09 in the same brain. The projection (E) and image sections at the γ3 (F) or β′1 (G) are shown.
(H) Diagrams of the three MBONs shown in E-G.
(I) A summary table for observation of MBON08 and MBON09 in male and female brains.
(J) All possible variations of 4 MBONs in MB083C driver, and estimated probability for each case. Panel (A) and (C) were adapted from **Figure 8** of (Aso et al., 2014a).

Although MBON08 was not found in brain samples used for the hemibrain or FAFB EM connectome (Dorkenwald et al., 2023; Scheffer et al., 2020; Zheng et al., 2018), DANs in the γ3 could be subdivided to two groups that innervate the medial or lateral part of the γ3 (**Figure 11-figure supplement 2C**) (Li et al., 2020). Therefore, subdivision of the γ3 compartment may exist irrespective of heterogeneity on the MBON side. In larval brains, two MBONs that correspond to adult MBON08/09 exhibit identical morphology (Eichler et al., 2017; Saumweber et al., 2018; Truman et al., 2023). Therefore, one of these MBONs acquires distinct morphology as MBON08 during metamorphosis at 21/209 odds, resulting in an asymmetric output pathway of the MB; We have never observed a brain with MBON08 on both hemispheres, and therefore MBON08 likely to appear in only one hemisphere, if at all (**Figure 11J**). This asymmetry could be one source of turning handedness and idiosyncratic learning performance (de Bivort et al., 2022; Smith et al., 2022), given that MBON09 forms extensive connection with other MBONs and fan-shaped body neurons (Li et al., 2020) and the activity of MBON08/MBON09 has strong influence on turning (Aso et al., 2023, 2014b; Matheson et al., 2022).

Conversion to split-LexA

Split-GAL4 lines can be converted into split-LexA lines by replacing the GAL4 DNA binding domain with that of LexA (Ting et al., 2011). To broaden the utility of our collection, we have generated over 20 LexADBD lines to test the conversions of split-GAL4 to split-LexA. The majority (22 out of 34) of the resulting split-LexA lines exhibited very similar expression patterns to their corresponding original split-GAL4 lines (**Figure 12**). For the failed cases, the expression level was either undetectable or too weak.

Concluding Remarks

The ability to define and manipulate a small group of neurons is crucial for studying neural circuits. Here, we have generated and characterized driver lines targeting specific cell types that are likely to be a part of associative learning circuits centered on the MB. We have provided these driver lines with a comprehensive lookup table linking these cell types with the EM hemibrain connectome. These lines, together with preceding collections of drivers (Aso et al., 2014a; Aso and Rubin, 2016; Davis et al., 2020; Dolan et al., 2018; Rubin and Aso, 2023; Shuai et al., 2015; see for examples: Sterne et al., 2021; Strother et al., 2017; Truman et al., 2023; Tuthill et al., 2013; Wang et al., 2021; Wolff and Rubin, 2018; Wu et al., 2016), collectively constitute a powerful resource for precise functional interrogation of associative learning in adult Drosophila melanogaster, and will be a foundation to reveal conserved principles of neural circuits for associative learning.

Materials and Methods

Fly strains

Drosophila melanogaster strains were reared at 22°C and 60% humidity on standard cornmeal food in 12:12 hour light:dark cycle. The genotypes of all split-GAL4 and split-LexA driver lines released here are listed in the Supplementary File 1. The new collection of split-GAL4 drivers reported here was designed based on confocal image databases (*http://flweb.janelia.org*) (Jenett et al., 2012; Tirian and Dickson, 2017), and screening expression patterns of p65ADZp and ZpGAL4DBD combinations was performed as described previously (Aso et al., 2014a; Pfeiffer et al., 2010).

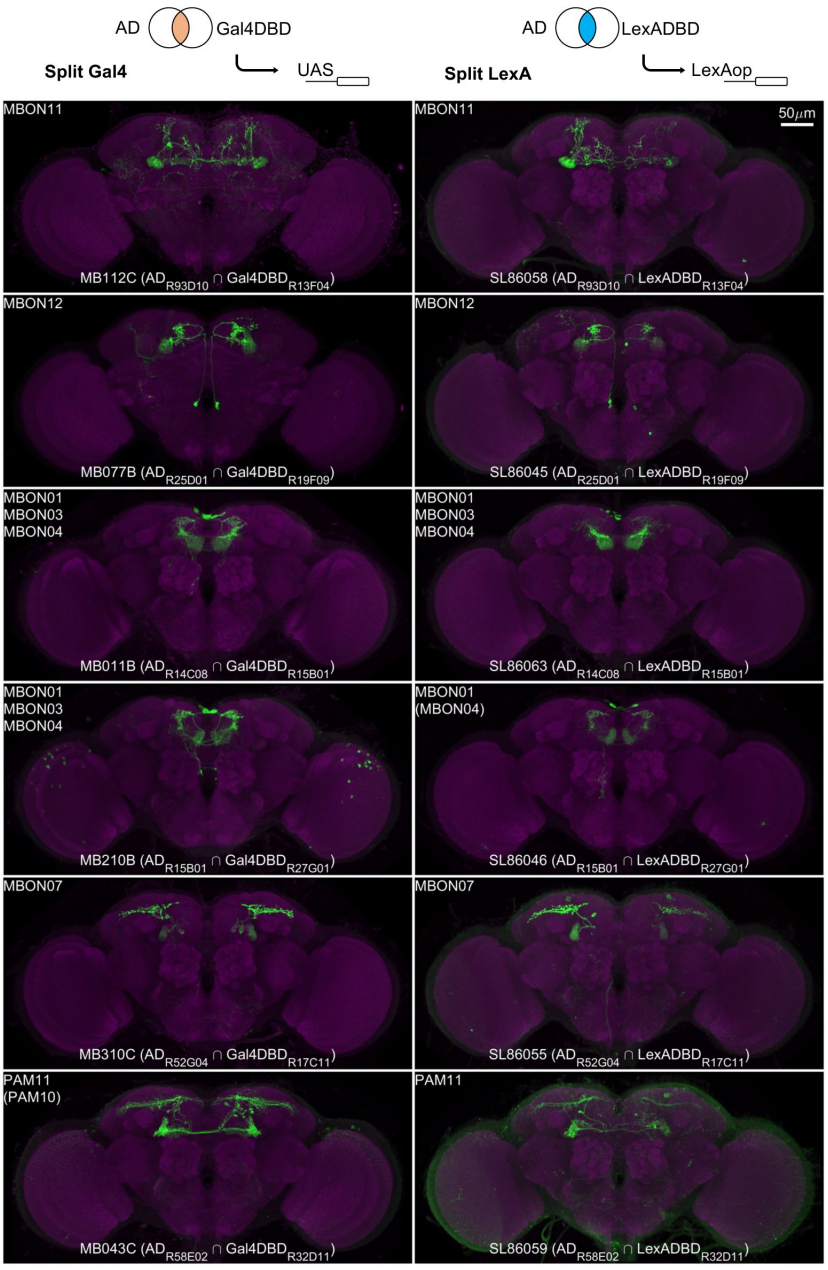

Figure 12

Examples of split-LexA conversion

Split-LexA shares the same enhancers with split-GAL4 but with the Gal4DBD replaced by LexADBD. Among 34 conversions tested, 22 were successful, with the split-LexA showing identical or similar expression patterns as the split-GAL4. The remaining 12 had weak/no expression or showed unintended intersectional patterns. See Supplementary File 2 for the hemidriver lines with p10 translational enhancers to enhance expression level.

Immunohistochemistry

Brains and ventral nerve cords of 3-10 days old flies were dissected, fixed and immunolabeled and imaged with confocal microscopes (Zeiss LSM710, LSM780 or LSM880) as previously described (Aso et al., 2014a; Jenett et al., 2012; Meissner et al., 2023; Nern et al., 2015). The detailed protocols and videos are available at *https://www.janelia.org/project-team/flylight/protocols*.

Whole-body sections

For sample preparation, flies were anesthetized on ice and briefly washed with 70% ethanol. Small incisions were made in the flanks of the thorax and abdomen under 2% paraformaldehyde in PBS with 0.1% Triton X-100 (PBS-T), and the flies were fixed in this solution overnight at 4°C. After washing in PBS containing 1% Triton X-100, the samples were embedded in 7% agarose and sectioned on Leica Vibratome (VT1000s) sagittally in slices of 0.3 mm. The slices were incubated in PBS with 1% Triton X-100, 0.5% DMSO, 3% normal goat serum, Texas Red-X Phalloidin (1:50, Life Technologies #T7471) and anti-GFP rabbit polyclonal antibodies (1:1000, Thermo Fisher, #A10262) at room temperature with agitation for 24 hours. After a series of three washes in PBS-T, the sections were incubated for another 24 hours in the solution containing secondary antibodies (1:1000, goat anti-rabbit, Thermo Fisher #A32731). The samples were then washed in PBS-T and mounted in Tris-HCL (pH 8.0)-buffered 80% glycerol + 0.5% DMSO. For imaging and rendering, serial optical sections were obtained at 2 µm intervals on a Zeiss 880 confocal microscope with a pan-apochromat 10x/0.45 NA objective using 488 and 594 nm lasers. Images were processed in Fiji (*http://fiji.sc/*) and Photoshop (Adobe Systems Inc.).

Behavioral assays

For flies expressing CsChrimson (Klapoetke et al., 2014), the food was supplemented with retinal (0.2 mM all-trans-retinal prior to eclosion and then 0.4 mM). Two- to six-day old adult females were collected and sorted on a Peltier cold plate 2-4 days before testing in behavioral assays. Flies were starved for 40–48 hr on 1% agar before they were subjected to behavioral experiments. Olfactory conditioning and optogenetic activation experiments were performed as previously described using the modified four-field olfactory arena equipped with the 627 nm LED board and odor mixers (Aso and Rubin, 2016; Pettersson, 1970). The odors were diluted in paraffin oil: pentyl acetate (PA, 1:10000, v/v) and ethyl lactate (EL, 1:10000, v/v). Videos were taken at 30 frames per second and analyzed using Fiji and Caltech FlyTracker (Eyjolfsdottir et al., 2014).

LM-EM matching

The confocal microscopy images of different split-GAL4 lines were registered to a common template JRC2018_unisex (Bogovic et al., 2020) and organized in Janelia Workstation software (*https://github.com/JaneliaSciComp/workstation*). Color depth MIP mask search (Otsuna et al., 2018) was used to search through the EM neuron library (hemibrain 1.2.1) for matching candidates. The searching target was obtained by either creating a mask on the full confocal image or using neurons of interest manually segmented in VVD viewer (*https://github.com/takashi310/VVD_Viewer*)(Wan et al., 2012). SWC files of top-matching EM neuron candidates were loaded into VVD viewer together with the confocal microscopy images in the same standard brain coordinates. By rotating the 3d images and manually scrutinizing the branching patterns, we picked the best matching candidate. Typically, we had high confidence of LM-to-EM matching for the line that labels only one cell per hemishere. For instance, we could unambiguously match the cell in SS67721 with SMP108 in the EM hemibrain volume. Our confidence of LM-to-EM matching tended to be lower for the lines that label multiple cells, because neurons of similar morphologies could be labeled together in those lines.

Connectivity analysis

Connectivity information was retrieved from neuPrint (*neuprint.janelia.org*), a publicly accessible website hosting the "hemibrain" dataset (Scheffer et al., 2020). For cell types, we used cell type name assignments reported in Sheffer et al., 2020. Only connections of the cells in the right hemisphere were used due to incomplete connectivity in the left hemisphere. The 3D renderings of neurons presented were generated using the visualization tools of NeuTu (Zhao et al., 2018) or VVD viewer.

Statistics

Statistical comparisons were performed on GraphPad Prism 7.0 using one-way ANOVA followed by Dunnett's test for multiple comparisons. Sample size was not predetermined based on pilot experiments.

Data Availability

The confocal images of expression patterns are available online (*http://www.janelia.org/split-gal4*). The values used for figures are summarized in Source Data.

Detailed fly genotypes used by figures

Figure 1F	*w/w, 20xUAS-CsChrimson-mVenus attP18; +/split-GAL4* *w/w, 20xUAS-CsChrimson-mVenus attP18; +/P{Gr64f-GAL4.9.7}5; +/P{Gr64f-GAL4.9.7}1*
Figure 2A	*w/w, 20xUAS-CsChrimson-mVenus attP18;+/SS45245-split-GAL4*
Figure 2B	w/w, pBPhsFlp2::PEST in attP3;; pJFRC201-10XUAS-FRT>STOP>FRT-myr::smGFP-HA in VK00005, pJFRC240-10XUAS-FRT>STOP>FRT-myr::smGFP-V5-THS-10XUAS-FRT>STOP>FRT-myr::smGFP-FLAG in su(Hw)attP1/SS45245-*split-GAL4*
Figure 2C	w/w;pJFRC225-5XUAS-IVS-myr::smFLAG in VK00005, pJFRC51-3XUAS-IVS-Syt::smHA in su(Hw)attP1/SS45245-*split-GAL4*
Figure 7E-J	*w/w, 20xUAS-CsChrimson-mVenus attP18;+/SS87269-split-GAL4* *w/w, 20xUAS-CsChrimson-mVenus attP18;+/SS87272-split-GAL4* *w/w, 20xUAS-CsChrimson-mVenus attP18;+/SS88801-split-GAL4* *w/w, 20xUAS-CsChrimson-mVenus attP18;+/SS87278-split-GAL4*
Figure 7K-Q	*w/w, 20xUAS-CsChrimson-mVenus attP18;+/Gr64f-split-GAL4s* *w/w, 20xUAS-CsChrimson-mVenus attP18;+/Gr66a-GAL4*
Figure 7 - figure supplement 1	*w/w; +/ P{Gr64f-GAL4.9.7}5; 5xUAS-myr-smFLAG in VK00005/P{Gr64f-GAL4.9.7}1*
Figure 8E-F, Figure 8 - figure supplement 2	*w/w, 20xUAS-CsChrimson-mVenus attP18; +/Gr64f-split-GAL4s* *w/w, 20xUAS-CsChrimson-mVenus attP18; +/ P{Gr64f-GAL4.9.7}5; +/P{Gr64f-GAL4.9.7}1* *w/w, 20xUAS-CsChrimson-mVenus attP18; +/empty-split-GAL4*
Figure 8 - figure supplement 1A	*w/w, 20xUAS-CsChrimson-mVenus attP18; +/SS87269-split-GAL4*
Figure 8 - figure supplement 1C	*w/w, 20xUAS-CsChrimson-mVenus attP18; +/SS87269-split-GAL4* *w/w, 20xUAS-CsChrimson-mVenus attP18; +/SS87278-split-GAL4* *w/w, 20xUAS-CsChrimson-mVenus attP18; +/empty-split-GAL4*
Figure 8I	*w/w, 20xUAS-CsChrimson-mVenus attP18;+/SS87269-split-GAL4* *w/w, 20xUAS-CsChrimson-mVenus attP18;+/SS88801-split-GAL4* *w/w, 20xUAS-CsChrimson-mVenus attP18;+/empty-GAL4*
Figure 9B-D	*w/w, 20xUAS-CsChrimson-mVenus attP18;+/SS01159-split-GAL4* *w/w, 20xUAS-CsChrimson-mVenus attP18;+/empty-GAL4*
Figure 10A	w/w;pJFRC225-5XUAS-IVS-myr::smFLAG in VK00005, pJFRC51-3XUAS-IVS-Syt::smHA in su(Hw)attP1/*SS01336-split-GAL4*
Figure 10B	w/w;pJFRC225-5XUAS-IVS-myr::smFLAG in VK00005, pJFRC51-3XUAS-IVS-Syt::smHA in su(Hw)attP1/ *SS01241-split-GAL4*

Figure 10C	w/w, pBPhsFlp2::PEST in attP3;; pJFRC201-10XUAS-FRT>STOP>FRT-myr::smGFP-HA in VK00005, pJFRC240-10XUAS-FRT>STOP>FRT-myr::smGFP-V5-THS-10XUAS-FRT>STOP>FRT-myr::smGFP-FLAG in su(Hw)attP1/*MB310C-split-GAL4*
Figure 10D	w/w, pBPhsFlp2::PEST in attP3;; pJFRC201-10XUAS-FRT>STOP>FRT-myr::smGFP-HA in VK00005, pJFRC240-10XUAS-FRT>STOP>FRT-myr::smGFP-V5-THS-10XUAS-FRT>STOP>FRT-myr::smGFP-FLAG in su(Hw)attP1/*MB082C-split-GAL4*
Figure 11A-B, Figure 11 - figure supplement 1	w/w;;pJFRC225-5XUAS-IVS-myr::smFLAG in VK00005, pJFRC51-3XUAS-IVS-Syt::smHA in su(Hw)attP1/ *MB083C-split-GAL4* *w/w;UAS-mCD8::GFP/MB083C-split-GAL4* *w/w, 20xUAS-CsChrimson-mVenus in attP18;;+/ MB083C-split-GAL4* *w/w, pJFRC12-10XUAS-IVS-myr::GFP in attP18/ MB083C-split-GAL4*
Figure 11 - figure supplement 2	*w, 10xUAS-IVS-myr::smGdP-HA in attP18, 13xLexAop2-IVS-myr::smGdP-V5 in su(Hw)attP8; +/R52G04-LexA (MBON08/09);+/MB312C-split-GAL4 (PAM-γ4)* *w, 10xUAS-IVS-myr::smGdP-HA in attP18, 13xLexAop2-IVS-myr::smGdP-V5 in su(Hw)attP8; +/R52G04-LexA (MBON08/09);+/MB441B-split-GAL4 (PAM-γ3)* *w/w;;VT006202-LexAp65 in attP2/pJFRC19-13XLexAop2-IVS-myr::GFP in attP2*
Figure 12	*w/w, 20xUAS-CsChrimson-mVenus attP18; +/split-GAL4s* *w/w, 13xLexAop2-CsChrimson-mVenus attp18; +/split-LexAs*

Supplemental information

Supplementary File 2 New transgenic flies generated in this study

The enhancer fragments, insertion sites, and inserted chromosomes used to construct the lines are listed. For some of the transgenes, an additional version with a *p10* 3'-UTR (Pfeiffer et al., 2012) was generated to increase the expression.

Supplementary File 3 Coverage of MBON-downstream and DAN-upstream

Connection matrix between MB interneurons and DANs and MBONs. A threshold was set to exclude connections with a low number of neuron-neuron connections, specifically, 10 connections for MBON to a downstream neuron and 5 connections for upstream neurons to a DAN (Li et al., 2020). Recurrent neurons are defined as cell types receiving input from MBONs and supplying output to DANs. Neurotransmitter (NT) prediction data were from (Eckstein et al., 2023), and the fraction of synapses predicted for the neurotransmitter was pooled from all cells of the cell type.

Supplementary File 4 Updated list of driver lines for cell types within the MB excluding Kenyon cells

This includes new or improved split-GAL4 and split-LexA lines from the present study, lines from the Aso 2014 collection (Aso et al., 2014a), a recent MBON collection (Rubin and Aso, 2023), MB630B (Aso and Rubin, 2016), SS01308 (Aso et al., 2019), MB063B (Dolan et al., 2019), SS46348 (Otto et al., 2020), and some regular Gal4 lines VT43924-Gal4.2 (Amin et al., 2020) and G0239 (Chiang et al., 2011). Lines listed in boldface are generally of higher quality.

Supplementary File 5 Coverage of PN cell types

A list of split-GAL4 lines and their coverage of PNs of the antennal lobe. Shading indicates expression level. Many of the multi-glomerular PN (mPN) cell types cannot be easily differentiated based on light microscopy images, so they are listed as a broad mPN category in the table.

Appendix 1 key resources table

Reagent type (species) or resource	Designation	Source or reference	Identifiers	Additional information
strain, strain background (*Drosophila melanogaster*)	New split-GAL4 and split-LexA lines	This paper	https://splitgal4.janelia.org/cgi-bin/splitgal4.cgi	Available from Aso lab
strain, strain background (*Drosophila melanogaster*)	20xUAS-CsChrimson-mVenus attP18	(Klapoetke et al., 2014); PMID: 24509633	N.A.	
strain, strain background (*Drosophila melanogaster*)	pJFRC200-10xUAS-IVS-myr::smGFP-HA in attP18	(Nern et al., 2015); PMID: 25964354	N.A.	
strain, strain background (*Drosophila melanogaster*)	pJFRC225-5xUAS-IVS-myr::smGFP-FLAG in VK00005	(Nern et al., 2015); PMID: 25964354	N.A.	
strain, strain background (*Drosophila melanogaster*)	pBPhsFlp2::PEST in attP3	(Nern et al., 2015); PMID: 25964354	N.A.	
strain, strain background (*Drosophila melanogaster*)	pJFRC201-10XUAS-FRT>STOP > FRT-myr::smGFP-HA in VK0005	(Nern et al., 2015); PMID: 25964354	N.A.	
strain, strain background (*Drosophila melanogaster*)	pJFRC240-10XUAS-FRT>STOP > FRT-myr::smGFP-V5-THS-10XUAS-FRT>STOP > FRT-myr::smGFP-FLAG_in_su(Hw)attP1	(Nern et al., 2015); PMID: 25964354	N.A.	

strain, strain background (*Drosophila melanogaster*)	empty-split-GAL4 (p65ADZp attP40, ZpGAL4DBD attP2)	(Hampel et al., 2015); PMID: 26344548	RRID:BDSC_79603	
strain, strain background (*Drosophila melanogaster*)	empty-Gal4 (pBDPGal4U attP2)	(Pfeiffer et al., 2008); PMID: 18621688	RRID:BDSC_68384	
strain, strain background (*Drosophila melanogaster*)	MB083C split-GAL4	(Aso et al., 2014a) ; PMID: 25535793	RRID:BDSC_68287	Available from Aso lab
strain, strain background (*Drosophila melanogaster*)	w*; P{Gr64f-GAL4.9.7}5/CyO; P{Gr64f-GAL4.9.7}1/TM3, Sb^1	(Haberkern et al., 2019); PMID: 31056392	RRID: BDSC_57668, BDSC_57669	
strain, strain background (*Drosophila melanogaster*)	Gr66a-Gal4	(Joseph and Heberlein, 2012); PMID: 22798487	N.A.	
antibody	anti-GFP (rabbit polyclonal)	Invitrogen	A11122 RRID:AB_221569	1:1000
antibody	anti-Brp (mouse monoclonal)	Developmental Studies Hybridoma Bank	nc82 RRID:AB_2341866	1:30
antibody	anti-HA-Tag (mouse monoclonal)	Cell Signaling Technology	C29F4; #3724 RRID:AB_10693385	1:300
antibody	anti-FLAG (rat monoclonal)	Novus Biologicals	NBP1-06712 RRID:AB_1625981	1:200
antibody	anti-V5-TAG Dylight-549 (mouse monoclonal)	Bio-Rad	MCA2894D549GA RRID:AB_10845946	1:500
antibody	anti-mouse IgG(H&L) AlexaFluor-568 (goat polyclonal)	Invitrogen	A11031 RRID:AB_144696	1:400
antibody	anti-rabbit IgG(H&L) AlexaFluor-488 (goat polyclonal)	Invitrogen	A11034 RRID:AB_2576217	1:800

antibody	anti-mouse IgG(H&L) AlexaFluor-488 conjugated (donkey polyclonal)	Jackson Immuno Research Labs	715-545-151 RRID:AB_2341099	1:400
antibody	anti-rabbit IgG(H&L) AlexaFluor-594 (donkey polyclonal)	Jackson Immuno Research Labs	711-585-152 RRID:AB_2340621	1:500
antibody	anti-rat IgG(H&L) AlexaFluor-647 (donkey polyclonal)	Jackson Immuno Research Labs	712-605-153 RRID:AB_2340694	1:300
antibody	anti-mouse IgG(H&L) ATTO 647 N (goat polyclonal)	ROCKLAND	610-156-121 RRID:AB_10894200	1:100
antibody	anti-rabbit IgG(H+L) Alexa Fluor 568 (goat polyclonal)	Invitrogen	A-11036 RRID:AB_10563566	1:1000
chemical compound, drug	Pentyl acetate	Sigma-Aldrich	109584	1:10000 in paraffin oil
chemical compound, drug	Ethyl lactate	Sigma-Aldrich	W244015	1:10000 in paraffin oil
chemical compound, drug	Paraffin oil	Sigma-Aldrich	18512	
software, algorithm	ImageJ and Fiji	NIH; (Schindelin et al., 2012)	https://imagej.nih.gov/ij/ http://fiji.sc/	
software, algorithm	MATLAB	MathWorks	https://www.mathworks.com/	
software, algorithm	Adobe Illustrator CC	Adobe Systems	https://www.adobe.com/products/illustrator.html	
software, algorithm	GraphPad Prism 9	GraphPad Software	https://www.graphpad.com/scientific-software/prism/	
software, algorithm	Python	Python Software Foundation	https://www.python.org/	

software, algorithm	Caltech FlyTracker(Eyjolfsdottir et al., 2014)	(Eyjolfsdottir et al., 2014)	https://github.com/kristinbranson/FlyTracker	
software, algorithm	Animal Part Tracker	(Kabra et al., 2022)	(https://github.com/kristinbranson/APT)	
software, algorithm	neuPrint	(Plaza et al., 2022)	https://neuprint.janelia.org/	
software, algorithm	Cytoscape	(Shannon et al., 2003)	https://cytoscape.org/	
software, algorithm	Janelia workstation	HHMI Janelia	https://doi.org/10.25378/janelia.8182256.v1	
software, algorithm	NeuTu	(Zhao et al., 2018)	https://github.com/janelia-flyem/NeuTu	
software, algorithm	VVD Viewer	(Wan et al., 2012)	https://github.com/takashi310/VVD_Viewer	
other	Grade 3 MM Chr Blotting Paper	Whatman	3030–335	Used in glass vials with paraffin-oil diluted odors
other	mass flow controller	Alicat	MCW-200SCCM-D	Mass flow controller used for the olfactory arena

Acknowledgements

We thank Toshihide Hige, Daisuke Hattori, members of the Y.A., G.M.R. and G.T. laboratories for valuable comments on the manuscript. We thank all the members of Janelia Flylight (*https://www.janelia.org/project-team/flylight*) and Project Technical Resources (*https://www.janelia.org/support-team/project-technical-resources*) for technical assistance for constructing split-GAL4 drivers and generating confocal microscopy images. During this effort, the FlyLight Project Team and Project Technical Resources included Gudrun Ihrke, Megan Atkins, Shelby Bowers, Kari Close, Gina DePasquale, Zack Dorman, Kaitlyn Forster, Jaye Anne Gallagher, Theresa Gibney, Asish Gulati, Joanna Hausenfluck, Yisheng He, Kristin Hendersen, Hsing Hsi Li, Nirmala Iyer, Jennifer Jeter, Lauren Johnson, Rebecca Johnston, Rachel Lazarus, Kelley Lee, Hua-Peng Liaw, Oz Malkesman, Geoffrey Meissner, Brian Melton, Scott Miller, Reeham Motaher, Alexandra Novak, Omatara Ogundeyi, Alyson Petruncio, Jacquelyn Price, Sophia Protopapas, Susana Tae, Athreya Tata, Jennifer Taylor, Allison Vannan, Rebecca Vorimo, Brianna Yarborough, Kevin Xiankun Zeng, and Chris Zugates, with Steering Committee of Y.A., G.M.R, Gwyneth Card, Barry Dickson, Reed George, Wyatt Korff, and James Truman. We also thank Kelly Ashley, Pria Chang, Tam Dang, Dona Fetter, Guillermo Gonzalez, Donald Hall, Jui-Chun Kao, James McMahon, Monti Mercer, Brenda Perez, Scarlett Pitts, Danielle Ruiz, Brandi Sharp, Viruthika Vallanadu, Grace Zheng, Amanda Cavallaro, Todd Laverty of Janelia Fly facility (*https://www.janelia.org/support-team/fly-facility*) for

husbandry of stocks, and Eric Trautman, Rob Svirskas, Hideo Otsuna, Takashi Kawase and other members of Janelia Scientific Computing (*https://www.janelia.org/support-team/scientific-computing-software*) for supporting organization and analysis of confocal and EM microscopy images.

Author contributions

Conceptualization, G.M.R., G.T., L.T. and Y.A.; Formal Analysis and Investigation, Y.S., M.S., G.B.., K.H., C.Y., C.M.., I.S., and Y.A.; Writing, Y.S., G.M.R., G.T., G.S., and Y.A.; Supervision, G.M.R., G.T., T.L., and Y.A..; Funding Acquisition, G.M.R., G.T., T.L. and Y.A.

Competing interests

The authors declare no competing interests.

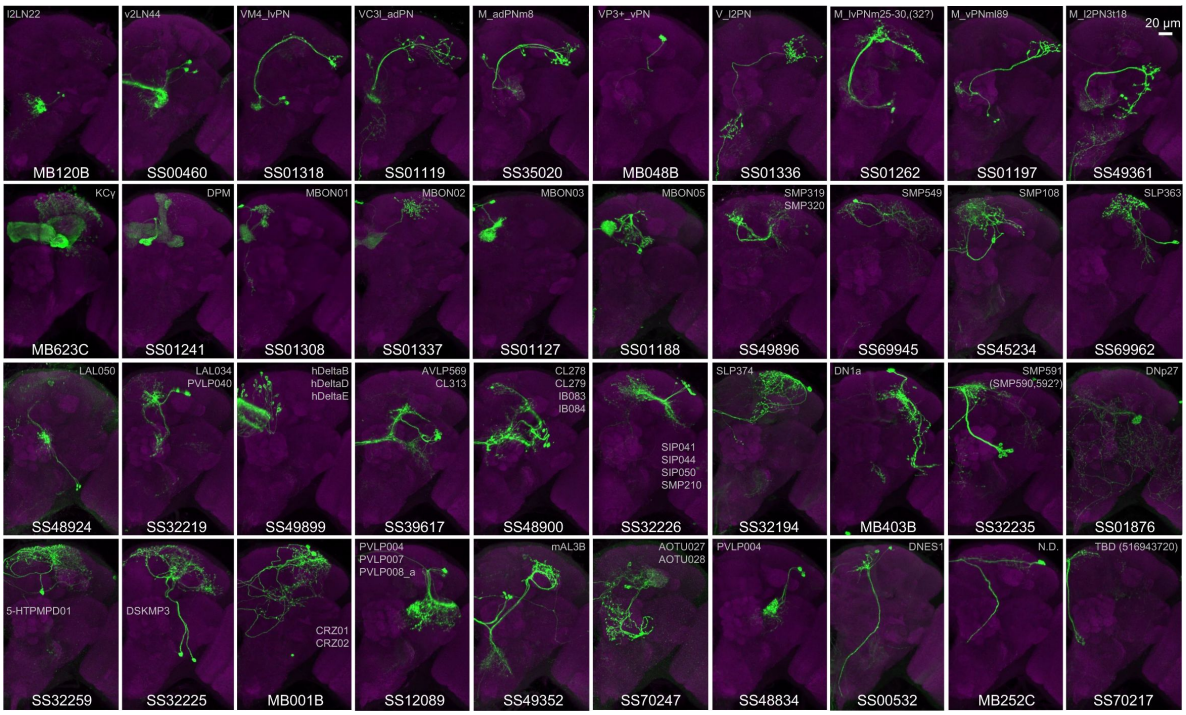

Figure 1-figure supplement 1

Examples of cell types covered by the split-GAL4 lines in this collection

Additional examples of cell types covered by the collection. Expression patterns of CsChrimson-mVenus (green) are shown with neuropil counterstaining of Brp (magenta). Only one brain hemisphere is shown.

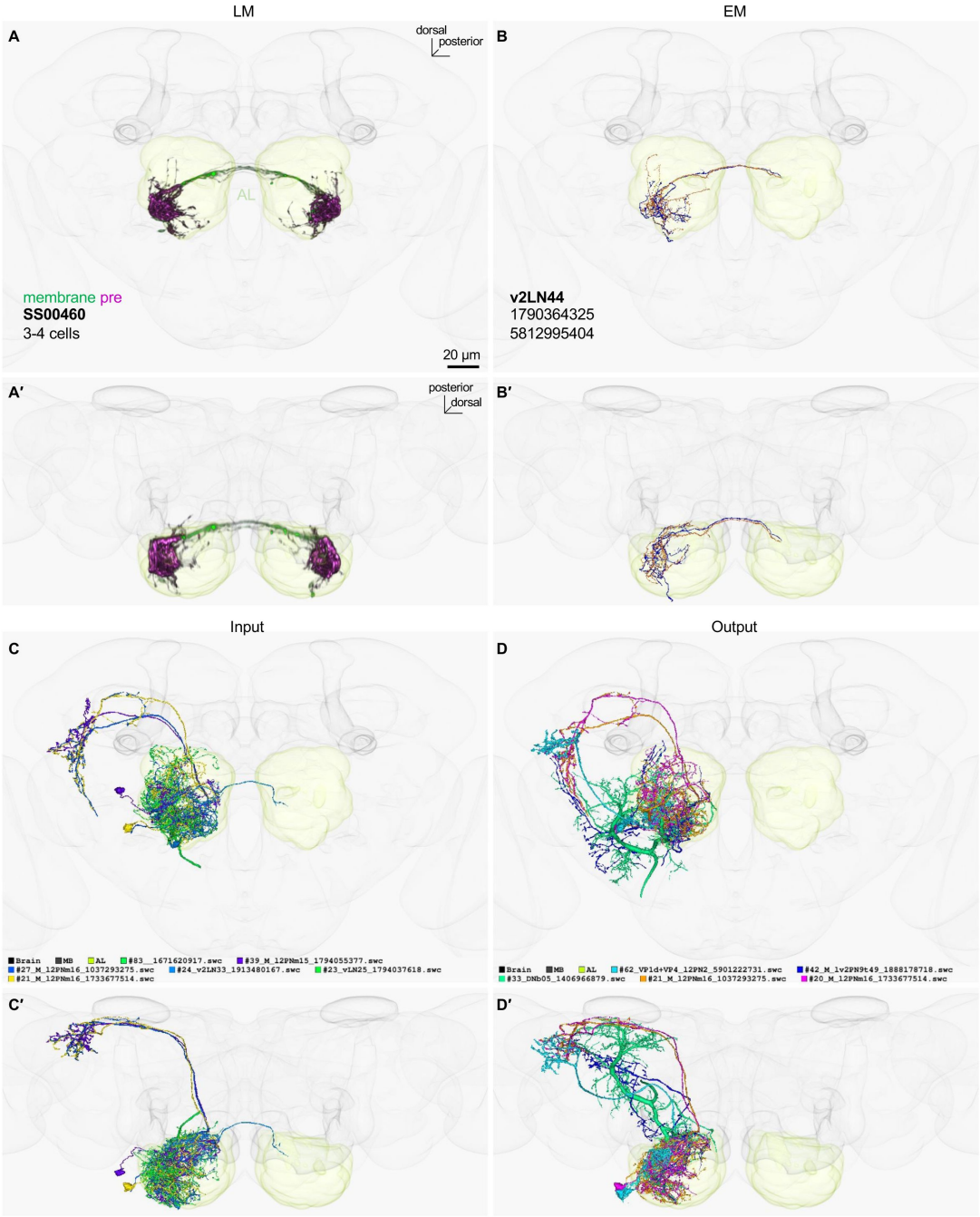

Figure 2-figure supplement 1

LM-EM match of SS00460

(A) Frontal and ventral views of segmented light microscopy (LM) images of SS00460 in the JRC2018 standard brain. Projections are shown with the outline of relevant neuropils. A' (ventral) is a rotated view of A (frontal) with the reference axis indicated.
(B) The skeleton reconstructed from electron microscopy (EM) data in the hemibrain volume of the matched cell type I2LN44.
(C) EM images of neurons with the most input connections (upstream) to I2LN44 in the hemibrain connectome. The number after "#" indicates the number of connections between the matched cell type (i.e. v2LN44) and its synaptic partners. The color code and EM BodyId for each EM-reconstructed neuron are also listed.
(D) EM images of neurons with the most output connections (downstream) from I2LN44 in the hemibrain connectome. In **Figure 2-figure supplement 1**-**20**, sensory neurons and KCs are not displayed as top upstream or downstream neurons.

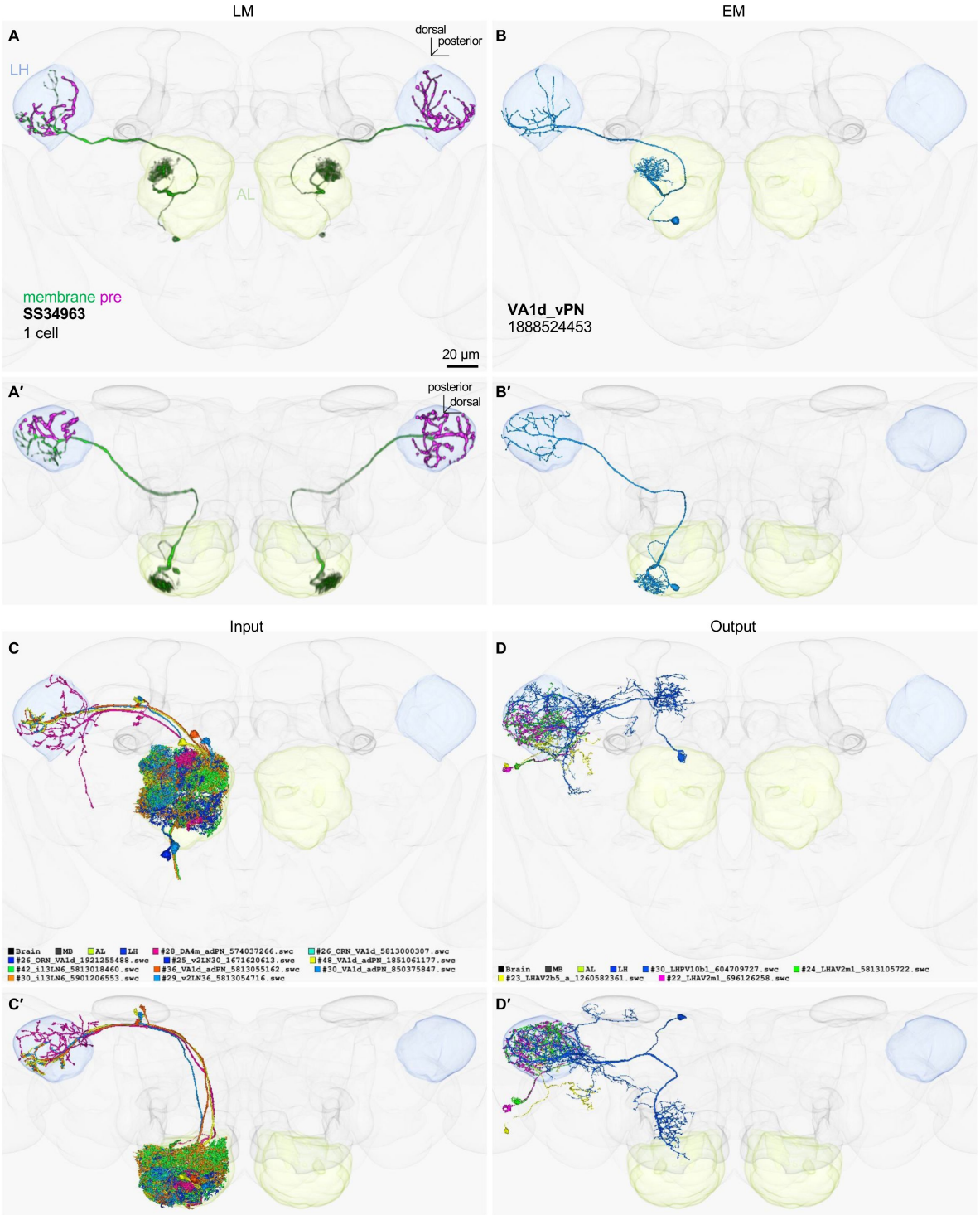

Figure 2-figure supplement 2

LM-EM match of SS34963

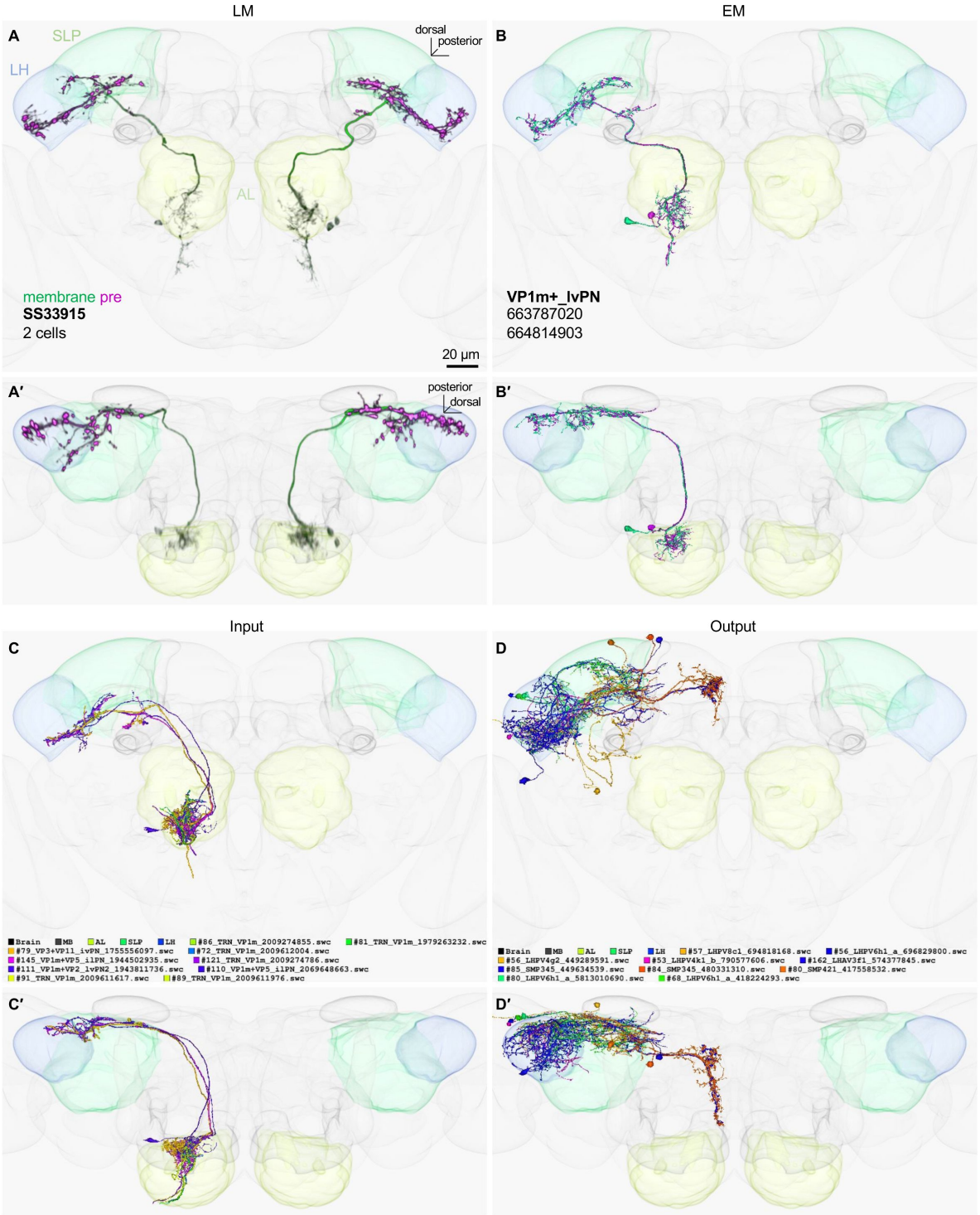

Figure 2-figure supplement 3

LM-EM match of SS33915

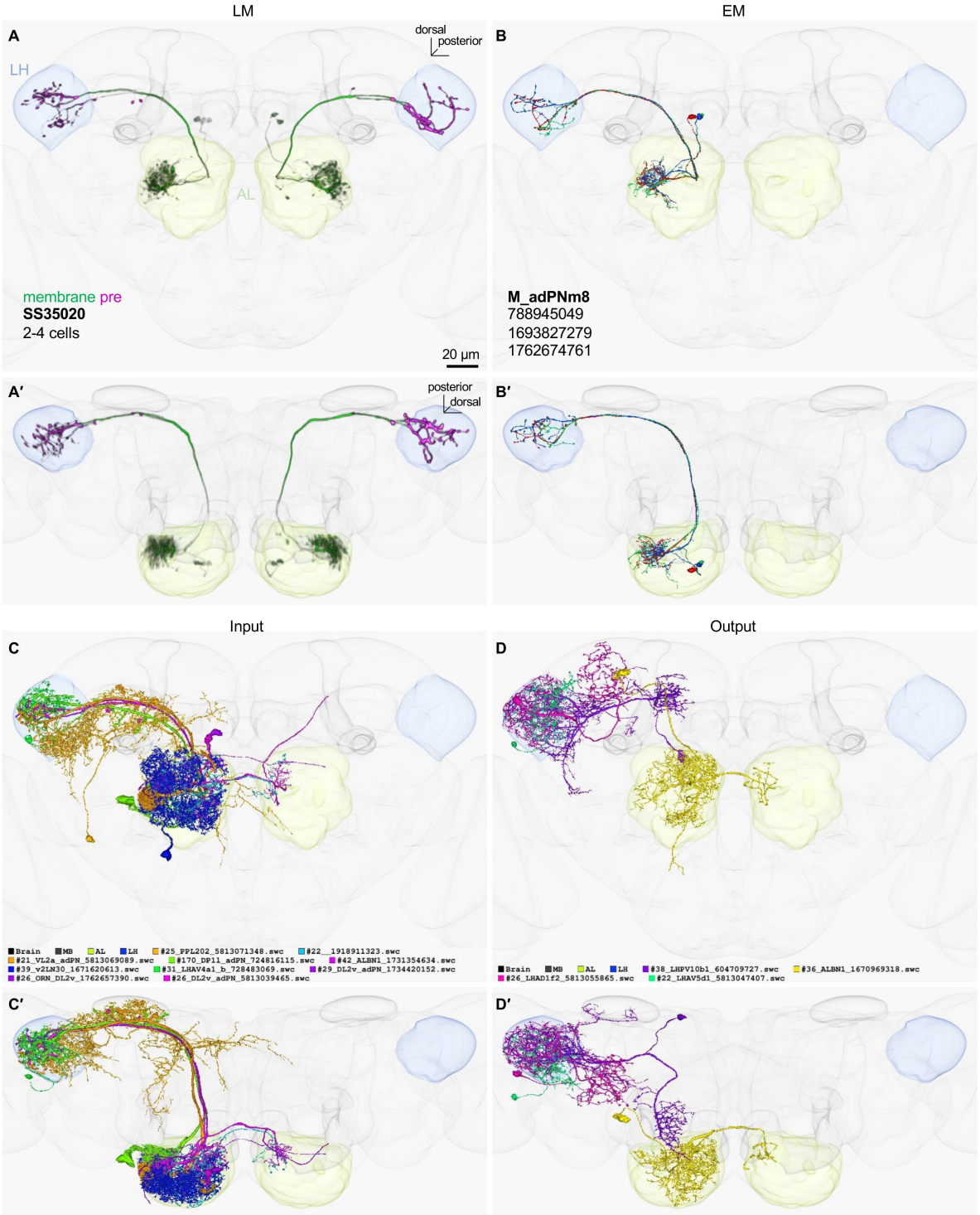

Figure 2-figure supplement 4

LM-EM match of SS35020

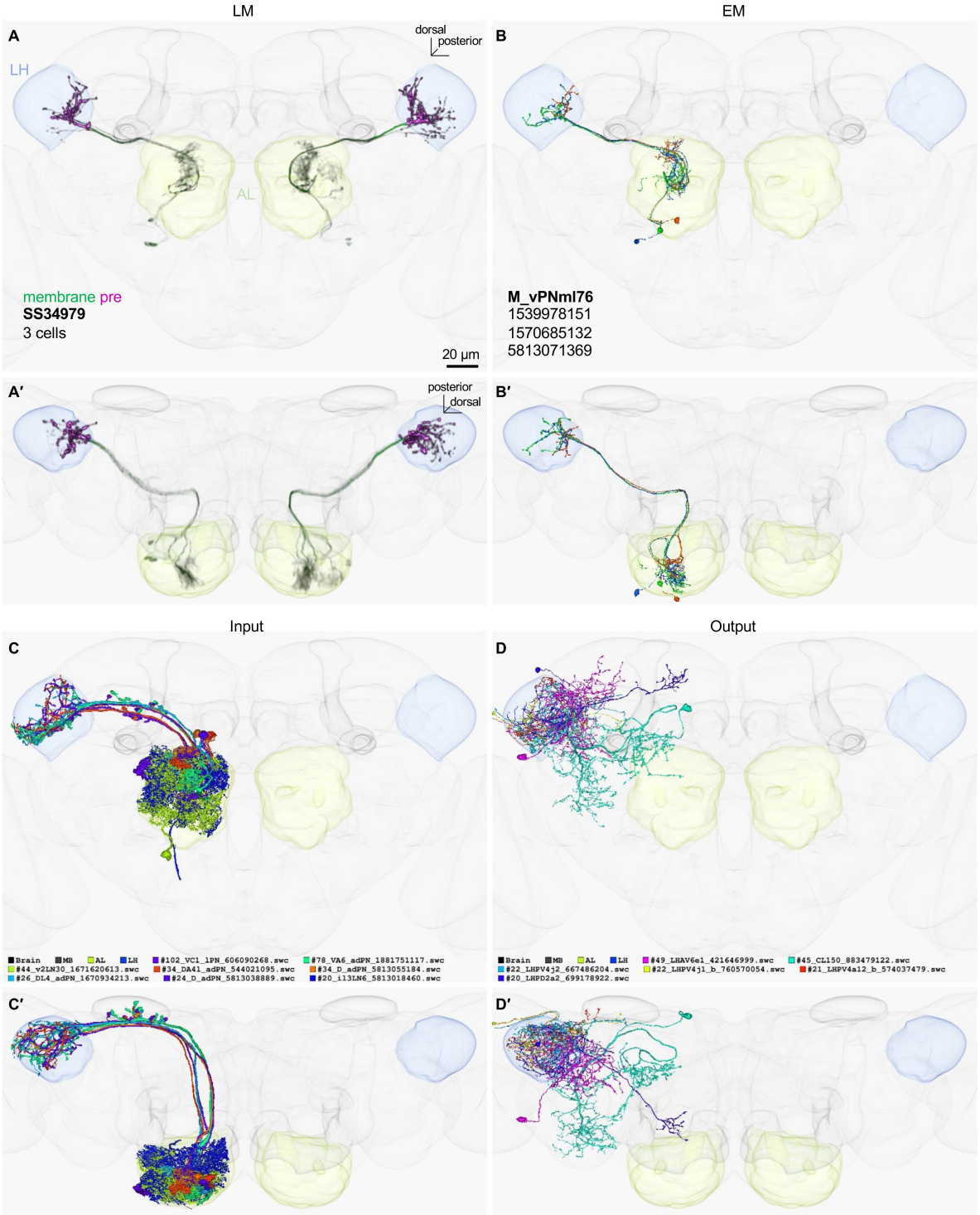

Figure 2-figure supplement 5

LM-EM match of SS34979

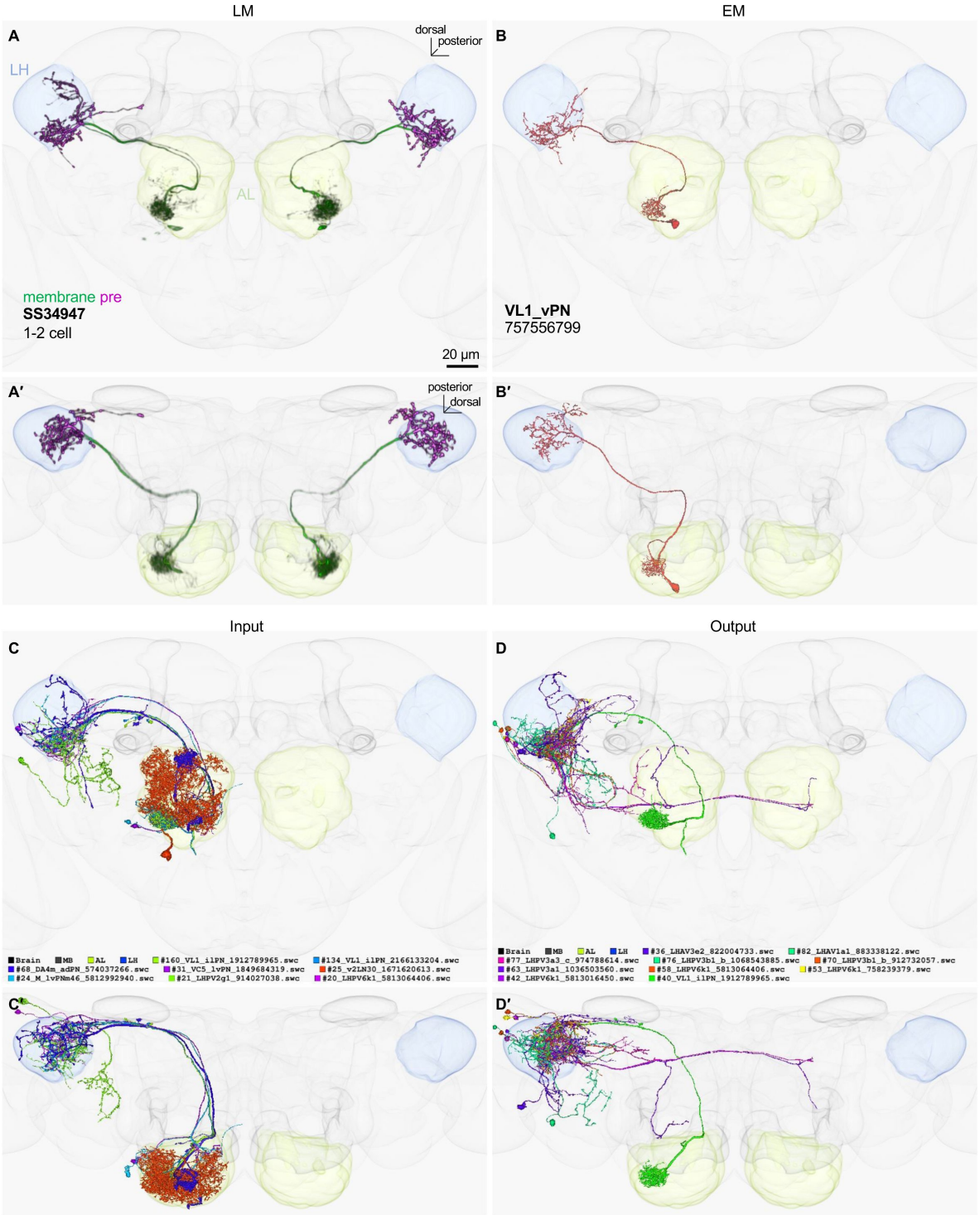

Figure 2-figure supplement 6

LM-EM match of SS34947

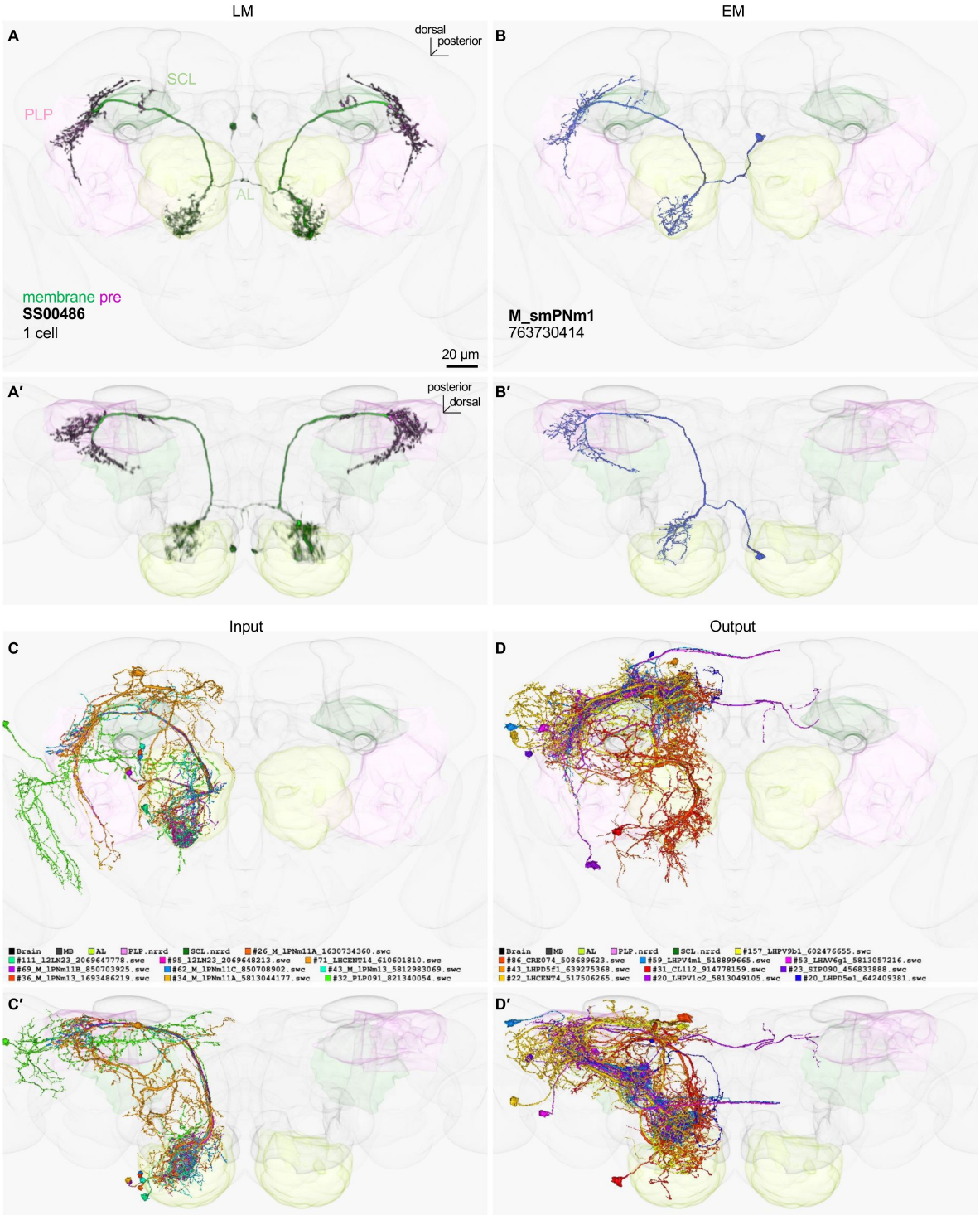

Figure 2-figure supplement 7

LM-EM match of SS00486

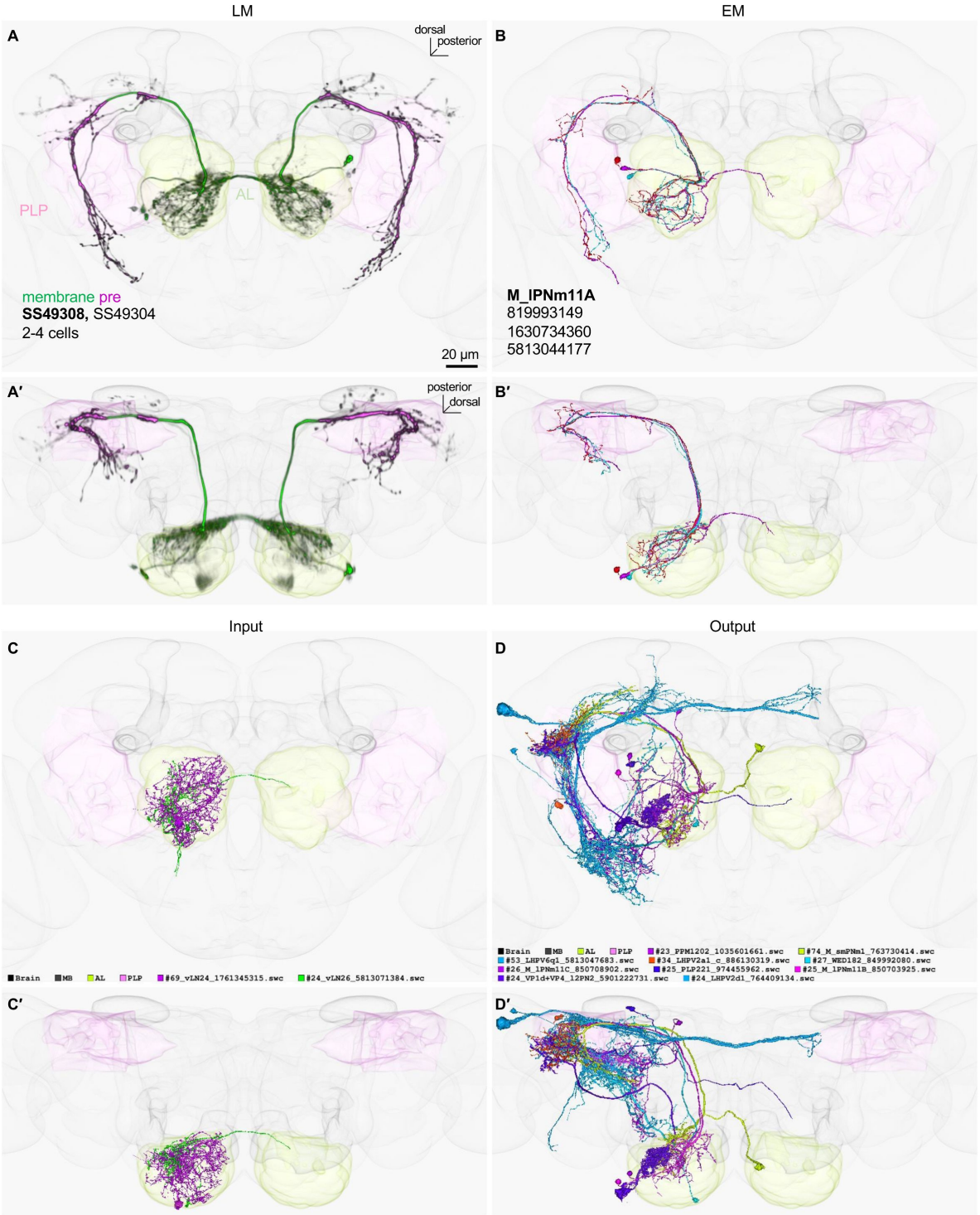

Figure 2-figure supplement 8

LM-EM match of SS49308

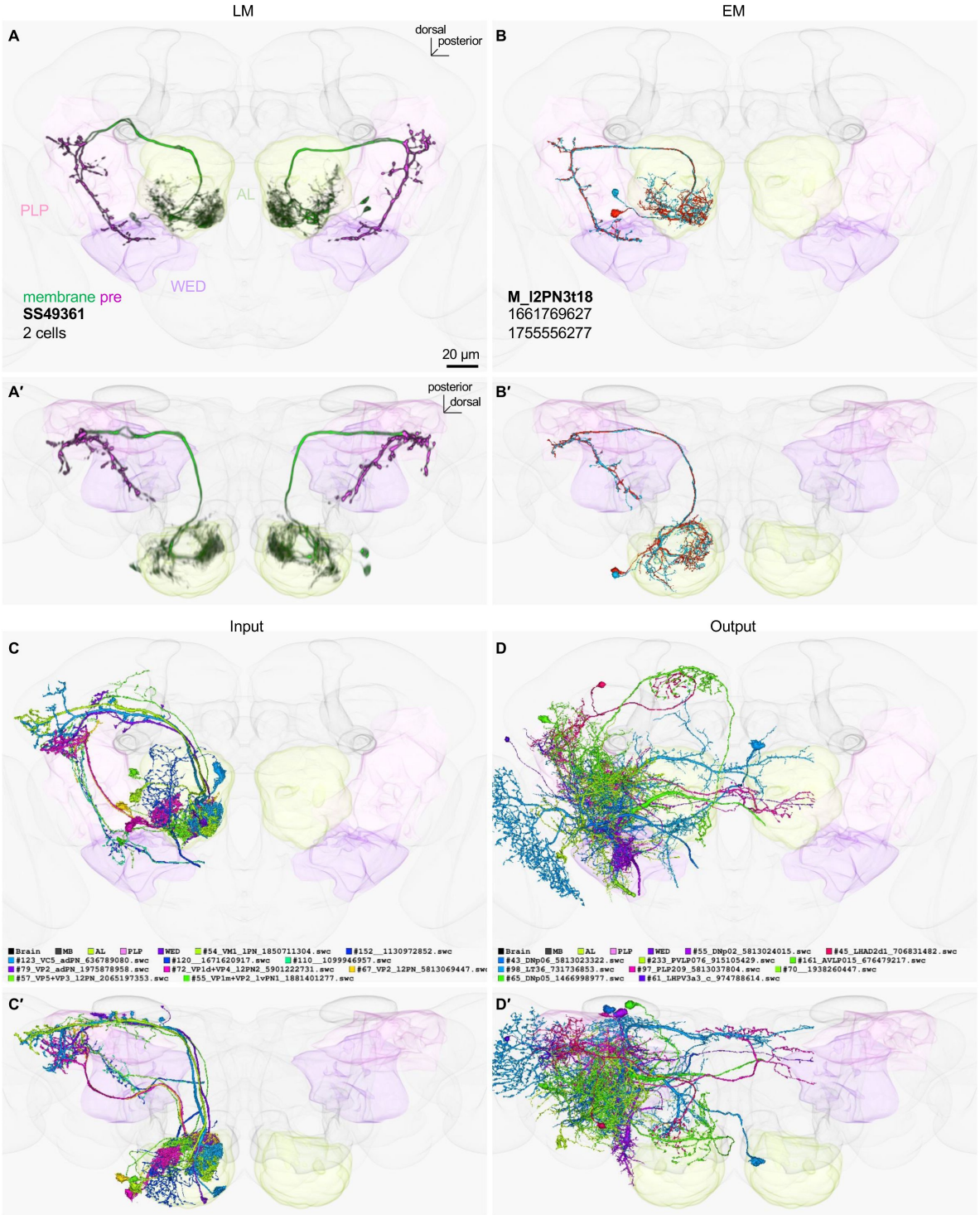

Figure 2-figure supplement 9

LM-EM match of SS49361

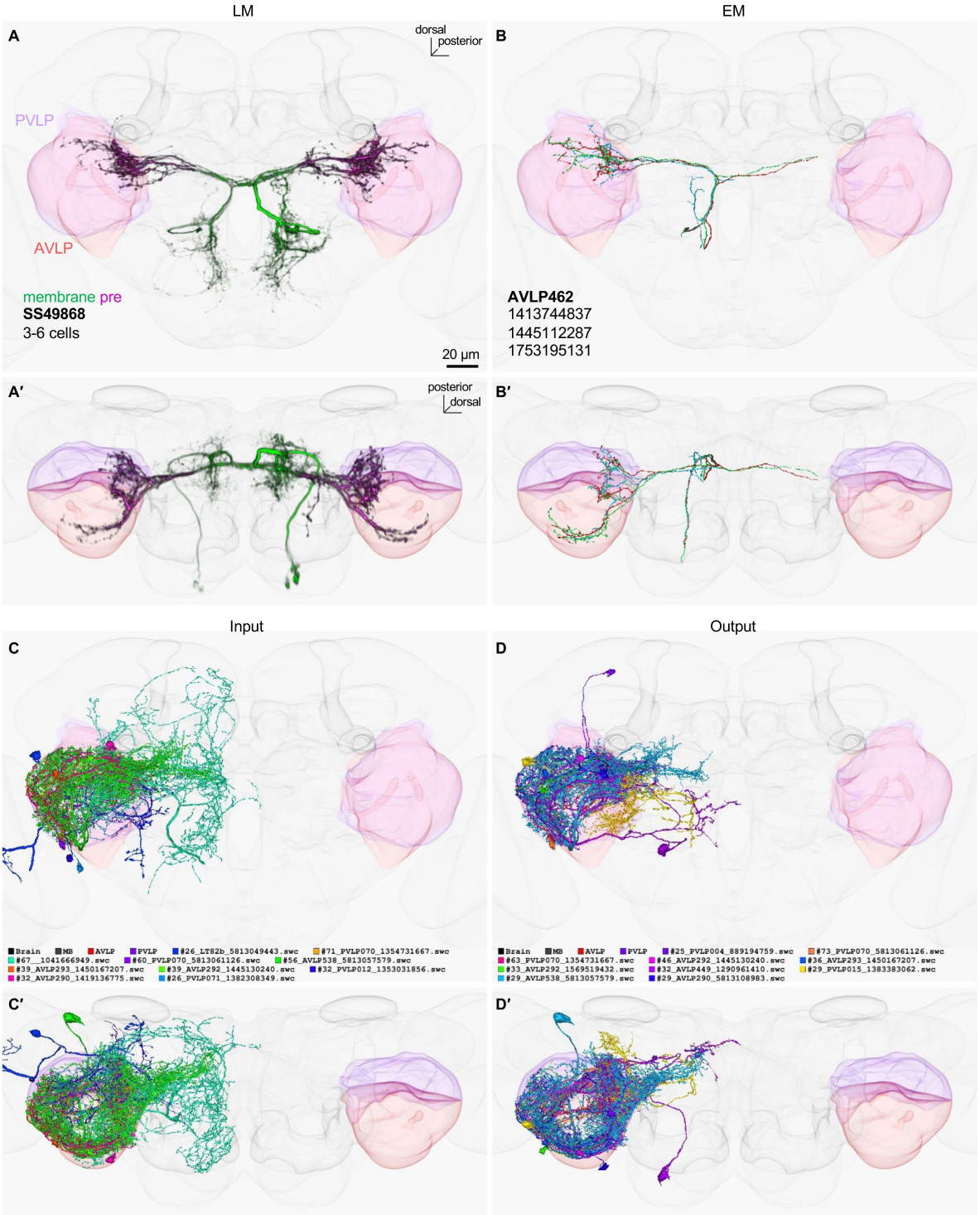

Figure 2-figure supplement 10

LM-EM match of SS49868

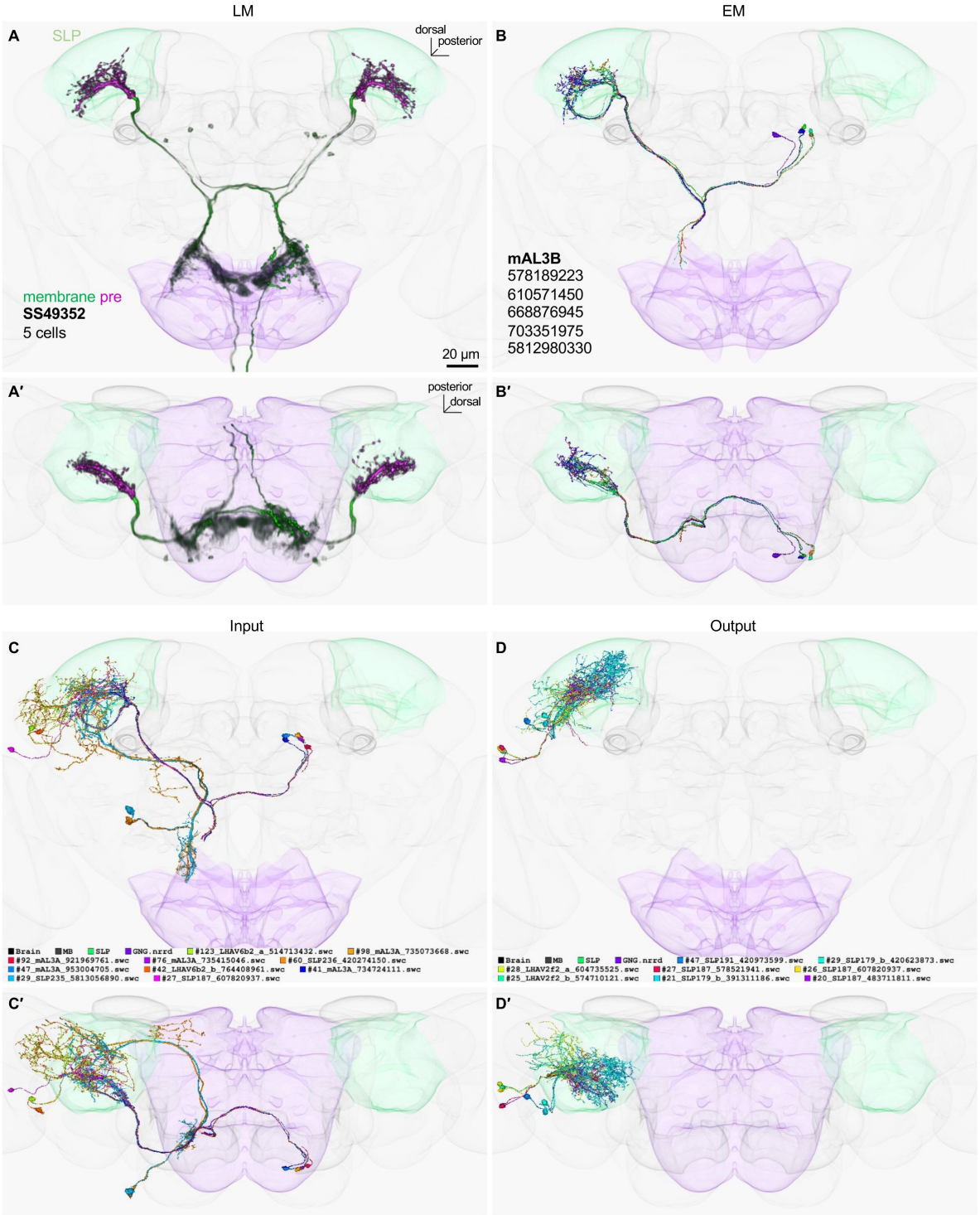

Figure 2-figure supplement 11

LM-EM match of SS49352

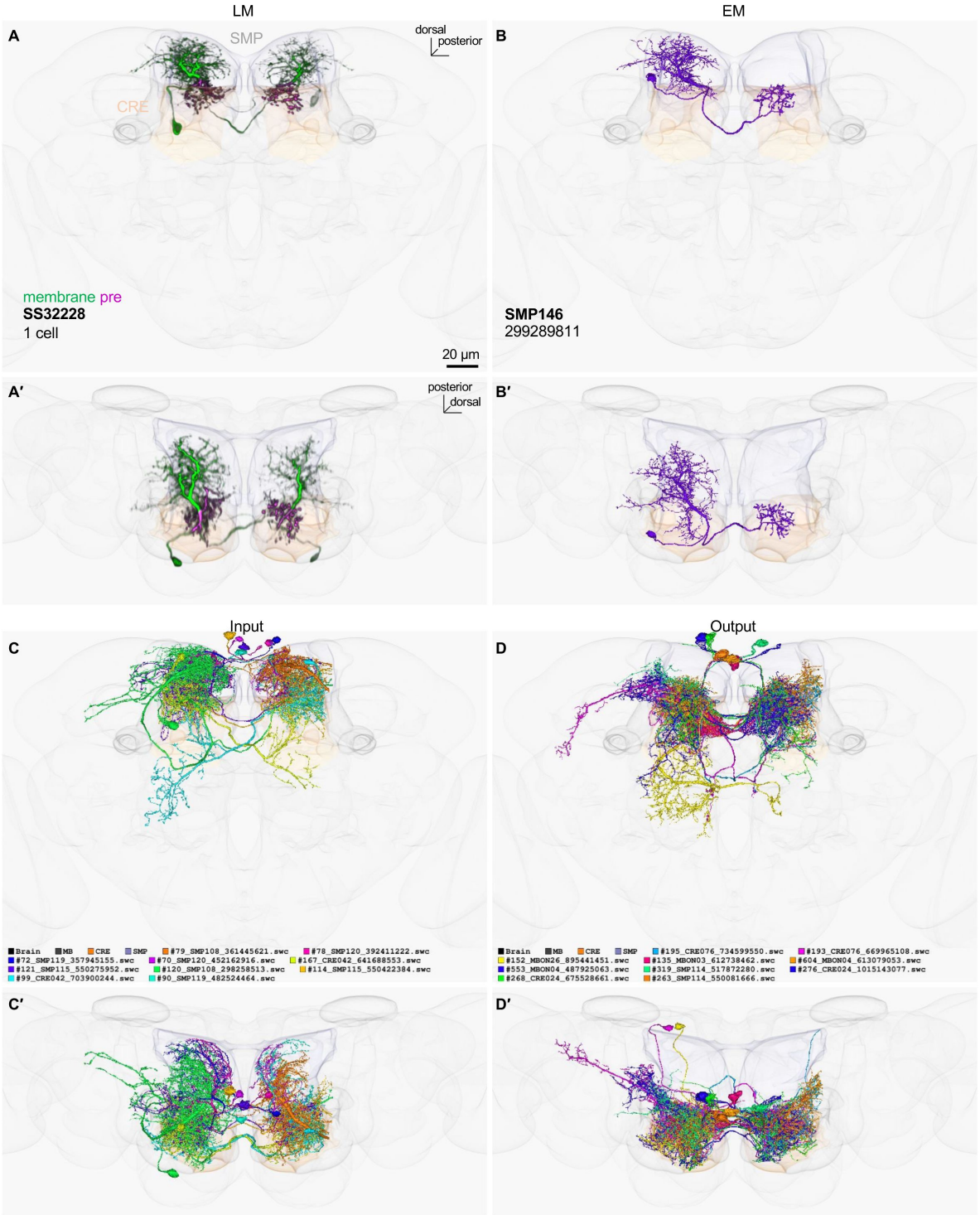

Figure 2-figure supplement 12

LM-EM match of SS32228

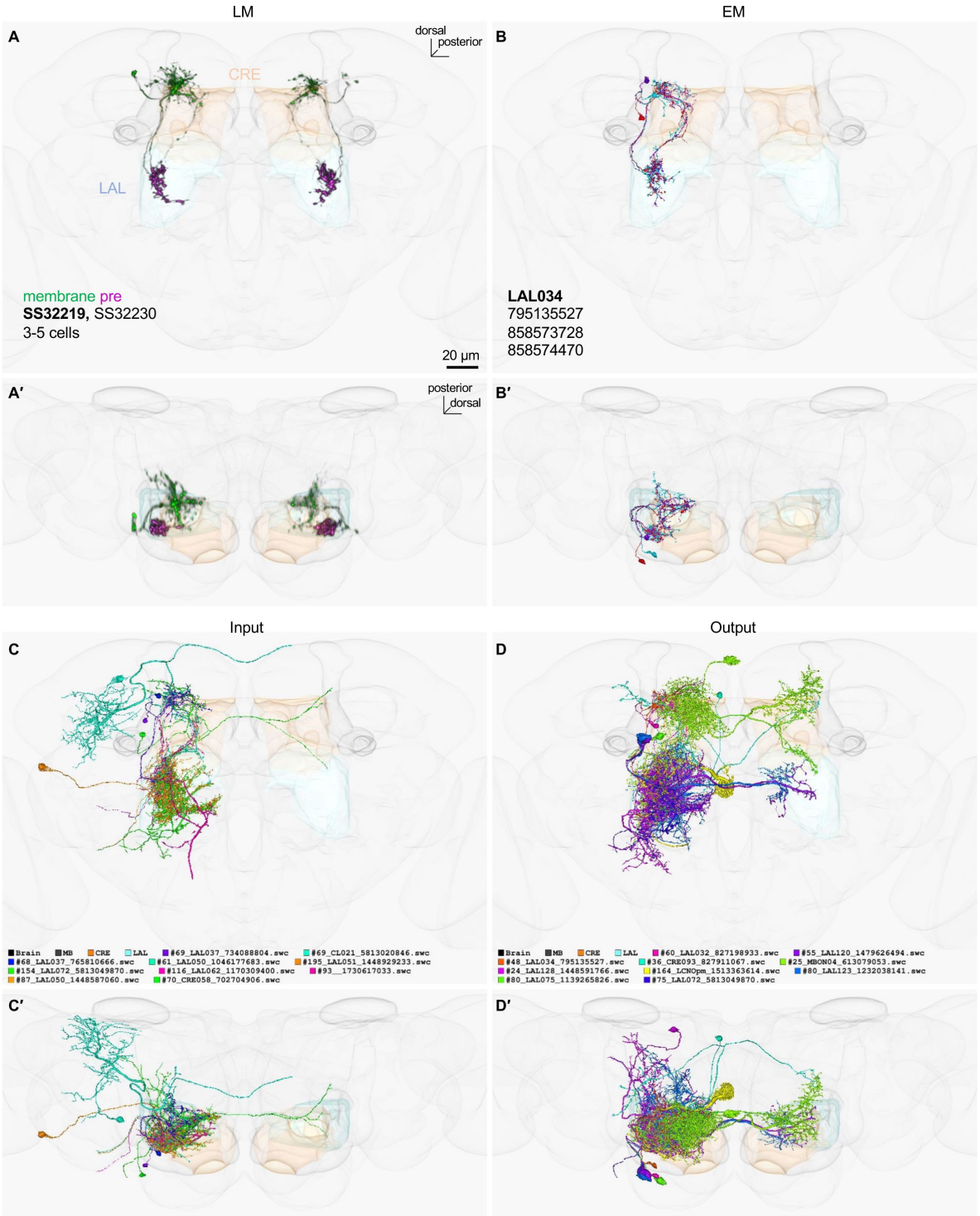

Figure 2-figure supplement 13

LM-EM match of SS32219

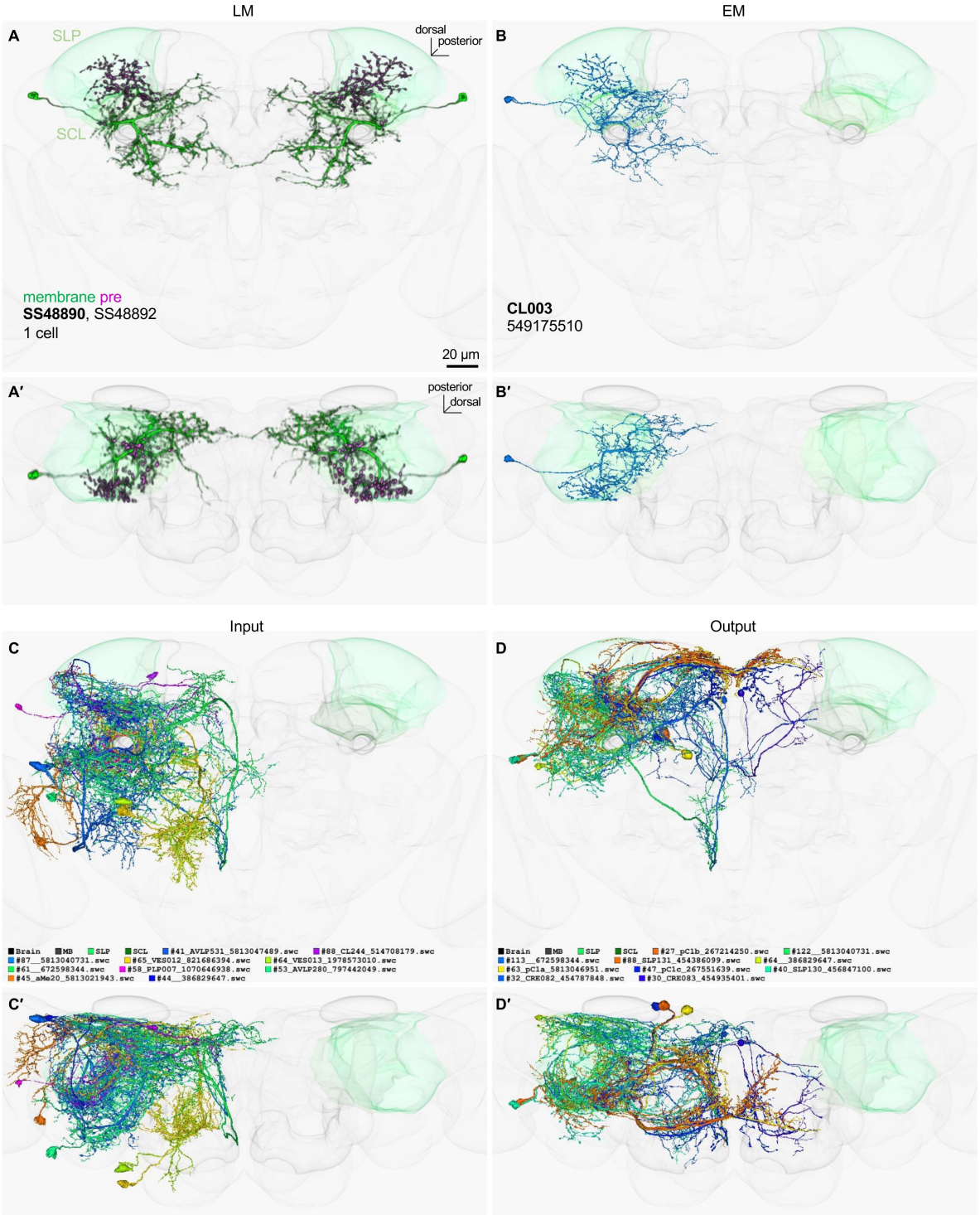

Figure 2-figure supplement 14

LM-EM match of SS48890

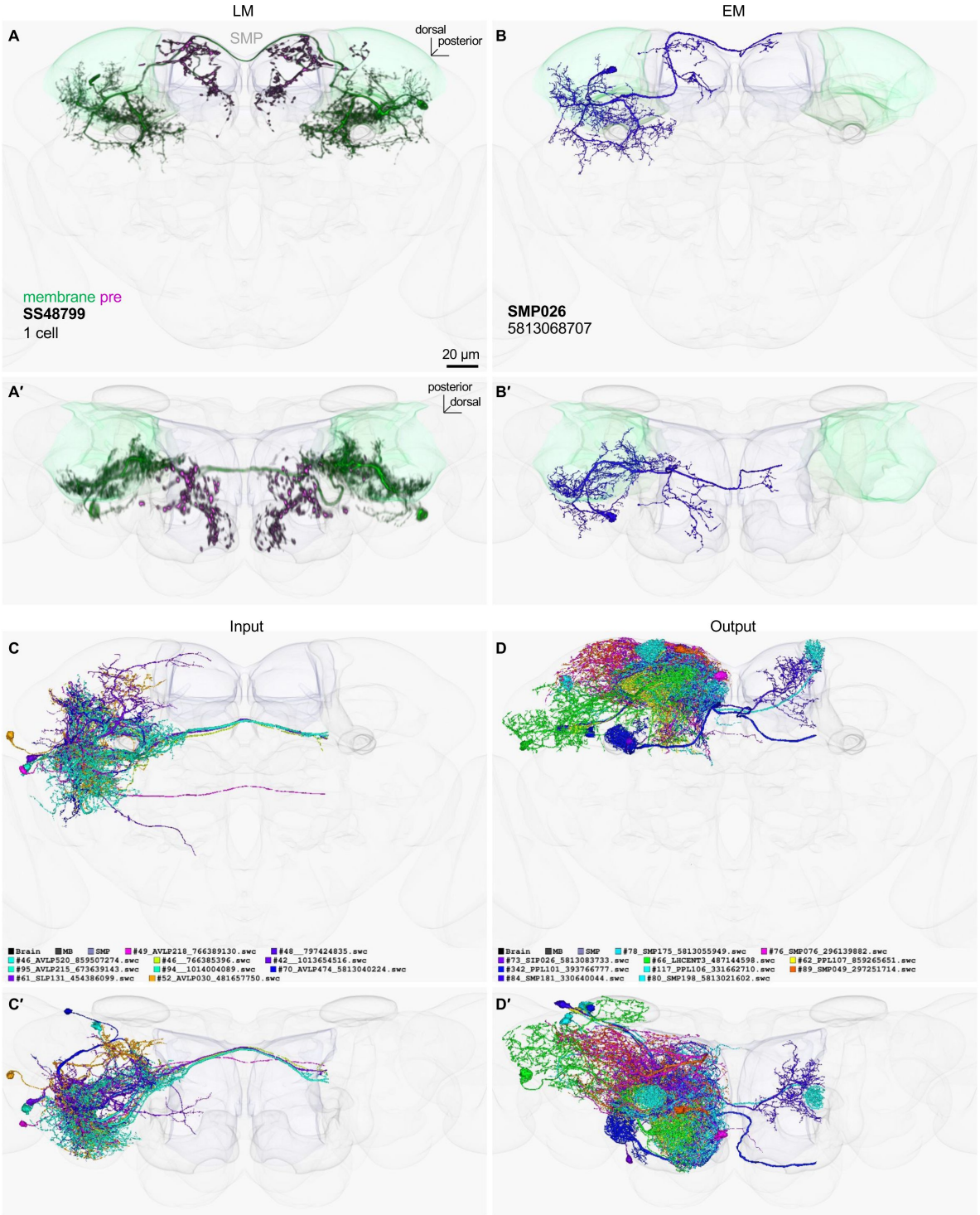

Figure 2-figure supplement 15

LM-EM match of SS48799

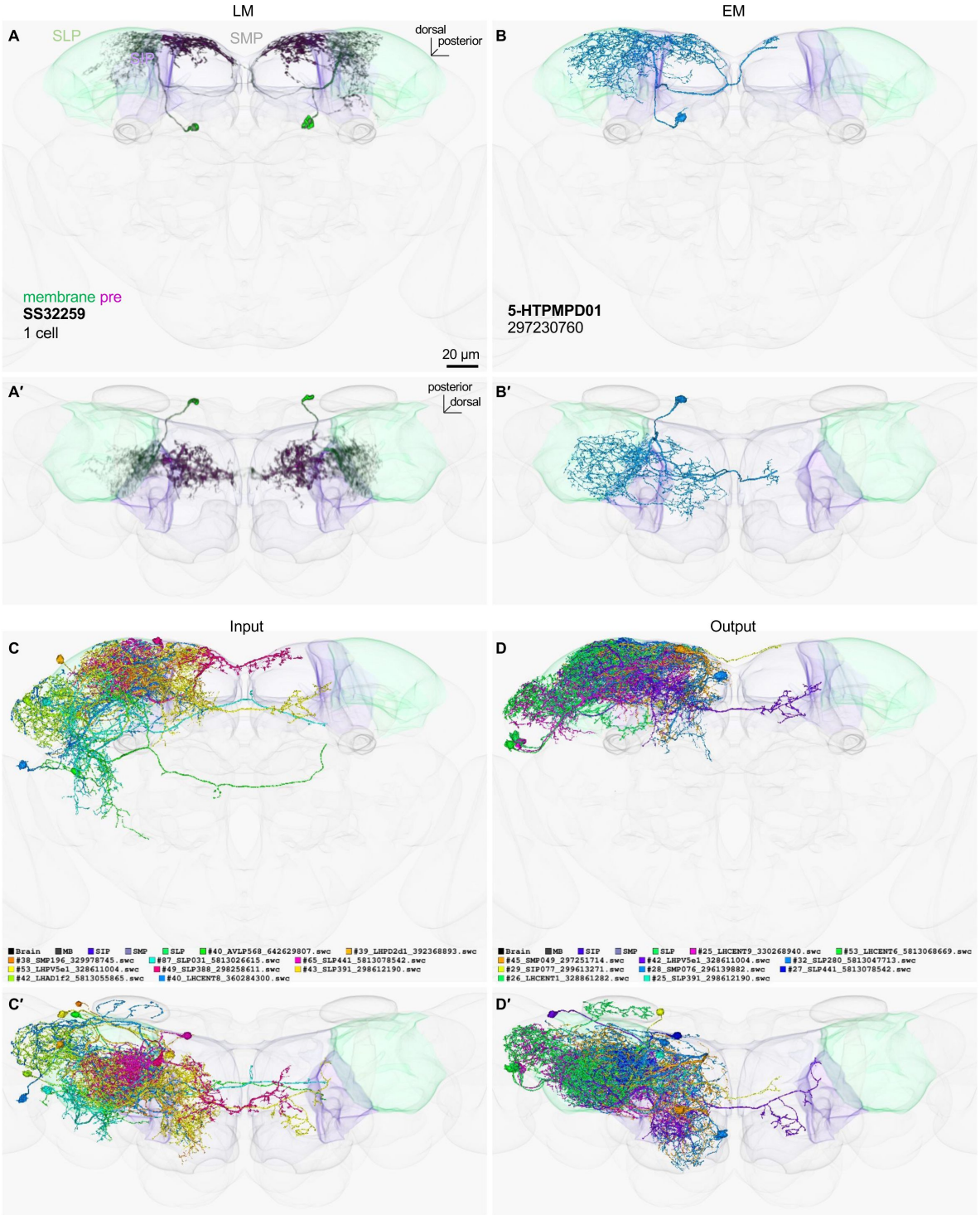

Figure 2-figure supplement 16

LM-EM match of SS32259

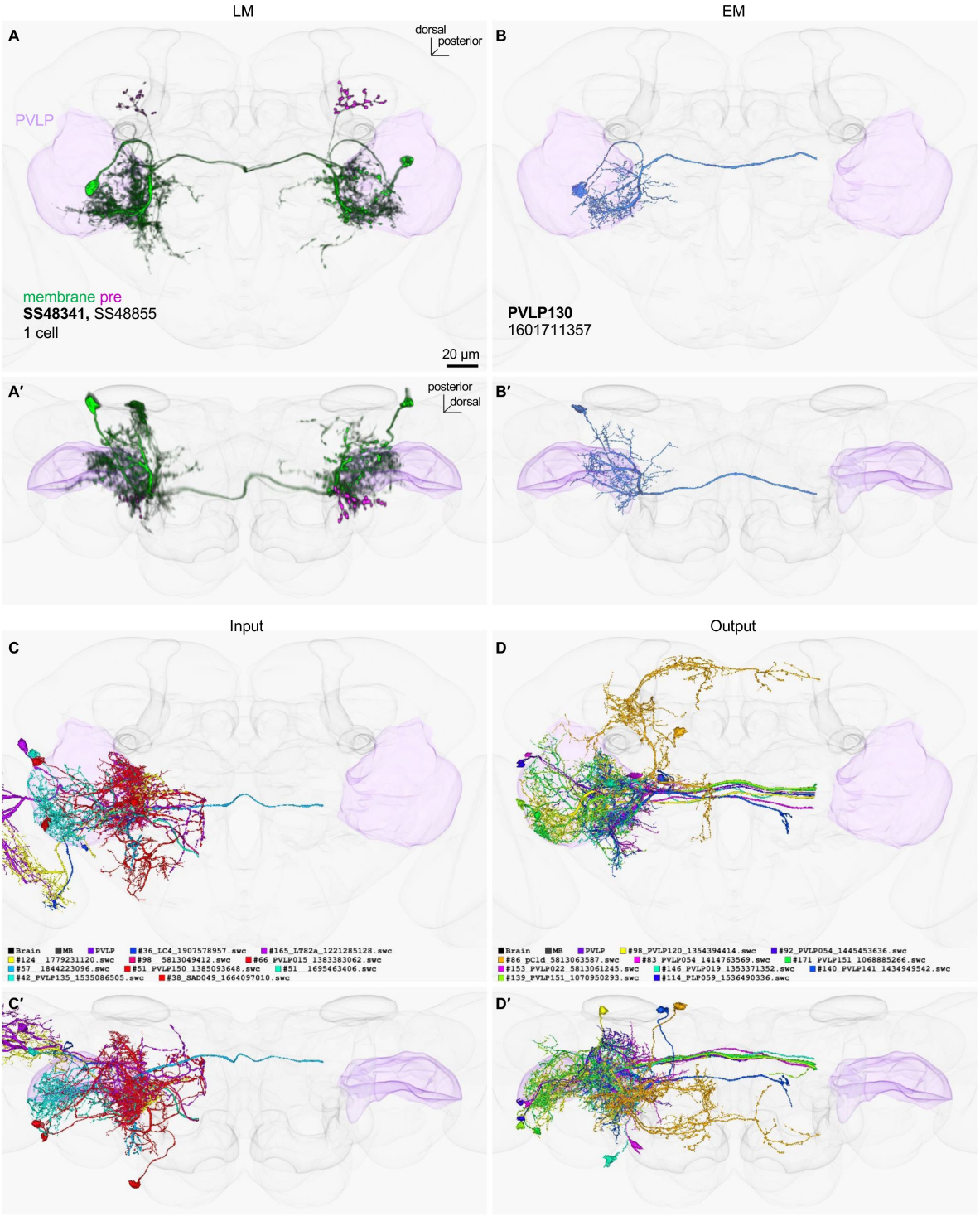

Figure 2-figure supplement 17

LM-EM match of SS48341

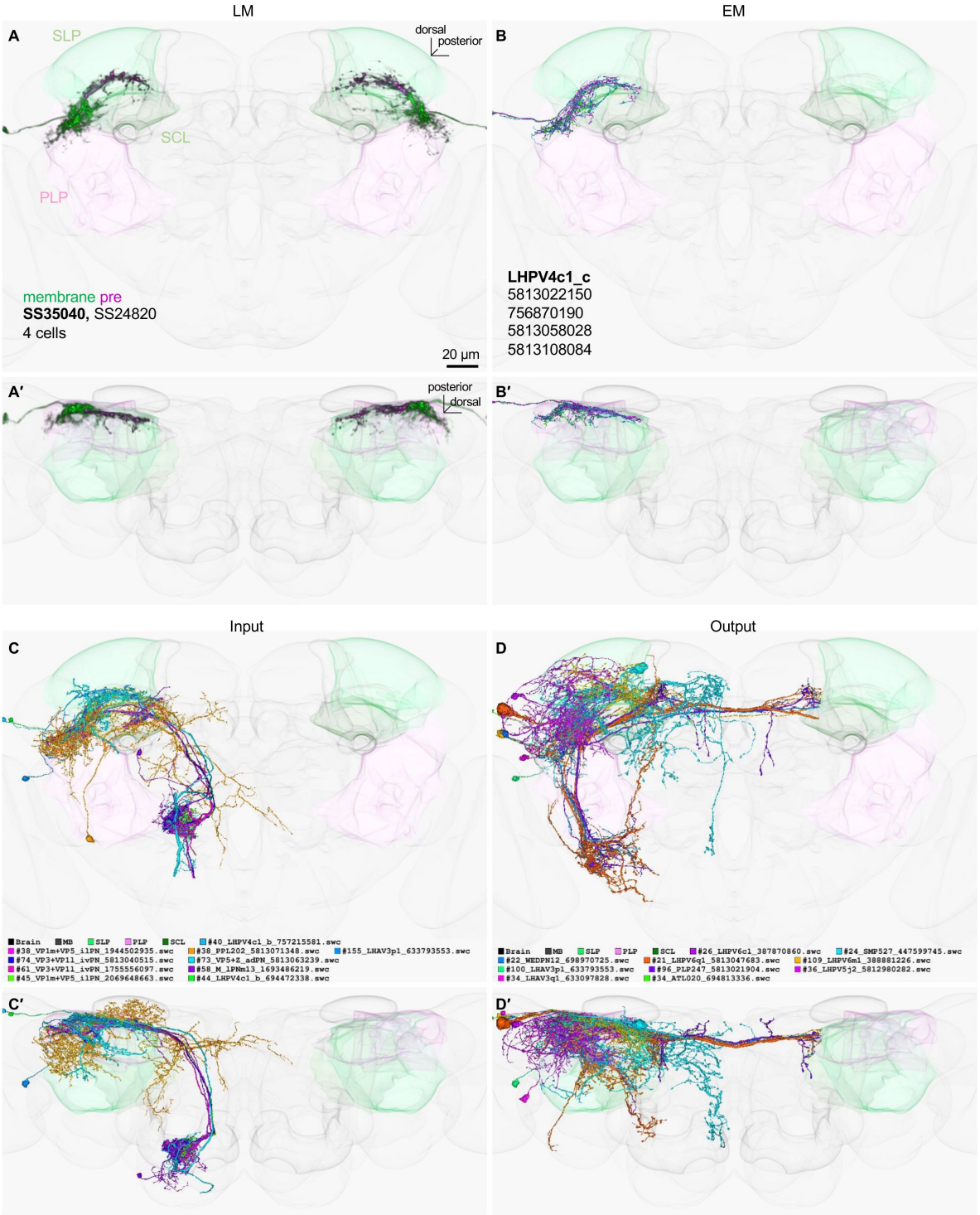

Figure 2-figure supplement 18

LM-EM match of SS35040

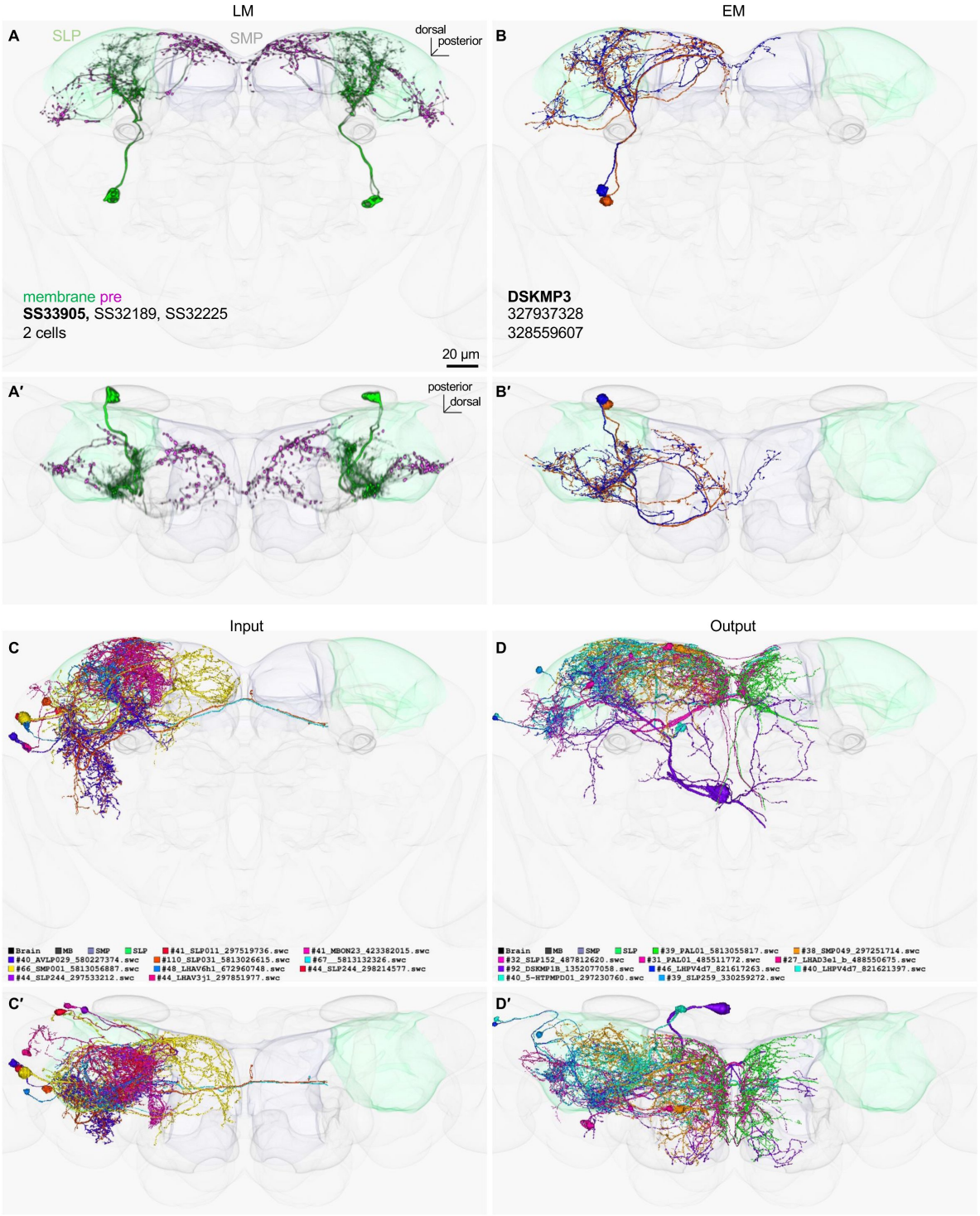

Figure 2-figure supplement 19

LM-EM match of SS33905

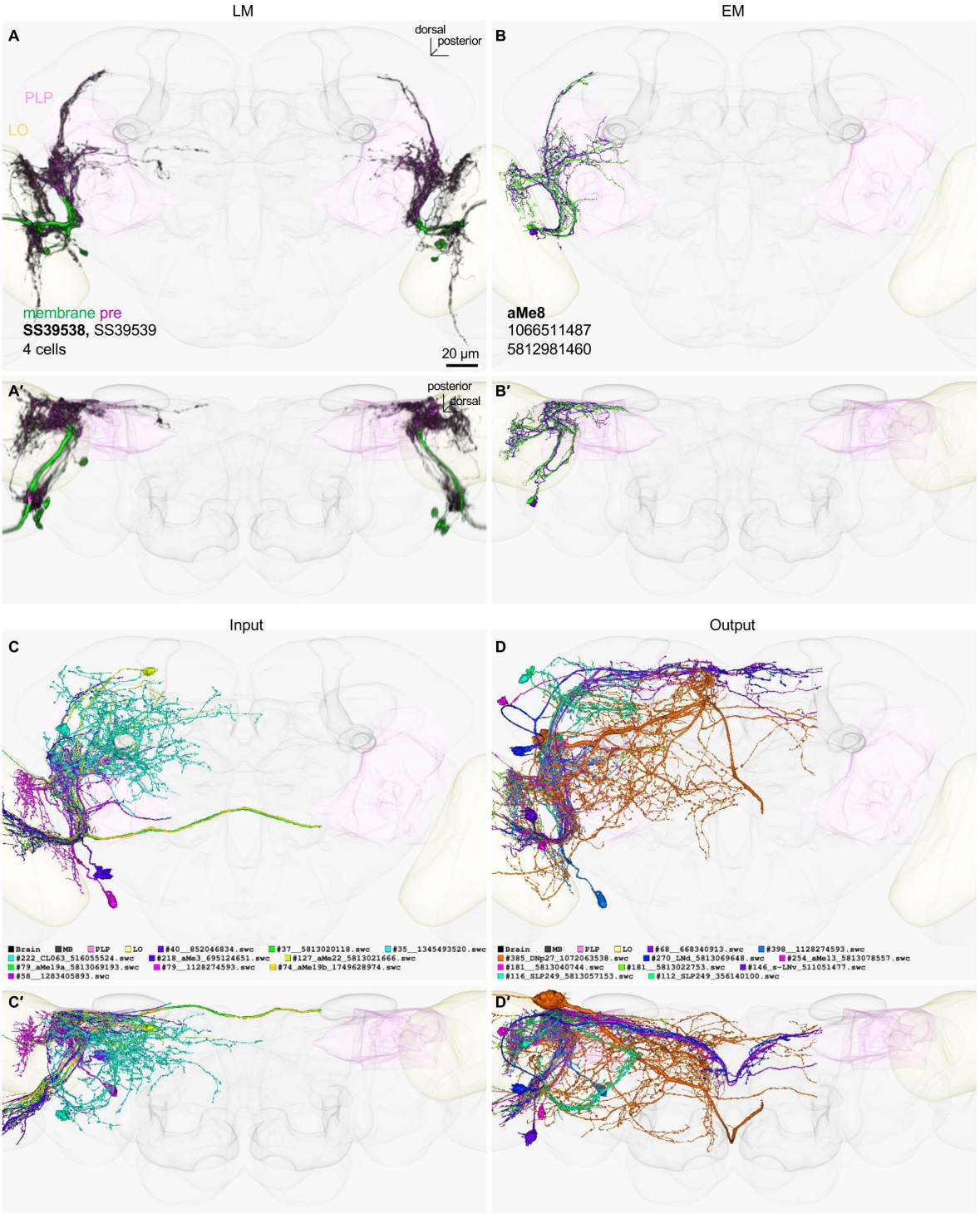

Figure 2-figure supplement 20

LM-EM match of SS39538

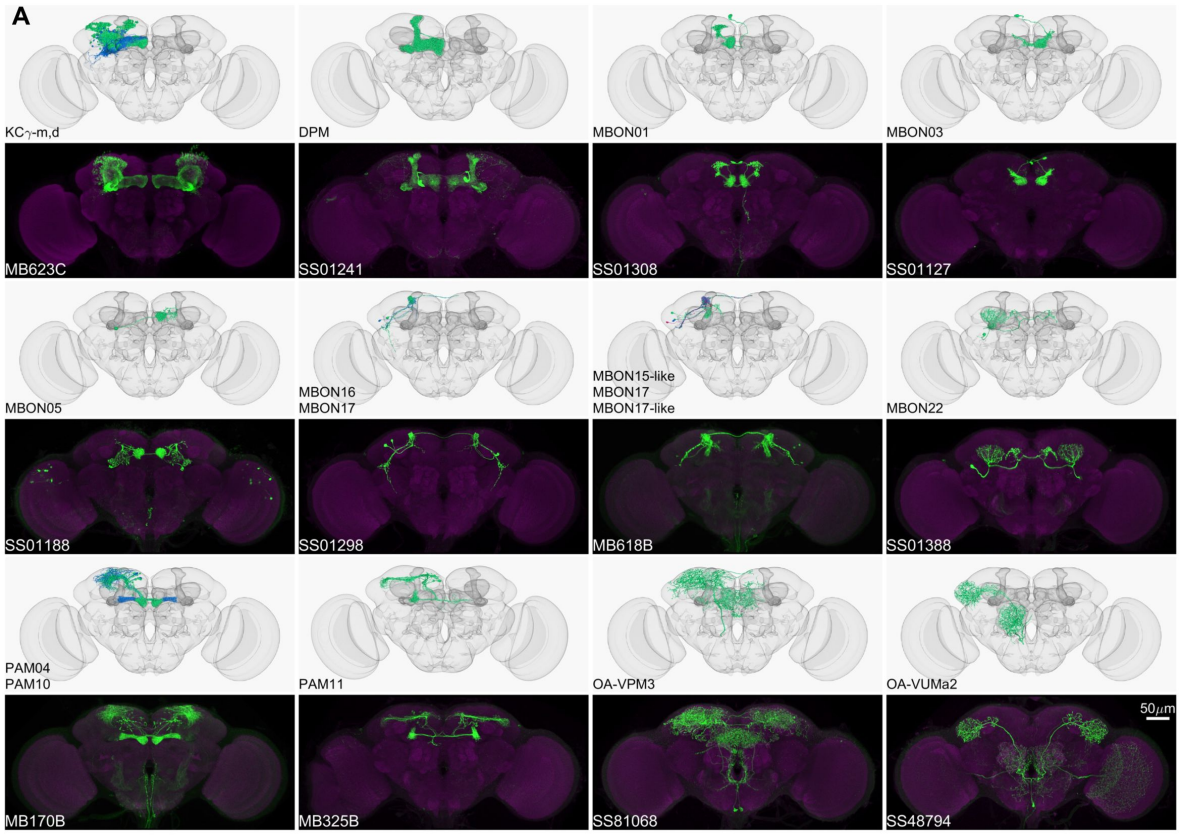

B

MB cell types	Covered cell types	Total cell types	Missed cell types
Intrinsic neurons (excluding KCs)	1	2	APL
MBONs	33	37	MBON24-25, 27, 34
DANs	18	23	PPL102, 201-202, PAM09,15
Other modulatory	6	6	
Total	58	68	

Figure 3-figure supplement 1

New or improved drivers for MB cell types

(A) Confocal images and matched EM cell types. CsChrimson-mVenus (green); Brp (magenta).
(B) Summary of within-MB split-GAL4 coverage. See Supplementary File 4 for details.

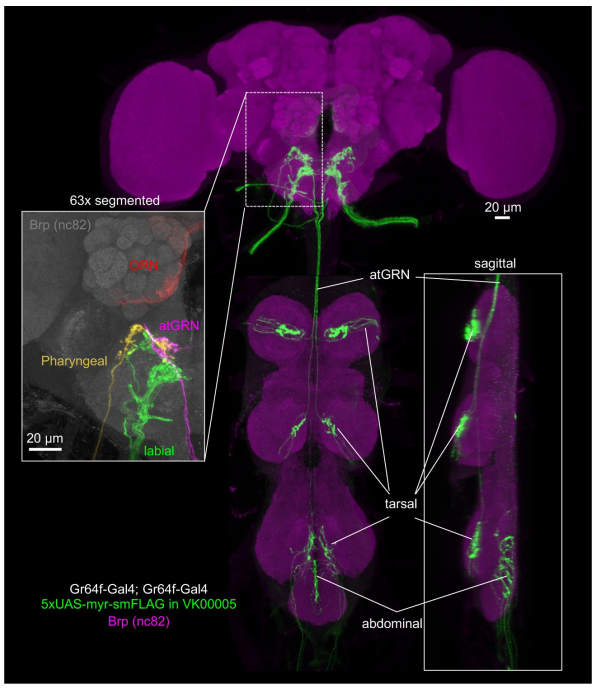

Figure 7-figure supplement 1

Expression pattern of Gr64f-Gal4

Expression pattern of Gr64f-GAL4 driving 5xUAS-myr-smFLAG in VK0005 in the brain and VNC (green) with neuropil counterstaining of Brp (magenta). The line used contains two copies of Gr64f-Gal4, with one copy on the second and one copy on the third chromosome. The insert on the left shows a magnified view of each cell type in different colors. The insert on the right shows a sagittal view of the VNC.

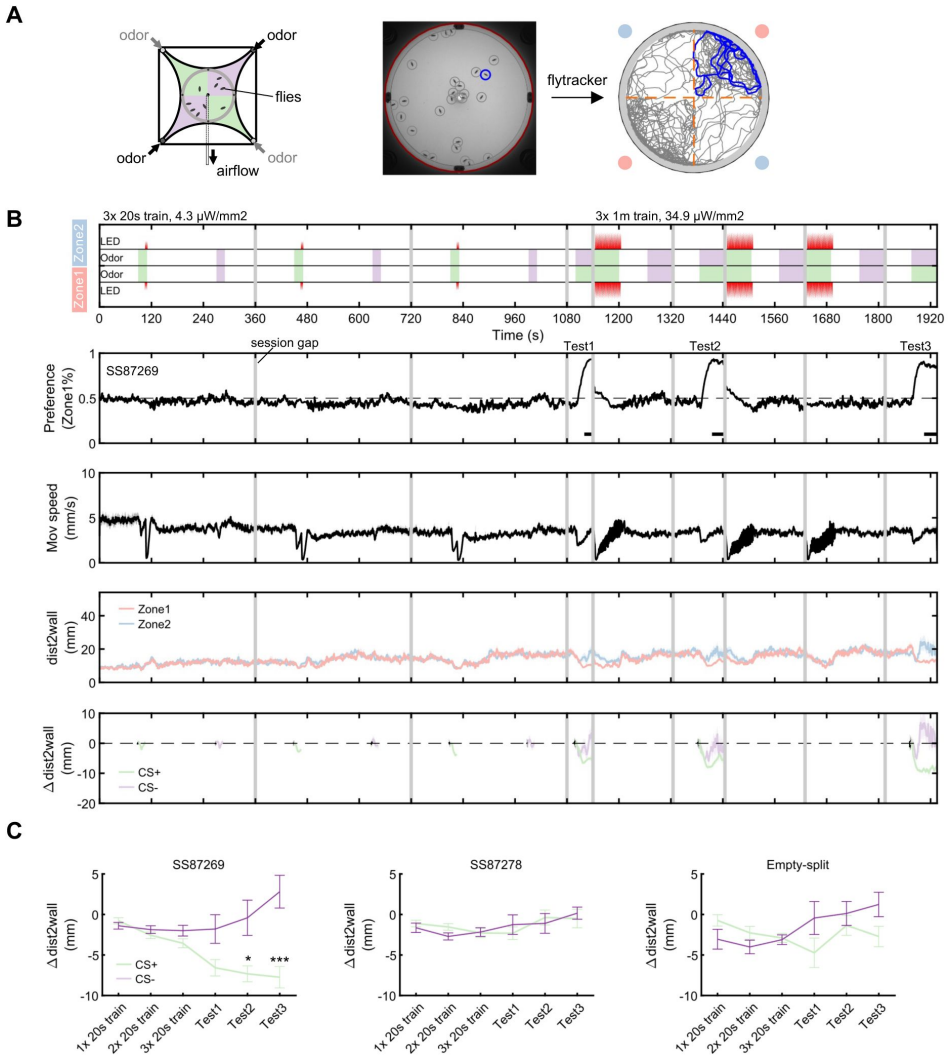

Figure 8-figure supplement 1

Olfactory arena learning experiment, fly tracking and data analysis

(A) To test associative learning in the olfactory circular arena, two different odors (A and B) were delivered to interleaved quadrants, defined as Zone 1 and Zone 2. The trajectory of an example fly during the odor choice period after automatic tracking of the experiment movies is shown.
(B) Experiment protocol for learning as in **Figure 8B**. Odors (green-A, purple-B) and LED delivered to the two zones are indicated. The transition between sessions that were not video-recorded are masked by gray. In the example data, the odor ethyl lactate (EL) served as CS+ and was paired with CsChrimson-activation of SS87269, while the other odor pentyl acetate (PA) served as CS- and was unpaired. The full data set included an additional reciprocal group with PA as CS+ and EL as CS-.
(C) Upwind displacement towards CS+ and CS- during the experiment was quantified by a change in the mean distance-to-wall for all flies (airflow came from the periphery of the arena and was drawn out in the center). In addition to the three testing periods (0-20 second after odor onset), the mean distance-to-wall during training in the odor periods before LED onset (0-10 second after odor onset) were also quantified. “CS+” and “CS-” groups were compared with a multi-comparison t-test with Bonferroni-Dunn’s correction. *, P<0.05; ***, P<0.001.

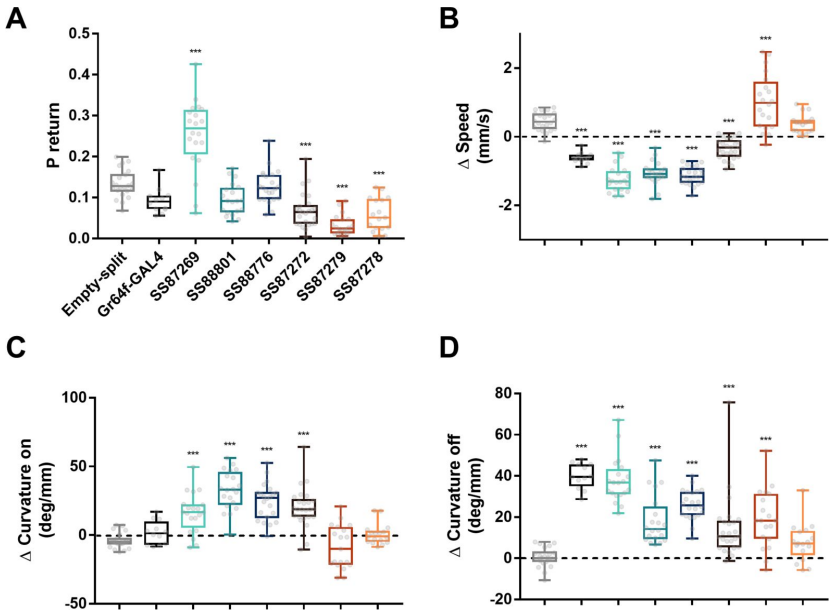

Figure 8-figure supplement 2

Summary data of Gr64f-split-Gal4 activation phenotypes

The data points during the time bin shown in **Figure 8F**.
(A) Probability of return during the post-activation period.
(B) Change of walking speed during the onset of activation period.
(C) Change of curvature during the onset of activation period.
(D) Change of curvature during the post-activation period.
One-way ANOVA followed by Dunnett's multiple comparisons test. ***, P<0.001. Individual data points are shown with minimum, maximum, median, and interquartile ranges.

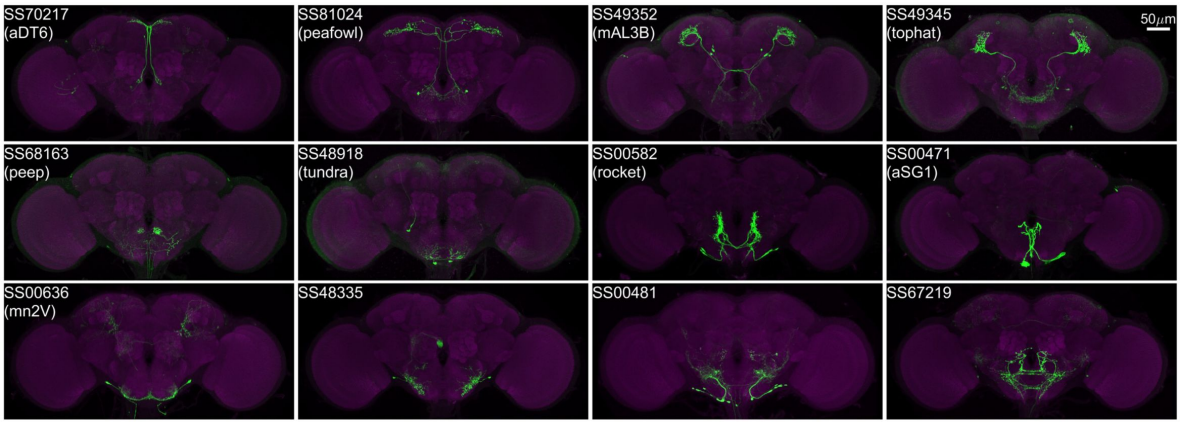

Figure 8-figure supplement 3

Examples of covered SEZ neurons.

(Top two rows) New or improved split-GAL4 drivers for cell types already covered by the SEZ Split-GAL4 Collection (Sterne et al., 2021). (Bottom row) Split-GAL4 drivers for cell types not included in the SEZ Split-GAL4 Collection. Cell types are from Hemibrain 1.2.1, Sterne 2021 or mn2V (McKellar et al., 2020).

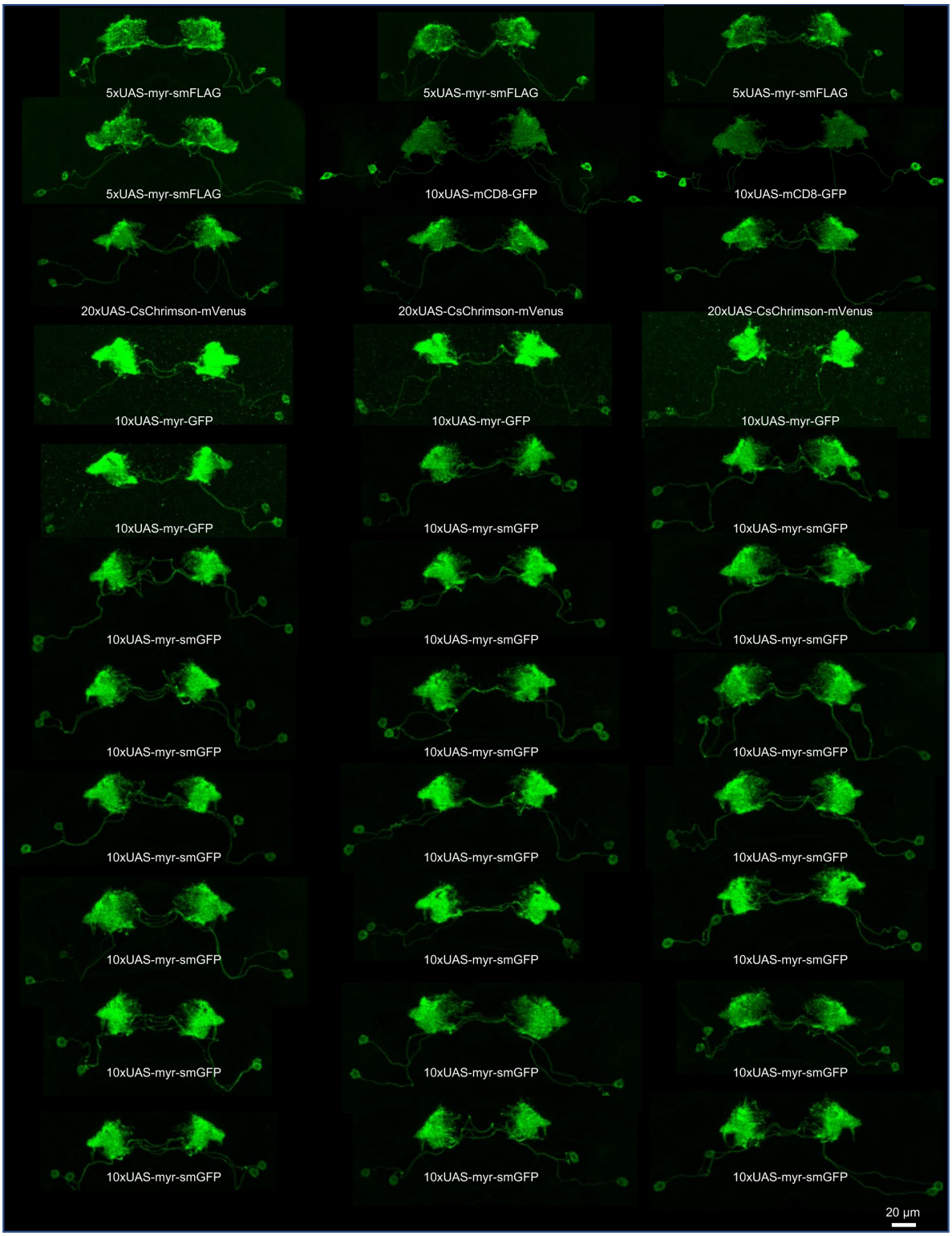

Figure 11-figure supplement 1

MB083C invariantly label two MBONs

Maximum intensity projection images of individual samples are shown. Note that two somas in each hemisphere are labeled in all samples. Reporters used are indicated in each panel.

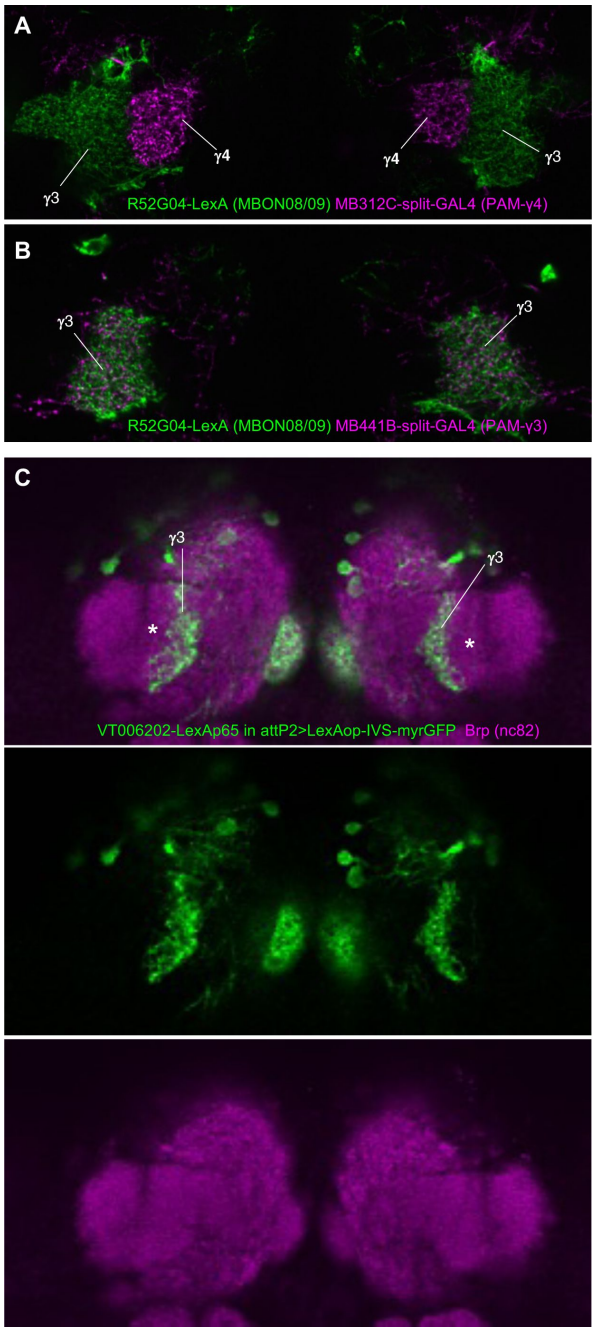

Figure 11-figure supplement 2

Subdivisions of medial and lateral γ3 compartments

(A) Overlay between the dendrites of MBON08/09 and axons of PAM-γ4 DANs.
(B) Overlay between the dendrites of MBON08/09 and axons of PAM-γ3 DANs.
(C) A subset of PAM-γ3 arborizes in the medial part of the γ3 compartment. Asterisk indicates the position of the lateral γ3 that is not labeled in this line.

References

Amin H, Apostolopoulou AA, Suárez-Grimalt R, Vrontou E, Lin AC (2020) **Localized inhibition in the Drosophila mushroom body** *Elife* **9** https://doi.org/10.7554/eLife.56954

Aso Y *et al.* (2014) **The neuronal architecture of the mushroom body provides a logic for associative learning** *Elife* **3**

Aso Y *et al.* (2019) **Nitric oxide acts as a cotransmitter in a subset of dopaminergic neurons to diversify memory dynamics** *Elife* **8** https://doi.org/10.7554/eLife.49257

Aso Y, Rubin GM (2016) **Dopaminergic neurons write and update memories with cell-type-specific rules** *Elife* **5** https://doi.org/10.7554/eLife.16135

Aso Y *et al.* (2014) **Mushroom body output neurons encode valence and guide memory-based action selection in Drosophila** *Elife* **3**

Aso Y, Siwanowicz I, Bräcker L, Ito K, Kitamoto T, Tanimoto H (2010) **Specific dopaminergic neurons for the formation of labile aversive memory** *Curr Biol* **20**:1445–1451

Aso Y, Yamada D, Bushey D, Hibbard KL, Sammons M, Otsuna H, Shuai Y, Hige T (2023) **Neural circuit mechanisms for transforming learned olfactory valences into wind-oriented movement** *Elife* **12** https://doi.org/10.7554/eLife.85756

Awata H, Takakura M, Kimura Y, Iwata I, Masuda T, Hirano Y (2019) **The neural circuit linking mushroom body parallel circuits induces memory consolidation in** *Proc Natl Acad Sci U S A* **116**:16080–16085

Bates AS *et al.* (2020) **Complete Connectomic Reconstruction of Olfactory Projection Neurons in the Fly Brain** *Curr Biol* **30**:3183–3199

Berry JA, Phan A, Davis RL (2018) **Dopamine Neurons Mediate Learning and Forgetting through Bidirectional Modulation of a Memory Trace** *Cell Rep* **25**:651–662

Bogovic JA *et al.* (2020) **An unbiased template of the Drosophila brain and ventral nerve cord** *PLoS One* **15**

Bohra AA, Kallman BR, Reichert H, VijayRaghavan K (2018) **Identification of a Single Pair of Interneurons for Bitter Taste Processing in the Drosophila Brain** *Curr Biol* **28**:847–858

Burke CJ, Huetteroth W, Owald D, Perisse E, Krashes MJ, Das G, Gohl D, Silies M, Certel S, Waddell S (2012) **Layered reward signalling through octopamine and dopamine in Drosophila** *Nature* **492**:433–437

Chen H-L, Motevalli D, Stern U, Yang C-H (2022) **A functional division of sweet taste neurons that is value-based and task-specific** *Proc Natl Acad Sci U S A* **119** https://doi.org/10.1073/pnas.2110158119

Chiang A-S *et al.* (2011) **Three-dimensional reconstruction of brain-wide wiring networks in Drosophila at single-cell resolution** *Curr Biol* **21**:1–11

Claridge-Chang A, Roorda RD, Vrontou E, Sjulson L, Li H, Hirsh J, Miesenböck G (2009) **Writing memories with light-addressable reinforcement circuitry** *Cell* **139**:405–415

Corfas RA, Sharma T, Dickinson MH (2019) **Diverse Food-Sensing Neurons Trigger Idiothetic Local Search in Drosophila** *Curr Biol* **29**:1660–1668

Costa M, Manton JD, Ostrovsky AD, Prohaska S, Jefferis GSXE (2016) **NBLAST: Rapid, Sensitive Comparison of Neuronal Structure and Construction of Neuron Family Databases** *Neuron* **91**:293–311

Dahanukar A, Lei Y-T, Kwon JY, Carlson JR (2007) **Two Gr genes underlie sugar reception in Drosophila** *Neuron* **56**:503–516

Datta SR, Vasconcelos ML, Ruta V, Luo S, Wong A, Demir E, Flores J, Balonze K, Dickson BJ, Axel R (2008) **The Drosophila pheromone cVA activates a sexually dimorphic neural circuit** *Nature* **452**:473–477

Davis FP, Nern A, Picard S, Reiser MB, Rubin GM, Eddy SR, Henry GL (2020) **A genetic, genomic, and computational resource for exploring neural circuit function** *Elife* **9** https://doi.org/10.7554/eLife.50901

Davis RL (2023) **Learning and memory using Drosophila melanogaster: a focus on advances made in the fifth decade of research** *Genetics* https://doi.org/10.1093/genetics/iyad085

de Bivort B *et al.* (2022) **Precise Quantification of Behavioral Individuality From 80 Million Decisions Across 183,000 Flies** *Front Behav Neurosci* **16**

Deere JU, Sarkissian AA, Yang M, Uttley HA, Martinez Santana N, Nguyen L, Ravi K, Devineni AV (2023) **Selective integration of diverse taste inputs within a single taste modality** *Elife* **12** https://doi.org/10.7554/eLife.84856

Dionne H, Hibbard KL, Cavallaro A, Kao J-C, Rubin GM (2018) **Genetic Reagents for Making Split-GAL4 Lines in** *Genetics* **209**:31–35

Dolan M-J *et al.* (2018) **Communication from Learned to Innate Olfactory Processing Centers Is Required for Memory Retrieval in Drosophila** *Neuron* **100**:651–668

Dolan M-J *et al.* (2019) **Neurogenetic dissection of the Drosophila lateral horn reveals major outputs, diverse behavioural functions, and interactions with the mushroom body** *Elife* **8** https://doi.org/10.7554/eLife.43079

Dorkenwald S *et al.* (2023) **Neuronal wiring diagram of an adult brain** *bioRxiv* https://doi.org/10.1101/2023.06.27.546656

Dunipace L, Meister S, McNealy C, Amrein H (2001) **Spatially restricted expression of candidate taste receptors in the Drosophila gustatory system** *Curr Biol* **11**:822–835

Eckstein N *et al.* (2023) **Neurotransmitter Classification from Electron Microscopy Images at Synaptic Sites in Drosophila Melanogaster** *bioRxiv* https://doi.org/10.1101/2020.06.12.148775

Eichler K *et al.* (2017) **The complete connectome of a learning and memory centre in an insect brain** *Nature* **548**:175–182

Enjin A, Zaharieva EE, Frank DD, Mansourian S, Suh GSB, Gallio M, Stensmyr MC (2016) **Humidity Sensing in Drosophila** *Curr Biol* **26**:1352–1358

Eschbach C *et al.* (2020) **Recurrent architecture for adaptive regulation of learning in the insect brain** *Nat Neurosci* **23**:544–555

Eyjolfsdottir E, Branson S, Burgos-Artizzu XP, Hoopfer ED, Schor J, Anderson DJ, Perona P (2014) **Detecting Social Actions of Fruit FliesComputer Vision – ECCV 2014** :772–787

Felsenberg J, Barnstedt O, Cognigni P, Lin S, Waddell S (2017) **Re-evaluation of learned information in Drosophila** *Nature* **544**:240–244

Frank DD, Jouandet GC, Kearney PJ, Macpherson LJ, Gallio M (2015) **Temperature representation in the Drosophila brain** *Nature* **519**:358–361

Fujii S, Yavuz A, Slone J, Jagge C, Song X, Amrein H (2015) **Drosophila sugar receptors in sweet taste perception, olfaction, and internal nutrient sensing** *Curr Biol* **25**:621–627

Gallio M, Ofstad TA, Macpherson LJ, Wang JW, Zuker CS (2011) **The coding of temperature in the Drosophila brain** *Cell* **144**:614–624

Gao R *et al.* (2019) **Cortical column and whole-brain imaging with molecular contrast and nanoscale resolution** *Science* **363** https://doi.org/10.1126/science.aau8302

Haberkern H, Basnak MA, Ahanonu B, Schauder D, Cohen JD, Bolstad M, Bruns C, Jayaraman V (2019) **Visually Guided Behavior and Optogenetically Induced Learning in Head-Fixed Flies Exploring a Virtual Landscape** *Curr Biol* **29**:1647–1659

Hammer M (1993) **An identified neuron mediates the unconditioned stimulus in associative olfactory learning in honeybees** *Nature* **366**:59–63

Hampel S, Franconville R, Simpson JH, Seeds AM (2015) **A neural command circuit for grooming movement control** *Elife* **4**

Handler A, Graham TGW, Cohn R, Morantte I, Siliciano AF, Zeng J, Li Y, Ruta V (2019) **Distinct Dopamine Receptor Pathways Underlie the Temporal Sensitivity of Associative Learning** *Cell* https://doi.org/10.1016/j.cell.2019.05.040

Harris DT, Kallman BR, Mullaney BC, Scott K (2015) **Representations of Taste Modality in the Drosophila Brain** *Neuron* **86**:1449–1460

Hattori D, Aso Y, Swartz KJ, Rubin GM, Abbott LF, Axel R (2017) **Representations of Novelty and Familiarity in a Mushroom Body Compartment** *Cell* **169**:956–969

Hige T, Aso Y, Modi MN, Rubin GM, Turner GC (2015) **Heterosynaptic Plasticity Underlies Aversive Olfactory Learning in Drosophila** *Neuron* **88**:985–998

Hige T, Aso Y, Rubin GM, Turner GC (2015) **Plasticity-driven individualization of olfactory coding in mushroom body output neurons** *Nature* **526**:258–262

Hiroi M, Marion-Poll F, Tanimura T. (2002) **Differentiated Response to Sugars among Labellar Chemosensilla in Drosophila** *jzoo*

Huetteroth W, Perisse E, Lin S, Klappenbach M, Burke C, Waddell S (2015) **Sweet taste and nutrient value subdivide rewarding dopaminergic neurons in Drosophila** *Curr Biol* **25**:751–758

Hwang RY, Zhong L, Xu Y, Johnson T, Zhang F, Deisseroth K, Tracey WD (2007) **Nociceptive Neurons Protect Drosophila Larvae from Parasitoid Wasps** *Curr Biol* **17**:2105–2116

Ichinose T, Aso Y, Yamagata N, Abe A, Rubin GM, Tanimoto H (2015) **Reward signal in a recurrent circuit drives appetitive long-term memory formation** *Elife* **4**

Jenett A *et al.* (2012) **A GAL4-driver line resource for Drosophila neurobiology** *Cell Rep* **2**:991–1001

Jiang L, Litwin-Kumar A (2021) **Models of heterogeneous dopamine signaling in an insect learning and memory center** *PLoS Comput Biol* **17**

Joseph RM, Heberlein U (2012) **Tissue-specific activation of a single gustatory receptor produces opposing behavioral responses in Drosophila** *Genetics* **192**:521–532

Kabra M, Lee A, Robie A, Egnor R, Huston S, Rodriguez IF, Edwards A, Branson K (2022) **APT: Animal Part Tracker v0.3.4** *Zenodo* https://doi.org/10.5281/ZENODO.6366082

Kanzaki R, Ikeda A, Shibuya T (1994) **[引用] Morphology and physiology of pheromone-triggered flip-flop descending interneurons of the male silkworm moth, Bombyx mori** *J Comp Physiol A*

Kim H, Kirkhart C, Scott K (2017) **Long-range projection neurons in the taste circuit of Drosophila** *Elife* **6** https://doi.org/10.7554/eLife.23386

Kirkhart C, Scott K (2015) **Gustatory learning and processing in the Drosophila mushroom bodies** *J Neurosci* **35**:5950–5958

Klapoetke NC *et al.* (2014) **Independent optical excitation of distinct neural populations** *Nat Methods* **11**:338–346

König C, Khalili A, Niewalda T, Gao S, Gerber B (2019) **An optogenetic analogue of second-order reinforcement in Drosophila** *Biol Lett* **15**

Li F *et al.* (2020) **The connectome of the adult Drosophila mushroom body provides insights into function** *Elife* **9** https://doi.org/10.7554/eLife.62576

Lin H-H, Chu L-A, Fu T-F, Dickson BJ, Chiang A-S (2013) **Parallel neural pathways mediate CO2 avoidance responses in Drosophila** *Science* **340**:1338–1341

Lin H-H, Lai JS-Y, Chin A-L, Chen Y-C, Chiang A-S (2007) **A Map of Olfactory Representation in the Drosophila Mushroom Body** *Cell* **128**:1205–1217

Liu C, Plaçais P-Y, Yamagata N, Pfeiffer BD, Aso Y, Friedrich AB, Siwanowicz I, Rubin GM, Preat T, Tanimoto H (2012) **A subset of dopamine neurons signals reward for odour memory in Drosophila** *Nature* https://doi.org/10.1038/nature11304

Liu WW, Mazor O, Wilson RI (2015) **Thermosensory processing in the Drosophila brain** *Nature* **519**:353–357

Luan H, Diao F, Scott RL, White BH (2020) **The Drosophila Split Gal4 System for Neural Circuit Mapping** *Frontiers in Neural Circuits* https://doi.org/10.3389/fncir.2020.603397

Luan H, Peabody NC, Vinson CR, White BH (2006) **Refined spatial manipulation of neuronal function by combinatorial restriction of transgene expression** *Neuron* **52**:425–436

Mao Z, Davis RL (2009) **Eight different types of dopaminergic neurons innervate the Drosophila mushroom body neuropil: anatomical and physiological heterogeneity** *Front Neural Circuits* **3**

Marin EC *et al.* (2020) **Connectomics Analysis Reveals First-, Second-, and Third-Order Thermosensory and Hygrosensory Neurons in the Adult Drosophila Brain** *Curr Biol* **30**:3167–3182

Martinez-Cervantes J, Shah P, Phan A, Cervantes-Sandoval I (2022) **Higher-order unimodal olfactory sensory preconditioning in** *Elife* **11** https://doi.org/10.7554/eLife.79107

Masek P, Worden K, Aso Y, Rubin GM, Keene AC (2015) **A dopamine-modulated neural circuit regulating aversive taste memory in Drosophila** *Curr Biol* **25**:1535–1541

Masse NY, Cachero S, Ostrovsky AD, Jefferis GSXE (2012) **A mutual information approach to automate identification of neuronal clusters in Drosophila brain images** *Front Neuroinform* **6**

Matheson AMM, Lanz AJ, Medina AM, Licata AM, Currier TA, Syed MH, Nagel KI (2022) **A neural circuit for wind-guided olfactory navigation** *Nat Commun* **13**:1–21

McCurdy LY, Sareen P, Davoudian PA, Nitabach MN (2021) **Dopaminergic mechanism underlying reward-encoding of punishment omission during reversal learning in Drosophila** *Nat Commun* **12**

McKellar CE, Siwanowicz I, Dickson BJ, Simpson JH (2020) **Controlling motor neurons of every muscle for fly proboscis reaching** *Elife* **9**

Meissner GW *et al.* (2023) **Meissner GW, Nern A, Dorman Z, DePasquale GM, Forster K, Gibney T, Hausenfluck JH, He Y, Iyer NA, Jeter J, Johnson L, Johnston RM, Lee K, Melton B, Yarbrough B, Zugates CT, Clements J, Goina C, Otsuna H, Rokicki K, Svirskas RR, Aso Y, Card GM, Dickson BJ, Ehrhardt E, Goldammer J, Ito M, Kainmueller D, Korff W, Mais L, Minegishi R, Namiki S, Rubin GM, Sterne GR, Wolff T, Malkesman O. 2023. A searchable image resource of Drosophila GAL4 driver expression patterns with single neuron resolution. doi:10.7554/eLife.80660** *A searchable image resource of Drosophila GAL4 driver expression patterns with single neuron resolution* https://doi.org/10.7554/eLife.80660

Miyamoto T, Slone J, Song X, Amrein H (2012) **A fructose receptor functions as a nutrient sensor in the Drosophila brain** *Cell* **151**:1113–1125

Miyazaki T, Lin T-Y, Ito K, Lee C-H, Stopfer M (2015) **A gustatory second-order neuron that connects sucrose-sensitive primary neurons and a distinct region of the gnathal ganglion in the Drosophila brain** *J Neurogenet* **29**:144–155

Modi MN, Shuai Y, Turner GC (2020) **The Drosophila Mushroom Body: From Architecture to Algorithm in a Learning Circuit** *Annu Rev Neurosci* **43**:465–484

Namiki S, Dickinson MH, Wong AM, Korff W, Card GM (2018) **Namiki S, Dickinson MH, Wong AM, Korff W, Card GM. 2018. The functional organization of descending sensory-motor pathways in Drosophila. doi:10.7554/eLife.34272** https://doi.org/10.7554/eLife.34272

Nern A, Pfeiffer BD, Rubin GM (2015) **Optimized tools for multicolor stochastic labeling reveal diverse stereotyped cell arrangements in the fly visual system** *Proc Natl Acad Sci U S A* **112**:E2967–76

Ohyama T *et al.* (2015) **A multilevel multimodal circuit enhances action selection in Drosophila** *Nature* **520**:633–639

Otsuna H, Ito M, Kawase T. (2018) **Color depth MIP mask search: a new tool to expedite Split-GAL4 creation** *bioRxiv* https://doi.org/10.1101/318006

Otto N *et al.* (2020) **Input Connectivity Reveals Additional Heterogeneity of Dopaminergic Reinforcement in Drosophila** *Curr Biol* **30**:3200–3211

Owald D, Felsenberg J, Talbot CB, Das G, Perisse E, Huetteroth W, Waddell S (2015) **Activity of defined mushroom body output neurons underlies learned olfactory behavior in Drosophila** *Neuron* **86**:417–427

Park J-H, Kwon JY (2011) **A systematic analysis of Drosophila gustatory receptor gene expression in abdominal neurons which project to the central nervous system** *Mol Cells* **32**:375–381

Pavlowsky A, Schor J, Plaçais P-Y, Preat T (2018) **A GABAergic Feedback Shapes Dopaminergic Input on the Drosophila Mushroom Body to Promote Appetitive Long-Term Memory** *Curr Biol* **28**:1783–1793

Perez-Orive J, Mazor O, Turner GC, Cassenaer S, Wilson RI, Laurent G (2002) **Oscillations and sparsening of odor representations in the mushroom body** *Science* **297**:359–365

Pettersson J (1970) **An Aphid Sex Attractant** *Insect Syst Evol* **1**:63–73

Pfeiffer BD *et al.* (2008) **Tools for neuroanatomy and neurogenetics in Drosophila** *Proc Natl Acad Sci U S A* **105**:9715–9720

Pfeiffer BD, Ngo T-TB, Hibbard KL, Murphy C, Jenett A, Truman JW, Rubin GM (2010) **Refinement of tools for targeted gene expression in Drosophila** *Genetics* **186**:735–755

Pfeiffer BD, Truman JW, Rubin GM (2012) **Using translational enhancers to increase transgene expression in Drosophila** *Proc Natl Acad Sci U S A* **109**:6626–6631

Plaçais P-Y, de Tredern É, Scheunemann L, Trannoy S, Goguel V, Han K-A, Isabel G, Preat T. (2017) **Upregulated energy metabolism in the Drosophila mushroom body is the trigger for long-term memory** *Nat Commun* **8**

Plaza SM, Clements J, Dolafi T, Umayam L, Neubarth NN, Scheffer LK, Berg S (2022) **neuPrint: An open access tool for EM connectomics** *Front Neuroinform* **16**

Rajagopalan AE, Darshan R, Fitzgerald JE, Turner GC. (2022) **Expectation-based learning rules underlie dynamic foraging in Drosophila** *bioRxiv* https://doi.org/10.1101/2022.05.24.493252

Rodrigues V, Siddiqi O (1978) **Genetic analysis of chemosensory pathway** *Proceedings / Indian Academy of Sciences* **87**:147–160

Rubin GM, Aso Y. (2023) **New genetic tools for mushroom body output neurons in Drosophila** *bioRxiv* https://doi.org/10.1101/2023.06.23.546330

Saumweber T *et al.* (2018) **Functional architecture of reward learning in mushroom body extrinsic neurons of larval Drosophila** *Nat Commun* **9**

Sayin S *et al.* (2019) **A Neural Circuit Arbitrates between Persistence and Withdrawal in Hungry Drosophila** *Neuron* **104**:544–558

Scaplen KM, Talay M, Fisher JD, Cohn R, Sorkaç A, Aso Y, Barnea G, Kaun KR (2021) **Transsynaptic mapping of Drosophila mushroom body output neurons** *Elife* **10** https://doi.org/10.7554/eLife.63379

Scheffer LK *et al.* (2020) **A connectome and analysis of the adult central brain** *Elife* **9** https://doi.org/10.7554/eLife.57443

Schindelin J *et al.* (2012) **Fiji: an open-source platform for biological-image analysis** *Nat Methods* **9**:676–682

Schlegel P *et al.* (2023) **Whole-brain annotation and multi-connectome cell typing quantifies circuit stereotypy in Drosophila** *bioRxiv* https://doi.org/10.1101/2023.06.27.546055

Schretter CE *et al.* (2020) **Cell types and neuronal circuitry underlying female aggression in Drosophila** *eLife* https://doi.org/10.7554/elife.58942

Schroll C *et al.* (2006) **Light-induced activation of distinct modulatory neurons triggers appetitive or aversive learning in Drosophila larvae** *Curr Biol* **16**:1741–1747

Schwaerzel M, Monastirioti M, Scholz H, Friggi-Grelin F, Birman S, Heisenberg M (2003) **Dopamine and octopamine differentiate between aversive and appetitive olfactory memories in Drosophila** *J Neurosci* **23**:10495–10502

Shannon P, Markiel A, Ozier O, Baliga NS, Wang JT, Ramage D, Amin N, Schwikowski B, Ideker T (2003) **Cytoscape: a software environment for integrated models of biomolecular interaction networks** *Genome Res* **13**:2498–2504

Shimono K, Fujimoto A, Tsuyama T, Yamamoto-Kochi M, Sato M, Hattori Y, Sugimura K, Usui T, Kimura K-I, Uemura T (2009) **Multidendritic sensory neurons in the adult Drosophila abdomen: origins, dendritic morphology, and segment- and age-dependent programmed cell death** *Neural Dev* **4**

Shuai Y, Hirokawa A, Ai Y, Zhang M, Li W, Zhong Y (2015) **Dissecting neural pathways for forgetting in Drosophila olfactory aversive memory** *Proc Natl Acad Sci U S A* **112**:E6663–72

Shyu W-H, Chiu T-H, Chiang M-H, Cheng Y-C, Tsai Y-L, Fu T-F, Wu T, Wu C-L (2017) **Neural circuits for long-term water-reward memory processing in thirsty Drosophila** *Nat Commun* **8**

Smith MA-Y, Honegger KS, Turner G, de Bivort B. (2022) **Idiosyncratic learning performance in flies** *Biol Lett* **18**

Sterne GR, Otsuna H, Dickson BJ, Scott K (2021) **Classification and genetic targeting of cell types in the primary taste and premotor center of the adult brain** *Elife* **10** https://doi.org/10.7554/eLife.71679

Stocker RF, Lienhard MC, Borst A, Fischbach KF (1990) **Neuronal architecture of the antennal lobe in Drosophila melanogaster** *Cell Tissue Res* **262**:9–34

Strother JA, Wu S-T, Wong AM, Nern A, Rogers EM, Le JQ, Rubin GM, Reiser MB. (2017) **The Emergence of Directional Selectivity in the Visual Motion Pathway of Drosophila** *Neuron* **94**:168–182

Suh GSB, Wong AM, Hergarden AC, Wang JW, Simon AF, Benzer S, Axel R, Anderson DJ (2004) **A single population of olfactory sensory neurons mediates an innate avoidance behaviour in Drosophila** *Nature* **431**:854–859

Takagi S *et al.* (2017) **Divergent Connectivity of Homologous Command-like Neurons Mediates Segment-Specific Touch Responses in Drosophila** *Neuron* **96**:1373–1387

Tanaka NK, Awasaki T, Shimada T, Ito K (2004) **Integration of chemosensory pathways in the Drosophila second-order olfactory centers** *Curr Biol* **14**:449–457

Tanaka NK, Endo K, Ito K (2012) **Organization of antennal lobe-associated neurons in adult Drosophila melanogaster brain** *J Comp Neurol* **520**:4067–4130

Tanaka NK, Tanimoto H, Ito K (2008) **Neuronal assemblies of the Drosophila mushroom body** *J Comp Neurol* **508**:711–755

Thoma V, Knapek S, Arai S, Hartl M, Kohsaka H, Sirigrivatanawong P, Abe A, Hashimoto K, Tanimoto H. (2016) **Functional dissociation in sweet taste receptor neurons between and within taste organs of Drosophila** *Nat Commun* **7**

Ting C-Y, Gu S, Guttikonda S, Lin T-Y, White BH, Lee C-H (2011) **Focusing transgene expression in Drosophila by coupling Gal4 with a novel split-LexA expression system** *Genetics* **188**:229–233

Tirian L, Dickson BJ. (2017) **The VT GAL4, LexA, and split-GAL4 driver line collections for targeted expression in the Drosophila nervous system** *bioRxiv* https://doi.org/10.1101/198648

Truman JW, Price J, Miyares RL, Lee T (2023) **Metamorphosis of memory circuits in Drosophila reveals a strategy for evolving a larval brain** https://doi.org/10.7554/eLife.80594

Tsao C-H, Chen C-C, Lin C-H, Yang H-Y, Lin S (2018) **. mushroom bodies integrate hunger and satiety signals to control innate food-seeking behavior** *Elife* **7** https://doi.org/10.7554/eLife.35264

Turner GC, Bazhenov M, Laurent G (2008) **Olfactory Representations by Drosophila Mushroom Body Neurons** *J Neurophysiol* https://doi.org/10.1152/jn.01283.2007

Tuthill JC, Nern A, Holtz SL, Rubin GM, Reiser MB (2013) **Contributions of the 12 neuron classes in the fly lamina to motion vision** *Neuron* **79**:128–140

Vogt K, Aso Y, Hige T, Knapek S, Ichinose T, Friedrich AB, Turner GC, Rubin GM, Tanimoto H (2016) **Direct neural pathways convey distinct visual information to Drosophila mushroom bodies** *Elife* **5** https://doi.org/10.7554/eLife.14009

Wang K, Wang F, Forknall N, Yang T, Patrick C, Parekh R, Dickson BJ (2021) **Neural circuit mechanisms of sexual receptivity in Drosophila females** *Nature* **589**:577–581

Wang Z, Singhvi A, Kong P, Scott K (2004) **Taste representations in the Drosophila brain** *Cell* **117**:981–991

Wan Y, Otsuna H, Chien C-B, Hansen C (2012) **FluoRender: An Application of 2D Image Space Methods for 3D and 4D Confocal Microscopy Data Visualization in Neurobiology Research** *IEEE Pac Vis Symp* :201–208

Winding M *et al.* (2023) **The connectome of an insect brain** *Science* **379**

Wolff T, Rubin GM (2018) **Neuroarchitecture of the Drosophila central complex: A catalog of nodulus and asymmetrical body neurons and a revision of the protocerebral bridge catalog** *J Comp Neurol* **526**:2585–2611

Wu J-K, Tai C-Y, Feng K-L, Chen S-L, Chen C-C, Chiang A-S (2017) **Long-term memory requires sequential protein synthesis in three subsets of mushroom body output neurons in Drosophila** *Sci Rep* **7**

Wu M, Nern A, Williamson WR, Morimoto MM, Reiser MB, Card GM, Rubin GM (2016) **Visual projection neurons in the lobula link feature detection to distinct behavioral programs** *Elife* **5** https://doi.org/10.7554/eLife.21022

Xie Q *et al.* (2021) **Temporal evolution of single-cell transcriptomes of olfactory projection neurons** *Elife* **10** https://doi.org/10.7554/eLife.63450

Yamada D, Bushey D, Li F, Hibbard KL, Sammons M, Funke J, Litwin-Kumar A, Hige T, Aso Y (2023) **Hierarchical architecture of dopaminergic circuits enables second-order conditioning in Drosophila** *Elife* **12** https://doi.org/10.7554/eLife.79042

Yamagata N, Ichinose T, Aso Y, Plaçais P-Y, Friedrich AB, Sima RJ, Preat T, Rubin GM, Tanimoto H (2015) **Distinct dopamine neurons mediate reward signals for short- and long-term memories** *Proc Natl Acad Sci U S A* **112**:578–583

Yavuz A, Jagge C, Slone J, Amrein H (2014) **A genetic tool kit for cellular and behavioral analyses of insect sugar receptors** *Fly* **8**:189–196

Zhang X, Noyes NC, Zeng J, Li Y, Davis RL (2019) **Aversive Training Induces Both Presynaptic and Postsynaptic Suppression in** *J Neurosci* **39**:9164–9172

Zheng Z *et al.* (2018) **A Complete Electron Microscopy Volume of the Brain of Adult Drosophila melanogaster** *Cell* **174**:730–743

Zheng Z *et al.* (2022) **Structured sampling of olfactory input by the fly mushroom body** *Curr Biol* **32**:3334–3349

Article and author information

Yichun Shuai
Janelia Research Campus, Howard Hughes Medical Institute, 19700 Helix Drive, Ashburn, VA 20147, USA
For correspondence: shuaiy@janelia.hhmi.org
ORCID iD: 0000-0001-9243-425X

Megan Sammons
Janelia Research Campus, Howard Hughes Medical Institute, 19700 Helix Drive, Ashburn, VA 20147, USA, Technion-Israel Institute of Technology, 1 Efron St., Haifa 32000, Israel
ORCID iD: 0000-0003-4516-5928

Gabriella Sterne
Janelia Research Campus, Howard Hughes Medical Institute, 19700 Helix Drive, Ashburn, VA 20147, USA, Department of Biomedical Genetics, University of Rochester Medical Center, Rochester, NY, USA
ORCID iD: 0000-0002-7221-648X

Karen Hibbard
Janelia Research Campus, Howard Hughes Medical Institute, 19700 Helix Drive, Ashburn, VA 20147, USA
ORCID iD: 0000-0002-2001-6099

He Yang
Janelia Research Campus, Howard Hughes Medical Institute, 19700 Helix Drive, Ashburn, VA 20147, USA

Ching-Po Yang
Janelia Research Campus, Howard Hughes Medical Institute, 19700 Helix Drive, Ashburn, VA 20147, USA, Life Sciences Institute, University of Michigan, Ann Arbor, USA

Claire Managan
Janelia Research Campus, Howard Hughes Medical Institute, 19700 Helix Drive, Ashburn, VA 20147, USA

Igor Siwanowicz
Janelia Research Campus, Howard Hughes Medical Institute, 19700 Helix Drive, Ashburn, VA 20147, USA
ORCID iD: 0000-0001-5819-1530

Tzumin Lee
Janelia Research Campus, Howard Hughes Medical Institute, 19700 Helix Drive, Ashburn, VA 20147, USA, Life Sciences Institute, University of Michigan, Ann Arbor, USA
ORCID iD: 0000-0003-0569-0111

Gerald M. Rubin
Janelia Research Campus, Howard Hughes Medical Institute, 19700 Helix Drive, Ashburn, VA 20147, USA
ORCID iD: 0000-0001-8762-8703

Glenn Turner
Janelia Research Campus, Howard Hughes Medical Institute, 19700 Helix Drive, Ashburn, VA 20147, USA
ORCID iD: 0000-0002-5341-2784

Yoshinori Aso
Janelia Research Campus, Howard Hughes Medical Institute, 19700 Helix Drive, Ashburn, VA 20147, USA
For correspondence: asoy@janelia.hhmi.org
ORCID iD: 0000-0002-2939-1688

Copyright

Editors

Reviewing Editor
Albert Cardona
University of Cambridge, Cambridge, United Kingdom

Senior Editor
Albert Cardona
University of Cambridge, Cambridge, United Kingdom

Reviewer #1 (Public Review):

Summary:
The emergence of Drosophila EM connectomes has revealed numerous neurons within the associative learning circuit. However, these neurons are inaccessible for functional assessment or genetic manipulation in the absence of cell-type-specific drivers. Addressing this knowledge gap, Shuai et al. have screened over 4000 split-GAL4 drivers and correlated them with identified neuron types from the "Hemibrain" EM connectome by matching light microscopy images to neuronal shapes defined by EM. They successfully generated over 800 split-GAL4 drivers and 22 split-LexA drivers covering a substantial number of neuron types across layers of the mushroom body associative learning circuit. They provide new labeling tools for olfactory and non-olfactory sensory inputs to the mushroom body; interneurons connected with dopaminergic neurons and/or mushroom body output neurons; potential reinforcement sensory neurons; and expanded coverage of intrinsic mushroom body neurons. Furthermore, the authors have optimized the GR64f-GAL4 driver into a sugar sensory neuron-specific split-GAL4 driver and functionally validated it as providing a robust optogenetic substitute for sugar reward. Additionally, a driver for putative nociceptive ascending neurons, potentially serving as optogenetic negative reinforcement, is characterized by optogenetic avoidance behavior. The authors also use their very large dataset of neuronal anatomies, covering many example neurons from many brains, to identify neuron instances with atypical morphology. They find many examples of mushroom body neurons with altered neuronal numbers or mistargeting of dendrites or axons and estimate that 1-3% of neurons in each brain may have anatomic peculiarities or malformations. Significantly, the study systematically assesses the individualized existence of

MBON08 for the first time. This neuron is a variant shape that sometimes occurs instead of one of two copies of MBON09, and this variation is more common than that in other neuronal classes: 75% of hemispheres have two MBON09's, and 25% have one MBON09 and one MBON08. These newly developed drivers not only expand the repertoire for genetic manipulation of mushroom body-related neurons but also empower researchers to investigate the functions of circuit motifs identified from the connectomes. The authors generously make these flies available to the public. In the foreseeable future, the tools generated in this study will allow important advances in the understanding of learning and memory in Drosophila.

Strengths:

1. After decades of dedicated research on the mushroom body, a consensus has been established that the release of dopamine from DANs modulates the weights of connections between KCs and MBONs. This process updates the association between sensory information and behavioral responses. However, understanding how the unconditioned stimulus is conveyed from sensory neurons to DANs, and the interactions of MBON outputs with innate responses to sensory context remains less clear due to the developmental and anatomic diversity of MBONs and DANs. Additionally, the recurrent connections between MBONs and DANs are reported to be critical for learning. The characterization of split-GAL4 drivers for 30 major interneurons connected with DANs and/or MBONs in this study will significantly contribute to our understanding of recurrent connections in mushroom body function.

2. Optogenetic substitutes for real unconditioned stimuli (such as sugar taste or electric shock) are sometimes easier to implement in behavioral assays due to the spatial and temporal specificity with which optogenetic activation can be induced. GR64f-GAL4 has been widely used in the field to activate sugar sensory neurons and mimic sugar reward. However, the authors demonstrate that GR64f-GAL4 drives expression in other neurons not necessary for sugar reward, and the potential activation of these neurons could introduce confounds into training, impairing training efficiency. To address this issue, the authors have elaborated on a series of intersectional drivers with GR64f-GAL4 to dissect subsets of labeled neurons. This approach successfully identified a more specific sugar sensory neuron driver, SS87269, which consistently exhibited optimal training performance and triggered ethologically relevant local searching behaviors. This newly characterized line could serve as an optimized optogenetic tool for sugar reward in future studies.

3. MBON08 was first reported by Aso et al. 2014, exhibiting dendritic arborization into both ipsilateral and contralateral γ3 compartments. However, this neuron could not be identified in the previously published Drosophila brain connectomes. In the present study, the existence of MBON08 is confirmed, occurring in one hemisphere of 35% of imaged flies. In brains where MBON08 is present, its dendrite arborization disjointly shares contralateral γ3 compartments with MBON09. This remarkable phenotype potentially serves as a valuable resource for understanding the stochasticity of neurodevelopment and the molecular mechanisms underlying mushroom body lobe compartment formation.

Weaknesses:
There are some minor weaknesses in the paper that can be clarified:

1. In Figure 8, the authors trained flies with a 20s, weak optogenetic conditioning first, followed by a 60s, strong optogenetic conditioning. The rationale for using this training paradigm is not explicitly provided. In Figure 8E, if data for training with GR64f-GAL4 using the same paradigm is available, it would be beneficial for readers to compare the learning performance using newly generated split-GAL4 lines with the original GR64f-GAL4, which has been used in many previous research studies. It is noteworthy that in previously published work, repeating training test sessions typically leads to an increase in learning performance in discrimination assays. However, this augmentation is not observed in any of the split-GAL4 lines presented in Figure 8E. The authors may need to discuss possible reasons for this.

2. In line 327, the authors state that in all samples, the β'1 compartment is arborized by MBON09. However, in Figure 11J, the probability of having at least one β'1 compartment not arborized is inferred to be 2%. The authors should address and clarify this conflict in the text to avoid misunderstanding.

3. In general, are the samples presented male or female? This sample metadata will be shown when the images are deposited in FlyLight, but it would be useful in the context of this manuscript to describe in the methods whether animals are all one sex or mixed sex, and in some example images (e.g. mAL3A) to note whether the sample is male or female.

https://doi.org/10.7554/eLife.94168.1.sa2

Reviewer #2 (Public Review):

Summary:
The article by Shuai et al. describes a comprehensive collection of over 800 split-GAL4 and split-LexA drivers, covering approximately 300 cell types in Drosophila, aimed at advancing the understanding of associative learning. The mushroom body (MB) in the insect brain is central to associative learning, with Kenyon cells (KCs) as primary intrinsic neurons and dopaminergic neurons (DANs) and MB output neurons (MBONs) forming compartmental zones for memory storage and behavior modulation. This study focuses on characterizing sensory input as well as direct upstream connections to the MB both anatomically and, to some extent, behaviorally. Genetic access to specific, sparsely expressed cell types is crucial for investigating the impact of single cells on computational and functional aspects within the circuitry. As such, this new and extensive collection significantly extends the range of targeted cell types related to the MB and will be an outstanding resource to elucidate MB-related processes in the future.

Strengths:
The work by Shuai et al. provides novel and essential resources to study MB-related processes and beyond. The resulting tools are publicly available and, together with the linked information, will be foundational for many future studies. The importance and impact of this tool development approach, along with previous ones, for the field cannot be overstated. One of many interesting aspects arises from the anatomical analysis of cell types that are less stereotypical across flies. These discoveries might open new avenues for future investigations into how such asymmetry and individuality arise from development and other factors, and how it impacts the computations performed by the circuitry that contains these elements.

Weaknesses:
Providing such an array of tools leaves little to complain about. However, despite the comprehensive genetic access to diverse sensory pathways and MB-connected cell types, the

manuscript could be improved by discussing its limitations. For example, the projection neurons from the visual system seem to be underrepresented in the tools produced (or almost absent). A discussion of these omissions could help prevent misunderstandings. Additionally, more details on the screening process, particularly the selection of candidate split halves and stable split-GAL4 lines, would provide valuable insights into the methodology and the collection's completeness.

https://doi.org/10.7554/eLife.94168.1.sa1

Reviewer #3 (Public Review):

Summary:
Previous research on the Drosophila mushroom body (MB) has made this structure the best-understood example of an associative memory center in the animal kingdom. This is in no small part due to the generation of cell-type specific driver lines that have allowed consistent and reproducible genetic access to many of the MB's component neurons. The manuscript by Shuai et al. now vastly extends the number of driver lines available to researchers interested in studying learning and memory circuits in the fly. It is an 800-plus collection of new cell-type specific drivers target neurons that either provide input (direct or indirect) to MB neurons or that receive output from them. Many of the new drivers target neurons in sensory pathways that convey conditioned and unconditioned stimuli to the MB. Most drivers are exquisitely selective, and researchers will benefit from the fact that whenever possible, the authors have identified the targeted cell types within the Drosophila connectome. Driver expression patterns are beautifully documented and are publicly available through the Janelia Research Campus's Flylight database where full imaging results can be accessed. Overall, the manuscript significantly augments the number of cell type-specific driver lines available to the Drosophila research community for investigating the cellular mechanisms underlying learning and memory in the fly. Many of the lines will also be useful in dissecting the function of the neural circuits that mediate sensorimotor circuits.

Strengths:
The manuscript represents a huge amount of careful work and leverages numerous important developments from the last several years. These include the thousands of recently generated split-Gal4 lines at Janelia and the computational tools for pairing them to make exquisitely specific targeting reagents. In addition, the manuscript takes full advantage of the recently released Drosophila connectomes. Driver expression patterns are beautifully illustrated side-by-side with corresponding skeletonized neurons reconstructed by EM. A comprehensive table of the new lines, their split-Gal4 components, their neuronal targets, and other valuable information will make this collection eminently useful to end-users. In addition to the anatomical characterization, the manuscript also illustrates the functional utility of the new lines in optogenetic experiments. In one example, the authors identify a specific subset of sugar reward neurons that robustly promotes associative learning.

Weaknesses:
While the manuscript succeeds in making a mass of descriptive detail quite accessible to the reader, the way the collection is initially described - and the new lines categorized - in the text is sometimes confusing. Most of the details can be found elsewhere, but it would be useful to know how many of the lines are being presented for the first time and have not been previously introduced in other publications/contexts. And where can the lines be found at Flylight? Are they listed as one collection or as many? Also, the authors say that some of the lines were included in the collection despite not necessarily targeting the intended type of neuron (presumably one that is involved in learning and memory). What percentage of the collection falls into this category? And what about the lines that the authors say they included in the collection despite a lack of specificity? How many lines does this represent?

https://doi.org/10.7554/eLife.94168.1.sa0